The Liprin-α protein family: common and diverging properties

Dissertation

zur

Erlangung des Doktorgrades (Dr. rer. nat.)

der

Mathematisch-Naturwissenschaftlichen Fakultät

der

Rheinischen Friedrich-Wilhelms-Universität Bonn

vorgelegt von

Magdalena Zürner

aus

Karlsruhe

Bonn 2010

Angefertigt mit Genehmigung der Mathematisch-Naturwissenschaftlichen Fakultät der Rheinischen Friedrich-Wilhelms-Universität Bonn.

1. Gutachter: Prof. Dr. Susanne Schoch
2. Gutachter: Prof. Dr. Albert Haas

Tag der mündlichen Prüfung: 19.11.2010

Diese Dissertation ist auf dem Hochschulschriftenserver der ULB Bonn unter http://hss.ulb.uni-bonn.de/diss online elektronisch publiziert.

Erscheinungsjahr: 2010

ERKLÄRUNG

Diese Dissertation wurde im Sinne von § 4 der Promotionsordnung vom 7.1.2004 am Institut für Neuropathologie und Klinik für Epilepsie der Universität Bonn unter der Leitung von Frau Prof. S. Schoch angefertigt. Hiermit versichere ich, dass ich die vorliegende Arbeit selbständig angefertigt habe und keine weiteren als die angegebenen Hilfsmittel und Quelle verwendet habe, die gemäß § 6 der Promotionsordnung kenntlich gemacht sind.

Teile dieser Arbeit wurden in Form von wissenschaftlichen Artikeln veröffentlicht:

Zurner M, Schoch S (2009) The mouse and human Liprin-alpha family of scaffolding proteins: genomic organization, expression profiling and regulation by alternative splicing. Genomics 93:243-253.

Zürner M, Mittelstaedt T, tom Dieck S, Becker A, Schoch S (2010) Differential spatiotemporal expression and subcellular localization of Liprin-α proteins indicate isoform specific functions. Submitted.

Bonn, den _____ _____

Summary:

The Liprin-α family of scaffolding proteins is highly evolutionary conserved. While one homologue is present in invertebrates, it has diversified into four isoforms in mammals. In invertebrates, Liprin-α plays a crucial role in synapse assembly and maintenance as well as in synaptic vesicle trafficking. Little is known about the functional role of the four Liprin-α isoforms in the mammalian brain. The aim of this study was to examine the common and diverging properties of the four Liprin-α isoforms in order to gain insight into their role at the mammalian synapse.

A comparative characterization of the structure of the human and mouse Liprin-α genes and their regulation by alternative splicing showed that even though the genomic organization of the four isoforms is very similar, Liprins-α can be modified differentially in a developmental manner.

To study the spatiotemporal expression pattern of the four Liprin-α isoforms we generated isoform-specific peptide antibodies. All four Liprin-α proteins are expressed in most neuronal populations of the brain, but each Liprin-α protein is characterized by a distinct expression profile. In particular, the spatiotemporal expression pattern of Liprin-α1 stands out. Expression of the most abundant isoforms, Liprin-α2 and -α3, and the more weakly expressed Liprin-α4 is restricted to the brain and increases during development. In contrast, Liprin-α1 is expressed in all tissues tested, is present in glia, and has the highest expression level during development. The overlapping and distinct regional and subcellular localization of the Liprins-α indicates common as well as diverging functional roles. These results support the hypothesis that Liprin-α1 might play a role in organizing protein complexes that are involved in cell migration.

Liprins-α are hypothesized to act as scaffolding proteins at the active zone. To gain a better understanding of the role of Liprin-α2 at the presynapse we analyzed its dynamics. We found that Liprin-α2 has a relatively slow turn-over which suggests that Liprin-α2 functions as a stably integrated scaffolding protein, thereby adding to the tenacity of the active zone.

For further investigations into the role of Liprins-α we identified shRNAs to knock down single isoforms as well as a point mutation to disrupt Liprin-α - RIMα interactions.

In summary, this study provides a thorough characterization of the Liprin-α family, and indicates a role in cell migration during brain development for Liprin-α1 and a role in synapse tenacity for Liprin-α2.

Table of contents **Page**

1 Introduction

1.1 The synapse

Chemical synapses are the sites of contact and communication between a neuron and its target cell and are characterized by their asymmetric nature (Fig. 1.1). On both sides of the synapse signal transduction takes place at specialized membrane subcompartments. There are highly organized structures consisting of unique proteinaceous networks. At the presynapse, the area at the plasma membrane where synaptic vesicle fusion takes place, is called the active zone (AZ). On the opposite side, at the synapse, the postsynaptic density (PSD) contains the neurotransmitter reception apparatus (Sudhof, 2004; Schoch and Gundelfinger, 2006; Sheng and Hoogenraad, 2007). The active zone and PSD are precisely aligned and connected by trans-synaptic proteins, which bridge the synaptic cleft.

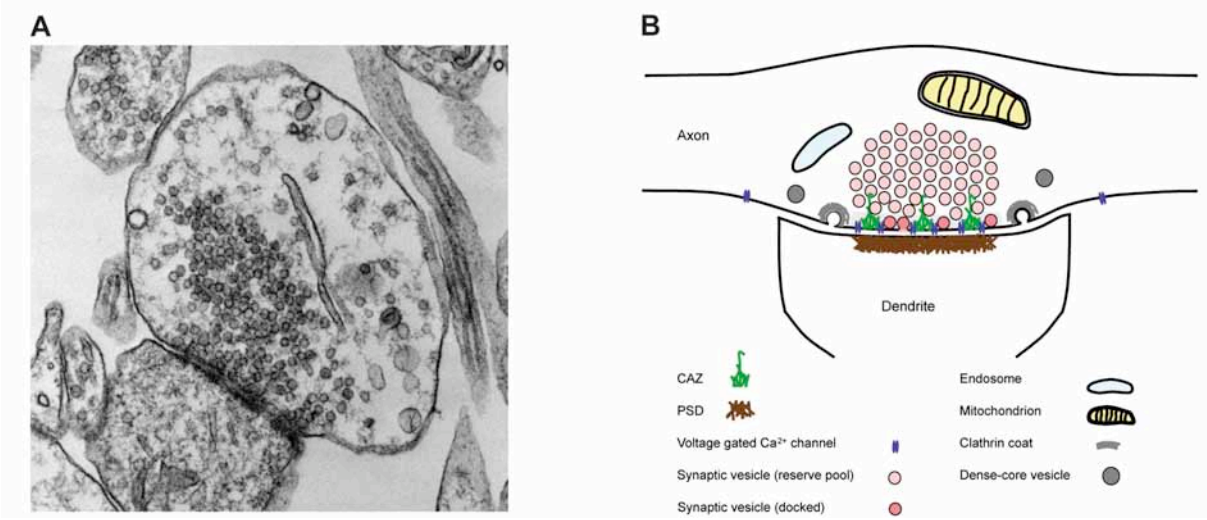

Fig.1.1: The chemical synapse
(A), Electron micrograph of a mouse hippocampal synapse (primary culture). (B), Schematic drawing of an enpassant presynaptic bouton taken from Ziv and Garner (2008) New Encyclopedia of Neuroscience.

Upon action potential arrival at the presynaptic bouton rapid fusion of synaptic vesicles (SVs) at the active zone is triggered as a response to Ca^{2+}-influx through voltage-gated Ca^{2+}-channels (Sudhof, 2004; Smith et al., 2008). Neurotransmitter is released into the synaptic cleft and bound by receptors in the PSD, where the chemical signal is converted to an electrical signal and is propagated. SVs are made available for this extremely fast fusion event at the active zone plasma membrane by consecutive events named docking and priming (Fig. 1.2). Following SV fusion

vesicle replenishment is mediated by different endocytotic mechanisms, e.g. clathrin mediated endocytosis and bulk endocytosis.

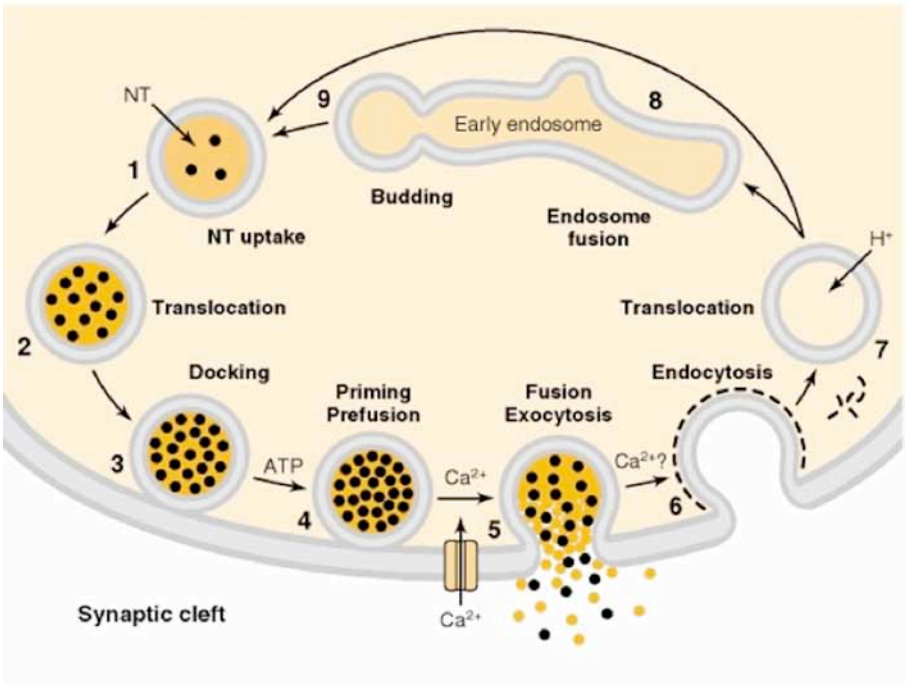

Fig. 1.2: The synaptic vesicle cycle
Taken from Basic Neurochemistry, 1999.

1.2 The presynaptic active zone

SV fusion takes place at a specialized domain of the plasma membrane, the active zone, which is tightly associated with an electron-dense structure, named cytomatrix at the active zone (CAZ). Fusion of SVs is extremely rapid and therefore needs to be tightly controlled. This poses specific requirements to the organization of the protein network at the active zone. In order to achieve the high speed, SVs need to be available in close proximity to the voltage-gated Ca^{2+}-channels as well as the required regulatory proteins (Siksou et al., 2007). Whereas exocytosis takes place at the active zone, endocytosis occurs in the perisynaptic region. Therefore the spatial segregation of membrane domains for exo- and endocytosis needs to be defined. These specific challenges suggest the need for a specialized structure at the active zone.

1.2.1. Models of the active zone structure

In recent years the morphology of the active zone of different synapse types and organisms has been analyzed in multiple studies using electron microscopy (EM). These studies showed that active zone morphology could vary considerably between synape types as well as species.

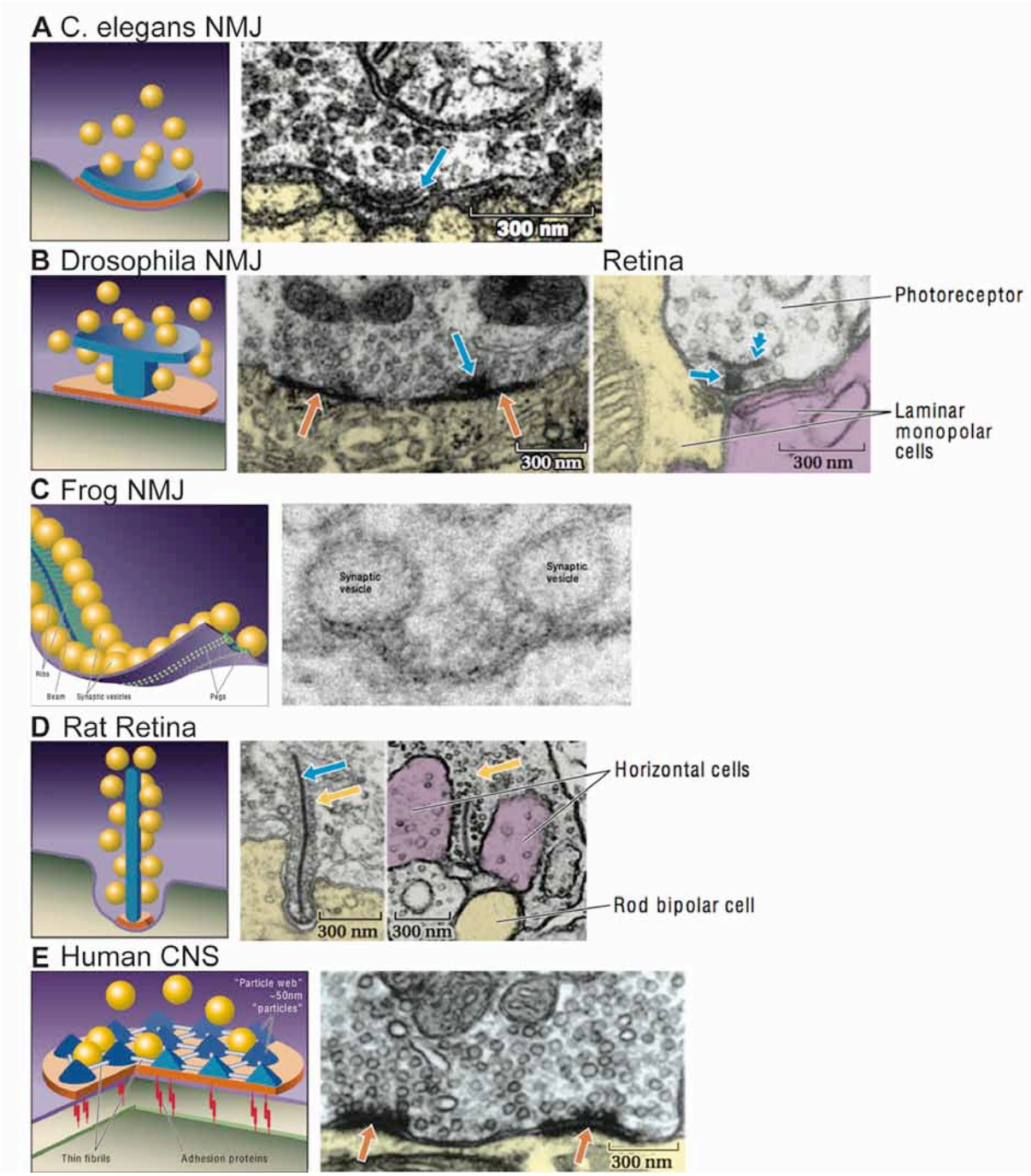

Fig.1.3: Overview of the active zone ultrastructur of different species and synapse types
(A), Neuromuscular junction (NMJ) terminal in *C. elegans.* (B), NMJ terminal in *Drosophila* with a dense projection called T bar (blue arrow). Retina: Tetrad synapse between photoreceptor and lamina monopolar cells. (C), Frog NMJ, where SV are docked to the plasma membrane through dense projections. (D), Triadic photoreceptor ribbon synapse between a rod photoreceptor and horizontal cell and a rod bipolar cell in rat. (E), Excitatory synaptic terminal in human hippocampus with two active zones (red arrows). On the left, diagrams of the active zone structure in the synaptic terminal electron micrograpahs are shown. All figures taken from (Zhai and Bellen, 2004).

For invertebrates two main types of active zone morphology were observed. In *C. elegans* the active zone at the neuromuscular junction (NMJ) was shown to have a

plaque like shape layered along the presynaptic plasma membrane (Hallam et al., 2002). In *Drosophila* a T-shaped dense projection, called T-bar, which extends into the presynaptic terminal and where SVs cluster around, was described for the NMJ, the tetrade synapse of the visual system as well as for a subset of CNS synapses. (Figure 1.3A, B) (Meinertzhagen, 1996). At the frog NMJ the active zone was shown to be layed out in a very organized, array like structure using EM tomography. So called beams and pegs connect SVs with putative Ca^{2+}-channels, so that each docked SV is perfectly aligned with at least one Ca^{2+}-channel (Figure 1.3C) (Harlow et al., 2001). In the mammalian visual system photoreceptor synapses are found to exhibit ribbons where SVs cluster around (Figure 1.3D) (Dick et al., 2003) while in classical EM studies of mammalian CNS synapses the active zone showed a regular arrangement of cone-shaped electron densities, that extended into the cytosol, the so-called presynaptic grid (Figure 1.3E, 1.4) (Gray, 1963; Bloom and Aghajanian, 1968; Pfenninger et al., 1969). Since then, many anatomical studies followed and different approaches for enhancement of EM aiming at better resolution and sample preperation were pursued. Using high pressure freezing of sampels instead of formaldeyde fixation followed by EM, docked vesicles were also described to clusterer around electron-dense material at the active zone, but these structures were not arranged in a regular pattern (Siksou et al., 2007). In the most recent approach using cryo-electron-tomography, where samples are vitrified, no cone shaped electron densities could be detected at the active zone (Figure 1.4) (Fernandez-Busnadiego et al., 2010) .

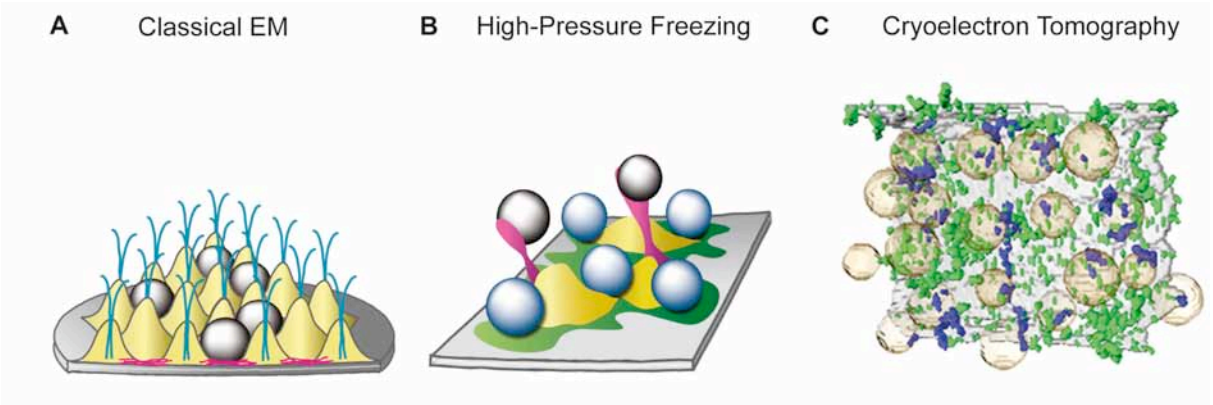

Fig. 1.4: Different models of the mammalian active zone ultrastructure
(A), Model of the AZ derived from classical EM studies. (B), Model of the AZ derived from a high pressure freezing EM study by Siksou et al. (C), Reconstruction of a cryo electron tomograph of the presynaptic bouton viewed from the cytoplasmic side where AZ membrane densities are mapped Gray, AZ; yellow (partially transparent), proximal synaptic vesicles; blue, synaptic vesicle tethers; green, other densities on the AZ that do not contact the vesicles (Fernandez-Busnadiego et al., 2010).

Many of the described electron-dense projections were shown to tether vesicles. Most prominently this has been shown for the frog NMJ but also at the vertebrate synapse tethers linking the active zone and SVs were described using a variety of methods (Harlow et al., 2001; Siksou et al., 2007; Fernandez-Busnadiego et al., 2010).

At some specific synapses proteins that are essential for the morphology and function of the active zone were identified. For example the retina of the Bassoon knock out mouse exhibits a severe disruption of the photoreceptor ribbon synapse morphology. The number of ribbons is reduced and they are no longer anchored at the active zone (Dick et al., 2003). In *Drosophila*, mutants of the ELKS family member Bruchpilot are lacking the T-shaped electron dense projections at the tetrade synapse of the visual system as well as at larval NMJ and show deficits in Ca^{2+}-channel clustering (Wagh et al., 2006). In *C. elegans* and *Drosophila,* mutants of the Liprin-α homolog (SYD-2/Dliprin-α) show a disrupted active zone morphology as well as an impairment of synaptic transmission at the NMJ (Zhen and Jin, 1999; Kaufmann et al., 2002).

1.2.2. CAZ proteins

Many proteins that are associated with the CAZ have been identified. Most of these proteins are not specifically localized at the active zone but are also found in other functional compartments of the cell. The CAZ is composed of cytoskeletal proteins, adhesion molecules, scaffolding proteins, voltage-gated Ca^{2+}-channels and components of the fusion machinery. Only four families of proteins are known so far to be highly enriched at the active zone, i.e. RIM, Munc13, ELKS and Bassoon/Piccolo (Schoch and Gundelfinger, 2006). RIMs play an important role in linking SV to the Ca^{2+}-channels and together with Munc13 are necessary for priming of SV (Schoch et al., 2002; Kiyonaka et al., 2007). ELKS, Bassoon and Piccolo are scaffolding proteins that interconnect many active zone proteins (Wang et al., 2009). Until now the molecular mechanisms underlying the organization of the active zone as well as the components essential for active zone formation and maintenance are unknown. A protein family enrichted at the active zone and implicated to play a role in active zone assembly are the Liprins-α.

1.3 Liprins-α

The evolutionary conserved Liprin-α family of scaffolding proteins plays a crucial role in synapse assembly and function (Schoch and Gundelfinger, 2006; Spangler and Hoogenraad, 2007; Stryker and Johnson, 2007a). Liprins-α were originally identified by their interaction with the LAR-RPTPs (leukocyte common antigen-related family of receptor protein tyrosine phosphatases) in non-neuronal cells (Pulido et al., 1995; Serra-Pages et al., 1995). Whereas in the invertebrates *C. elegans* and *Drosophila* only a single Liprin-α gene was described, *SYD-2* (synapse-defective-2) (Zhen and Jin, 1999) and Dliprin-α (Kaufmann et al., 2002), respectively, four Liprin-α isoforms were found in vertebrates, Liprin-α1, -α2, -α3 and -α4 (Serra-Pages et al., 1998). Liprins-α exhibit a striking degree of conservation, with 40% amino acid identity between the worm SYD-2 and human Liprin-α1.

1.3.1. Liprin-α domains and their interaction partners

Liprin-α proteins are composed of an N-terminal region predicted to form coiled-coil structures and three C-terminal SAM (sterile-α-motif)- domains that constitute the LH (liprin homology) region (Fig. 1.5A) (Pulido et al., 1995; Serra-Pages et al., 1995; Serra-Pages et al., 1998).

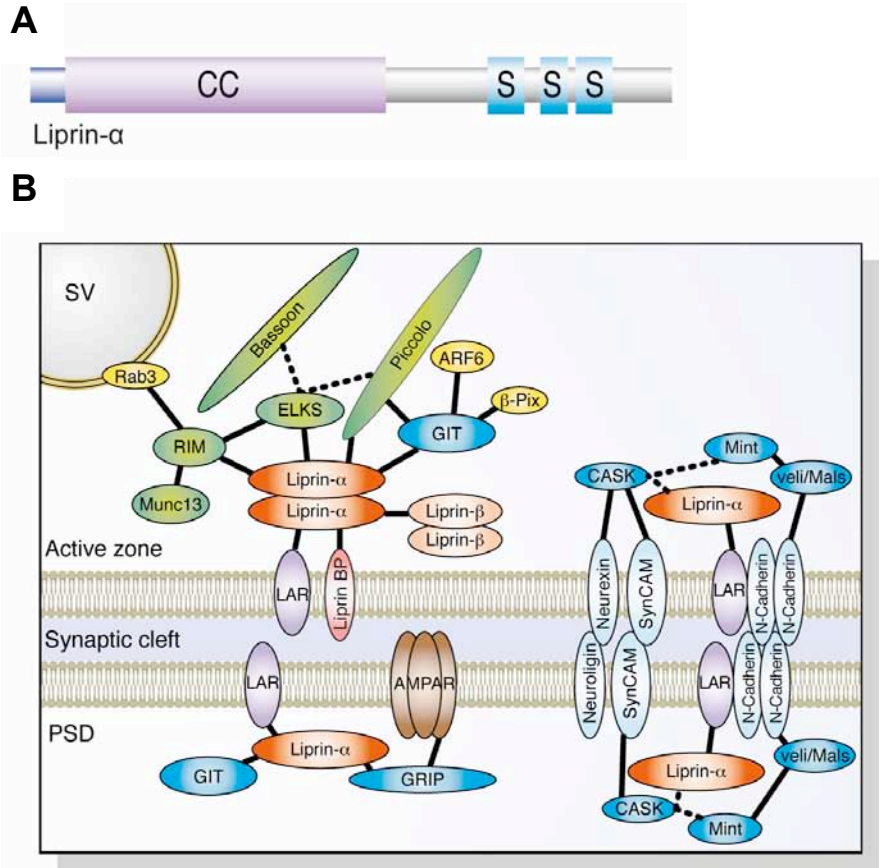

C

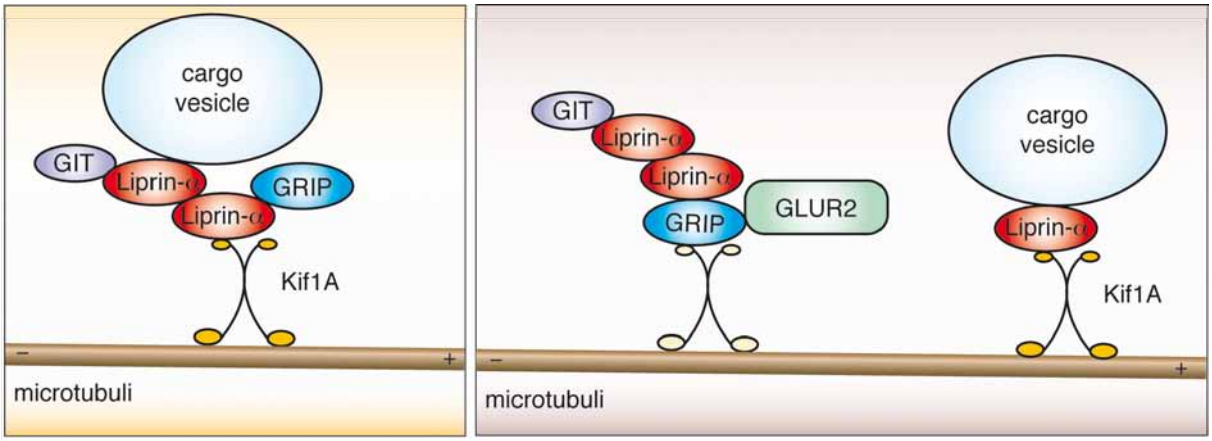

Fig.1.5: Liprins-α domains and their putative interaction partners
(A), Schematic drawing of the structural domains of Liprins-α. CC: Coiled-coil domain, S: SAM- (sterile-α-motive) domain. (B), Schematic drawing of the known interaction partners for Liprins-α at the pre- and postsynaptic side. In green: AZ enriched proteins. (C), Schematic drawing of the potential role of Liprin-α as an adaptor protein between Kif1A and its cargo.

The SAM-domains have been reported to interact with the intracellular domain of LAR-RPTPs (Pulido et al., 1995), the MAGUK (membrane-associated guanylate kinase) protein CASK (calcium/calmodulin-dependent serine protein kinase) (Olsen et al., 2005; Samuels et al., 2007), CaMKII (Ca^{2+}/calmodulin-dependent protein kinase II) (Hoogenraad et al., 2007), Liprin-ß and ATP (Serra-Pages et al., 2005). The N-terminal coiled-coil region mediates homo- and hetero-dimerization as well as interactions with various synaptic proteins, including the presynaptic active zone proteins RIM (Rab3-interacting molecule) (Schoch et al., 2002) and ELKS (also CAST/ERC (ELKS/RAB6-interacting/CAST)) (Ko et al., 2003a), the GTPase activating protein for the family of ADP-ribosylation factor GTPases GIT1 (G protein-coupled receptor kinase interactor) (Ko et al., 2003b), and the kinesin motor protein KIF1A (kinesin family member 1A) (Shin et al., 2003). At their C-terminus vertebrate Liprins-α contain a PDZ-binding motif that interacts with GRIP (glutamate receptor interacting protein) (Wyszynski et al., 2002). Through these interactions Liprins-α are directly linked to essential components of the presynaptic active zone and the postsynaptic density (Fig. 1.5B) as well as the machinery required for vesicular transport.

1.3.2. Functional role of Liprin-α in C.elegans and Drosophila

A loss of function mutant for the *C. elegans* Liprin-α homolog *SYD-2* was identified in a genetic screen for mutations affecting the localization of a SV marker. These

mutants showed a diffuse localization of SVs at the neuromuscular junction of motor neurons. In addition, the presynaptic Aactive zones were significantly lengthened while being less electron-dense. Mutants exhibited uncoordinated movement as well as defects in egg-laying behavior, indicative of a defect in synaptic transmission (Zhen and Jin, 1999). A subsequent study showed that SYD-2 is important for the correct localization of presynaptic proteins, e.g. ELKS, GIT SAD1, endophillin, RIM and synapsin (Ackley et al., 2005; Patel et al., 2006). Another candidate gene that was identified in the initial screen is *SYD-1*. *SYD-1* loss-of-function mutants show a similar phenotyp as *SYD-2* mutants. At the NMJ of *SYD-1* mutants fewer presynaptic punta were detected and an abberant active zone shape was observed. Presynaptic proteins were diffusely distributed and mutants exhibited uncoordinated movement as well as defects in egg-laying behavior (Hallam et al., 2002). At HSN (hermaphrodite specific neurons) motorneurons that control egg-laying behaviour identical phenotypes of the *SYD-1* and *SYD-2* mutants were observed. In the *SYD-1* mutant the punctate pattern of SYD-2 is diffuse compared to wild type. For this set of neurons a gain of function mutation in *SYD-2* was identified that was able to rescue the egg-laying phenotype (Dai et al., 2006). In these double mutants the presynaptic localization of SYD-2 is restored. In addition an increased interaction of SYD-2 with ELKS was observed. For the rescue of the *SYD-1* mutant phenotype the presence of ELKS was critical. It was hypothesized that SYD-1 acts upstream of SYD-2 and is important for the precise localization of SYD-2 at the synapse, thereby promoting SYD-2 activity.

Drosophila Dliprin-α mutants show a very similar defect in active zone morphology (Kaufmann et al., 2002). While at the wild type NMJ the size and shape of the active zone is very consistent, the loss of the functional Liprin-α homolog leads to elongated and larger active zone. The evoked excitatory junctional potentials and quantal content per synaptic event were decreased at the NMJ of Dliprin-α mutants pointing to a specific impairment of presynaptic function (Kaufmann et al., 2002). Furthermore, lack of Dliprin-α during synapse development at the larval NMJ lead to a reduction of bouton number and branch complexity of the terminal arbor (Kaufmann et al., 2002). This suggests that Dliprin-α plays an important role in synapse growth and thus in the formation of new boutons at the ends of terminal branches.

Additionally, invertebrate Liprins-α are involved in the regulation of synaptic vesicular transport through their interaction with the motor protein KIF1A/UNC-104. In Dliprin-α

mutants SVs abberantly accumulate along the axon, indicating that Dliprin-α plays a role in trafficking of SVs (Miller et al., 2005). In *C. elegans*, Liprin-α controls motor clustering along axons as well as motor motility. Loss of SYD-2 binding reduces net anterograde movement and velocity of the cargo (Wagner et al., 2009).

In the visual system Dliprin-α is required for the correct targeting of photoreceptor axons (Choe et al., 2006; Hofmeyer et al., 2006). Dliprin-α, N-cadherin and Dlar mutants show similar phenotypes in a set of photoreceptor cells (R1-6). The authors hypothesized that theses proteins act at the same step of axon targeting i.e. during target stabilization. A subsequent study showed that complex positive as well as inhibitory interactions amongst Dliprin-α, N-cadherin and DLAR regulate photoreceptor targeting (Prakash et al., 2009). During development of the visual system this protein complex regulates adhesive interactions between the pre- and post- synaptic cells at the axonal growth cone.

1.3.3. Functional role of Liprins-α in mammals

Mammalian Liprins-α were shown to be localized in axons and dendrites, in agreement with their association with pre- and postsynaptic protein complexes (Wyszynski et al., 2002). Liprins-α have been reported to regulate clustering and localization of LAR in cultured cell lines (Serra-Pages et al., 1995; Serra-Pages et al., 1998). At the presynaptic active zone of primary neurons Liprins-α colocalize with ELKS and RIM, two interaction partners known to be highly enriched at the active zone. These two proteins link Liprins-α to the tight net of active zone proteins. Interestingly, in RIM1α as well ELKS knock out mice levels of Liprin-α are unchanged (Kaeser et al., 2008; Kaeser et al., 2009). In dendrites Liprins-α are key proteins for the dendritic targeting of AMPA receptors. Liprin-α forms a complex with GRIP-LAR and GluR2/3 and the interaction of Liprin-α with GRIP is important for surface expression of AMPA receptors (Wyszynski et al., 2002). In addition, interfering with the Liprin-α - GIT interaction leads to disruption of dendritic clustering and surface expression of AMPA receptors (Ko et al., 2003b).

Furthermore, the Liprin-α-LAR-GRIP complex is involved in the development and maintenance of excitatory synapses as LAR mutants lead to decreased synapse density. The complex plays a role in the dendritic targeting of cadherin-ß-catenin, which is dependent on LAR phosphatase activity (Dunah et al., 2005). Recently, the interactions between Liprin-α, GRIP and the AMPA receptor subunit GluR2 were

identified as required for muscarinic receptor-triggered long term depression (LTD) (Dickinson et al., 2009).

A first study addressing possible functional differences of the four Liprin-α isoforms reported that Liprin-α1 is regulated in an activity-dependent manner. Liprin-α1 but not Liprin-α2 was degraded either in response to CaMKII phosphorylation or via the E3 ubiquitin ligase anaphase promoting complex (APC) (Hoogenraad et al., 2007). Expression of non-degradable Liprin-α1 mutants resulted in impaired dendritic targeting of LAR and a reduction of dendritic branching and synapse number.

Outside the nervous system Liprins-α have been found to localize LAR to the proximal edge of focal adhesions of human cell lines (Serra-Pages et al., 1995). Increasing evidence suggest that Liprin-α1 plays a role in the dynamic regulation of focal adhesions during cell motility. Depletion of Liprin-α1 inhibits cell spreading while overexpression enhances motility as well lamellipodia and focal-adhesion formation at the cell edge. Increased levels of Liprin-α1 lead to a redistribution of inactive, low-affinity integrins to focal adhesions while depletion increases the rate of integrin internalization. This indicates that Liprins-α regulate focal adhesion turn-over by influencing the localization and stability of integrins (Shen et al., 2007; Asperti et al., 2009; Asperti et al., 2010).

Taken together, Liprins-α are critically involved in the assembly, organization and function of presynaptic active zones, in the development and maintenance of dendritic spines and excitatory synapses and in the regulation of vesicular trafficking and cell motility.

1.4 Assembly of the active zone

Synapse assembly, i.e. the establishment of an axo-dendritic contact and the assembly of the active zone and postsynaptic density, is a key process during synaptogenesis as well as synaptic plasticity. In recent years genetic studies in invertebrates and vertebrates have allowed first insights into the formation of the active zone. Dissecting the underlying processes of synapse assembly has proven difficult among others due to genetic redundancies.

Establishing a synaptic contact is a multi-step process. First contact and recognition of an axon and dendrite takes place. Then the essential modules necessary to build a synapse e.g. the active zone components, the exo- and endocytosis machinery, the

components of the PSD and the trans-synaptic adhesion molecules need to be assembled at the site of contact. Many findings indicate that the assembly of these modules takes place by self-assembly of units (Owald and Sigrist, 2009).

The assembly is best studied in the model organisms *C. elegans* and *Drosophila.* Several presynaptic proteins important for the regulation of active zone formation were identified (Fig. 1.6). In *C. elegans* the definition of a patch of membrane where the active zone is assembled is dependent on the immunoglobulin cell adhesion molecules (IgCAM) UNC-44/DCC or the hetrophilic interaction pair SYG-1/Neph1 and SYG-2/Nephrin in different synapses (Shen et al., 2004; Colon-Ramos et al., 2007; Chao and Shen, 2008). Other IgCAM proteins might have similar functions in *Drosophila* and vertebrates. The cell adhesion molecules that trigger initial assembly seem to have diverged between synapse types and species.

Following the trans-synaptic interaction of the IgCAMs SYG-1 and SYG-2, which define the sites of active zone assembly, these proteins then recruit SYD-1 and SYD-2. SYD-2 in turn localizes other proteins such as ELKS and RIM to the active zone. SYD-1 and SYD-2/Liprin-α are key molecules that are tightly regulated to ensure correct assembly of the active zone. Their protein levels are critical for normal active zone size. RSY-1 (regulator of synaptogenesis-1), a protein identified in a genetic screen for mutants that rescue the synaptic phenotype of *SYD*-1 mutants, directly interacts with and regulates SYD-1 and SYD-2 (Patel and Shen, 2009). RSY-1 locally inhibits synapse assembly through negatively regulating these key assembly molecules. In *Drosophila* it was shown that presynaptic Dliprin-α levels, which are critical for normal active zone size are regulated through ubiquitylation by the ubiquitin-ligase APC/C (anaphase-promoting complex/cyclosome) (van Roessel et al., 2004). This allows regulation of the size of the presynaptic active zone by regulation of Dliprin-α through APC/C.

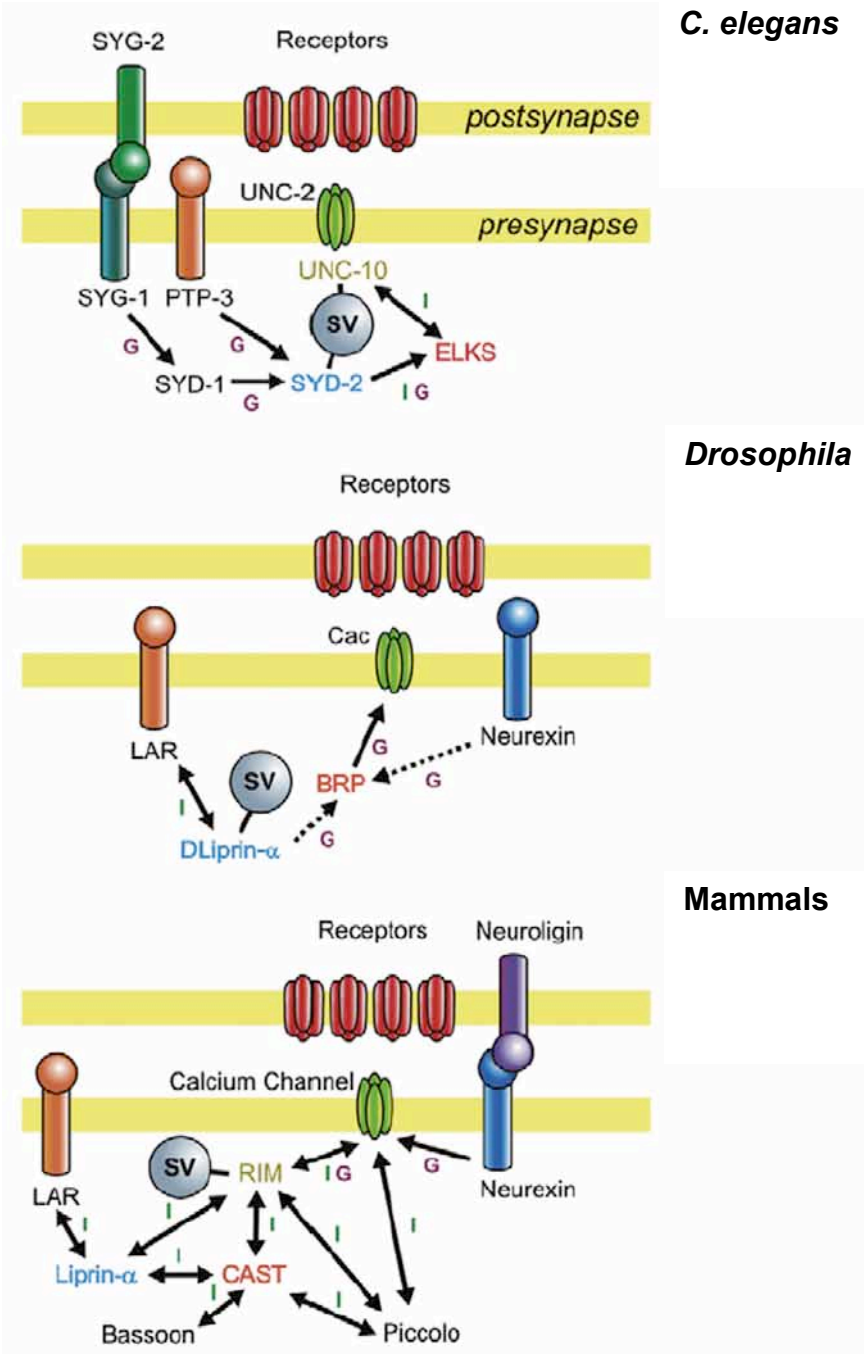

Fig.1.6: Molecular mechanisms involved in active zone assembly
A cartoon depicting proteins implicated in active zone assembly in different model organisms. Type of interactions are indicated by letters above the arrows: I = direct physical interaction, G = genetic interaction/ regulation inferred from genetic findings. Dashed lines indicate indirect evidence of interaction from imaging data. Figure taken from (Owald and Sigrist, 2009).

To better understand the modular assembly of the synapse different studies were carried out to define the time course. While cell culture experiments suggested a very rapid assembly in the course of 1-3 hours, data from slice cultures indicated that establishing a functional synapse takes many hours to one day (Owald and Sigrist, 2009). A recent study using time lapse imaging and electrophysiological analysis

followed by EM showed that synapses formed in the time frame of a few hours after spine formation occurred (Zito et al., 2009). There are different possible explanations for the differing results from the two systems. Synaptogenesis could be more tightly regulated in the slice and in addition the course of assembly might differ between high activity and low activity situations.

In summary, in invertebrates Liprin-α is a master assembly molecule that recruits numerous synaptic components to presynaptic sites as a result of contact initation by IgCAMs. To assure correct assembly of the active zone Liprin-α is regulated on different levels. At the mammalian synapse even though multiple components of the active zone have been described, no component critical for the assembly was yet identified.

1.5 Aims of this study

Liprins-α are a highly evolutionary conserved protein family with one homolog present in invertebrates and four isofoms in mammals. Studies in invertebrates showed that Liprins-α play a key role in synapse assembly and maintenance as well as in synaptic vesicle (SV) trafficking. So far little is known about the role of this protein family in the mammalian synapse. The aim of this study is to gain a better understanding of the role of Liprins-α at the mammalian synapse and to resolve the similarities and differences on the level of expression as well as function of the four isoforms.

Our first objective is to thoroughly characterize the genetic structure of the mammalian gene family as well as their alternative splicing as a way to obtain first insights into possible differences between the four isoforms. To verify our bioinformatic analysis we will subclone all four Liprin-α cDNAs and verify the sites of alternative splicing using RT-PCR.

So far no isoform specific antibodies are available, thus our second aim is to generate isoform specific antibodies to be able to dissect the distribution of the four isoforms on the cellular and subcellular level using immunoblots as well as immunostainings of primary neurons and brain sections.

In invertebrates the lack of Liprin-α led to a disruption of active zone morphology, mislocalization of other presynaptic proteins as well as to defects in synaptic vesicle trafficking. To be able to analyze the functional role of the family of Liprins-α and to study if Liprins-α fulfill a similar role in mammals we plan to develop tools to interfere with Liprin-α function. We would like to use shRNAs to analyze the effect of the lack of single Liprins-α on cell morphology as well as localization of other presynaptic proteins. In addition, we aim to identify point mutations to inhibit specific interactions. Disrupting interactions with specific binding partners would allow for a dissection of the functional role of these interactions.

Liprins-α are hypothesized to operate as scaffolds at the active zone (AZ), the site of synaptic vesicle fusion at the presynapse. Employing time-lapse imaging allows to study the dynamics of individual proteins and thus gives insights into their role at the presynapse. We plan to elucidate the turn over of Liprins-α at the presynapse by using FRAP (fluorescent recovery after photobleaching) and FRAPA (fluorescent recovery after photoactivation) experiments.

2 Materials

2.1 Equipment

Application	Model	Company
Acrylamid electrophoresis system	Mini-PROTEAN 3 Electrophoresis System	BioRad
Agarose electrophoresissystem	SUB-CELL GT	BioRad
Analytical balance	BP210S	Sartorius
Autoclave	Varioklav 75T	H + P
Balance	SBC53	SCALTEC
Capillary Sequencer	3130/xl/Genetic Analyzer	Applied Biosystems
Cell-cultur hood	MSC-Advantage	Thermo Scientific
Centrifuge	1-15K	Sigma
Centrifuge	5415C	Eppendorf
Centrifuge	Micro 22R	Hettich
Centrifuge	Avanti J-20	Beckman Coulter
Confocal laser scanning microscop	Leica TCS	Leica
Confocal laser scanning microscop	LSM710	Zeiss
Cryostat	FV300	MICROM
Gel documentation system	AlphaImager	Alpha Innotech
Incubator	T6	Heraeus Instruments
Infrared imaging system	Odyssey	Li-cor
Inverse microscope	Axio Observer 1A	Zeiss
PCR-Cycler	UNOII	Biometra
PCR-Cycler	MY Cycler	Biorad
Real time PCR (Taqman)	9700HT	ABI Prism
pH-meter	HI 9025	HANNA Instruments
Photometer	BIO	Eppendorf
Spectrophotometer	ND-1000	NanoDrop
Thermo shaker	MK13	HLC
Transfer System	Mighty Small Transphor/Hoefer TE22	Amersham
Ultrasonicator	UP50H	Hilscher
Vortex	Vortex-Genie 2	Scientific Industries

2.2 Material and Reagents

2.2.1. *Antibodies*

Table 3.1: Primary antibodies

Antibody	Assay	Dilution	Company
Bassoon (clone SAP7F407)	ICC	1:200-400	Stressgen
ß-actin	WB	1:5000	Abcam
CtBP2	ICC	1:10000	BD Bioscience
GAD 67	ICC	1:400	Chemicon
GAPDH	WB	1:1000	Abcam
GFAP	ICC	1:400	Synaptic Sytems
GFP (T3743)	WB	1:3000	Südhof lab
HA	WB	1:5000	Sigma
Liprin-α1	ICC/IHC/WB	1:20/1:50/1:100	Pineda
Liprin-α2	ICC/IHC/WB	1:50/1:50/1:200	Pineda
Liprin-α3	ICC/IHC/WB	1:20/1:50/1:200	Pineda
Liprin-α4	ICC/IHC/WB	1:20/1:50/1:200	Pineda
Pan-Liprin-α	WB	1:10000	Südhof lab
PSD-95	ICC	1:200	Chemicon
RIM1α	ICC	1:100	BD Bioscience
Synaptophysin	IHC	1:200	Synaptic Systems

Table 3.2: Secondary antibodies

Antibody	Assay	Dilution	Company
anti-mouse Cy5	ICC/IHC	1:200	Jackson immuno reagents Europe Ltd
anti-rabbit Alexa 594	ICC/IHC	1:1000	Molecular Probes
anti-rabbit Alexa 488	ICC/IHC	1:100	Invitrogen
IRDye anti-mouse 680nm	WB	1:20.000	Licor
IRDye anti-rabbit 800nm	WB	1:20.000	Licor
horseradish peroxidase coupled anti-mouse	WB	1:3000	Jackson immuno reagents Europe Ltd
horseradish peroxidase coupled anti-rabbit	WB	1:3000	Jackson immuno reagents Europe Ltd

2.2.2. Cell culture media

Dulbecco's Modified Eagle's Medium (DMEM)	Gibco BRL
Basal Medium Eagle (BME)	Invitrogen
IMDM	Gibco BRL
Fetales calf serum (FCS)	Invitrogen
Opti-MEM	Gibco BRL
Phospate saline buffer (PBS)	Gibco BRL
Hank's Buffered Salt Solution (HBSS)	Gibco BRL
Penicillin-Streptomycin	Gibco BRL
Glucose	Invitrogen
B27	Invitrogen

2.2.3. Chemicals

Chemicals were ordered from standard sources (Roth, Sigma-Aldrich, Merck).

Bovine serum albumin (BSA)	Sigma Aldrich
Cold water fish gelantine	Sigma
Complete Protease Inhibitor Cocktail Tablets	Roche
DMSO	Roth
Fetal calve serum (FCS)	Invitrogen
Glutathion	Sigma
Milk powder	Roth
Normal goat serum (NGS)	GIBCO BRL
Paraform aldehyd (PFA)	Merck
Poly-L-lysine	Sigma
Triton X-100	Sigma
Vectashield mouting medium	Vector Laboratories

2.2.4. Diverse materials

Glutathion-agarose beads	Sigma-Aldrich
HyperFilm	Amersham
Nitrocellulose membrane (Protan 0,4 mm)	Watman, GE Healthcare
Tissue tek	Sakura Finetek

2.2.5. Enzymes

GoTaq	Promega
pfu DNA polymerase	Promega
Restriction enzymes:	
BamHI, EcoRI, HindIII, KpnI, Xho	Fermentas
BamHI, BglII, PacI	New England Biolabs
Trypsin	GIBCO BRL
T4 Ligase	Fermentas

2.2.6. Kits

Amersham ECL Plus Western	GE Healthcare Europe
BigDye Terminator v3.1cycle Sequencing kit	Applied Biosystems
Blotting Detection Reagents	GE Healthcare Europe
DNA Clean and Concentration kit	Zymo Research
DyeEx 2.0 (Purification of Sequencing)	Qiagen
GeneJET Plasmid Miniprep kit	Fermentas
iScript cDNA synthesis kit	Biorad
Lipofectamine 2000	Invitrogen
Long PCR Enzyme Mix	Fermentas
QuickChangeII XL Site Directed Mutagenesis kit	Stratagen
PRISM Big Dye Terminator (Sequencing)	Applied Biosystems
Pure link Midi kit (DNA purification)	Invitrogen
TOPO vectors	Invitrogen
RNeasy Lipid Tissue Kit	Qiagen
Superscript RT III kit	Invitrogen
SYBR Green PCR kit	Qiagen
Zymoclean Gel DNA recovery kit	Zymo Research

2.3 Oligonucleotides

For all oligonucleotides the entry number under which it is listed in our data bank is stated (#).

2.3.1. Cloning

Table 3.3: Primers used for cloning of full length Liprins-α.

Gen		#	5´-SEQUENCE-3´	Vector
Liprin-α1	fw	900	CCCGCCGGCCAAGATGATGT	pcDNA 3.1-TOPO
Liprin-α1	rev	903	ATGTGGTTGGGGTAAGGGCTGTT	pcDNA 3.1-TOPO
Liprin-α2	fw	984	TCTTTCTCCTCCCGTTGCTA	pcDNA 3.1-TOPO
Liprin-α2	rev	985	TTGAGCCATCACAGTGCTTC	pcDNA 3.1-TOPO
Liprin-α3	fw	904	CCCCGGGGAACACGAGACTTAG	pcDNA 3.1-TOPO
Liprin-α3	rev	907	GCCCCCTTTCAGTCCATTTCTTA	pcDNA 3.1-TOPO
Liprin-α4	fw	650	CCCCTGACCCGACGCTGAGA	pcDNA 3.1-TOPO
Liprin-α4	rev	651	CGGGCTTGAGGACGGGTAGTTG	pcDNA 3.1-TOPO

Table 3.4: Primers used for cloning of constructs for pull down assay to test the interaction of GRIP with the alternatively spliced C-termini of Liprin-α1 and -α4.

Gen		#	5´-SEQUENCE-3´	Vector
Liprin-α1a fl	fw	1156	CCGGCCAAGATGATGTGC	pcDNA6.2 N-termGFP TOPO
Liprin-α1a fl	rev	1158	CTAGCAGGAGTAAGTCCTGACTGT	pcDNA6.2 N-termGFP TOPO
Liprin-α1b C-term.	fw	1274	TGGAGGAAGAAGTTCAGACCA	NT-GFP Fusion TOPO TA
Liprin-α1b C-term.	rev	1275	CATCTGTAGAAGTAGTGTGGG	NT-GFP Fusion TOPO TA
Liprin-α4b	fw	1168	TCCATTCCCATCATGTGTGAGG	pcDNA6.2 N-termGFP TOPO
Liprin-α4b	rev	1169	GGGGGTCAGCAGGAGTAGGTC	pcDNA6.2 N-termGFP TOPO

Table 3.5: Primers for cloning of deletion constructs and constructs for time-lapse imaging. RE: restriction enzyme.

Gen	Domain		#	5´-SEQUENCE-3´	RE	Vector
GFP	GFP N-term. fw	fw	819	GGCGGTACCGGTCGCCACCATGGT	KpnI	pCMV
GFP	GFP N-term. rev	rev	1134	GGCGGTACCCTCCTCCCTTGTACAGCTCGTCCATGCCG	KpnI	pCMV
paGFP	paGFP N-term. fw	fw	819	GGCGGTACCGGTCGCCACCATGGT	KpnI	pCMV
paGFP	paGFP N-term. fw	rev	1134	GGCGGTACCCTCCTCCCTTGTACAGCTCGTCCATGCCG	KpnI	pCMV
GFP	GFP N-term. fw	fw	1272	GGCGAATTCACCGGTCGCCACCATGGT	EcoRI	pCMV-RIM1α
GFP	GFP N-term rev	rev	1273	GGCCTCGAGCACCCTCCTCCCTTGTACAGCTCGTCCATGCCG	XhoI	pCMV-RIM1α
Cherry	Cherry N-term. fw	fw	1272	GGCGAATTCACCGGTCGCCACCATGGT	EcoRI	pCMV-RIM1α
Cherry	Cherry N-term. rev	rev	1273	GGCCTCGAGCACCCTCCTCCCTTGTACAGCTCGTCCATGCCG	XhoI	pCMV-RIM1α
paGFP	paGFP N-term. fw	fw	1272	GGCGAATTCACCGGTCGCCACCATGGT	EcoRI	pCMV-RIM1α
paGFP	paGFP N-term. rev	rev	1273	GGCCTCGAGCACCCTCCTCCCTTGTACAGCTCGTCCATGCCG	XhoI	pCMV-RIM1α
Liprin-α2	Full lenth	fw	1208	GGCAGATCTCAATGATGTGTGAAGTGATGCCC	BglII	pCMVMCS N-term. GFP
Liprin-α2	Full lenth	rev	1228	GGCTTAATTAATCAACATGAGTATGTGCGAAC	PacI	pCMVMCS N-term. GFP
Liprin-α2	Full lenth	fw	1208	GGCAGATCTCAATGATGTGTGAAGTGATGCCC	BglII	pCMVMCS N-term. paGFP
Liprin-α2	Full lenth	rev	1228	GGCTTAATTAATCAACATGAGTATGTGCGAAC	PacI	pCMVMCS N-term. paGFP
Liprin-α2	N-term. half	fw	1241	GGCAGATCTACATGATGTGTGAAGTGATGCCCACG	BglII	pCMV-GFP N-term.
Liprin-α2	N-term. half	rev	1242	GGCTTAATTAAACGGCTCTGGGTGTTGG	PacI	pCMV-GFP N-term.
Liprin-α3	CC domain	fw	1136	GGCAGATCTACCATGGGAATGACTGTGGTGAAACGCC	BglII	pCMV-GFP N-term.
Liprin-α3	CC domain	rev	1137	GGCTTAATTAATCGGCCTATGGACGACTTGAT	PacI	pCMV-GFP N-term.
Liprin-α2	C-term. half	fw	1239	GGCAGATCTCAGCCGTCAGAATGACTCACAC	BglII	pCMV-GFP N-term.
Liprin-α2	C-term. half	rev	1240	GGCTTAATTAATCAACATGAGTATGTGCGAACAGTGG	PacI	pCMV-GFP N-term.

Table 3.6: Primers used for constructs employed in pull down assays to test effect of point mutations on Liprin-α- RIM1α interaction. RE: restriction enzym

Gen	Domain		#	5´-SEQUENCE-3´	RE	Vector
Liprin-α2	RBD	fw	1429	GCGAGATCTACCACAAAGCCT TGGATGAA	BglII	pCMV-HA N-term.
Liprin-α2	RBD	rev	1430	GCGTTAATTAATATTGGCCCTC GAGGTGTCTCATAC	PacI	pCMV-HA N-term.
Liprin-α2	RBD	fw	1556	GCGGGATCCAGAGTCTCTGCA CTGGAAGAGG	BamHI	pGEX-KG
Liprin-α2	RBD	rev	1557	GCGAAGCTTAGCGCAAGATGG CTTCCTTGT	HindIII	pGEX-KG
RIM1α	C2B	fw	1431	GCGAGATCTTGTCGGGCCACA AGAAGTTG	BglII	pCMV-HA N-term.
RIM1α	C2B	rev	1432	GCGTTAATTAACTATGACCGGA TGCAGGGAG	PacI	pCMV-HA N-term

2.3.2. Diverse oligos

Table 3.6: Primers for cloning of peptides used for affinity anaysis of newly generated Liprin-α antibodies.

Ab peptid		#	5´-SEQUENCE-3´	Vector
Liprin-α1 fw	fw	1634	GATCCAGCCATGGGTCAGGCTCCCCTTCACA GCCAGATGCTGATTCGCATTTTGAGA	pGEX-KG
Liprin-α1 rev	rev	1635	AGCTTCTCAAAATGCGAATCAGCATCTGGCTG TGAAGGGGAGCCTGACCCATGGCTG	pGEX-KG
Liprin-α2 fw	fw	1636	GATCCTCTTCCTACCACAATGATGCCCGGAG CAGTTTATCTGCCTGCA	pGEX-KG
Liprin-α2 rev	rev	1637	AGCTTGCAGGCAGATAAACTGCTCCGGGCAT CATTGTGGTAGGAAGAG	pGEX-KG
Liprin-α3 fw	fw	1638	GATCCCGGGGAAGGCCGCCCTCCTCCTATTC CAGGTCCCTTCCTGGCAGTTGCA	pGEX-KG
Liprin-α3 rev	rev	1639	AGCTTGCAACTGCCAGGAAGGGACCTGGAAT AGGAGGAGGGCGGCCTTCCCCG	pGEX-KG
Liprin-α4 fw	fw	1640	GATCCGAGGGGGACCCCCTGGGGCCCCCCC ACGGTGCCGATGCTGAGGCCAACTTTGAGA	pGEX-KG
Liprin-α4 rev	rev	1641	AGCTTCTCAAAGTTGGCCTCAGCATCGGCAC CGTGGGGGGGCCCCAGGGGGTCCCCCTCG	pGEX-KG

Tabel 3.7: Position and sequence of primers for detection of alternative splicing.

Exon		#	5´-SEQUENCE-3´	Position (bp)
Liprin-α1 exon10	fw	1170	GCACCGACAGACAGAAGACA	1276
Liprin-α1 exon10	rev	1171	GCTGCAGCTCCTGATTTTTC	1577
Liprin-α1 exon18	fw	1097	GAAGGGTCCCTCACAGTCCT	2391
Liprin-α1 exon18	rev	1098	GGGGGAGAGGTTTCACATTT	2541
Liprin-α1 exon 24/25	fw	1101	GCTGGCCATCCAAGAGATAA	3118
Liprin-α1 exon 24/25	rev	1102	GGTTCATGTCCCCATATGCT	3296
Liprin-α1 exon 31	fw	1106	TTTTGATCACGGGGACTGAT	3756
Liprin-α1 exon 31	rev	1107	TTGCCAGACGAGCTCTACAC	4092
Liprin-α2 exon 6	fw	990	AAGAATGACGGTGGTCAAGC	711
Liprin-α2 exon 6	rev	1130	GAACATTTTGCTCACGCAAG	928
Liprin-α4 exon 22	fw	1124	TCAGCTCCACCTACCTCCAG	3100
Liprin-α4 exon 22	rev	1125	ATTCGTTTCCAATCCACTCG	3259
Liprin-α4b exon 28	fw	1174	ACCATAGCGGTGGCATGT	3794
Liprin-α4b exon 28	rev	1175	GGAGAGCATGTGTCCGTAGAG	4056
Liprin-α4b exon 28	fw	1174	ACCATAGCGGTGGCATGT	3794
Liprin-α4b exon 28	rev	1175	GGAGAGCATGTGTCCGTAGAG	4056
Liprin-α4 exon 22	fw	1124	TCAGCTCCACCTACCTCCAG	3100
Liprin-α4 exon 22	rev	1125	ATTCGTTTCCAATCCACTCG	3259
Liprin-α4b exon 28	fw	1174	ACCATAGCGGTGGCATGT	3794
Liprin-α4b exon 28	rev	1175	GGAGAGCATGTGTCCGTAGAG	4056
Liprin-α4b exon 28	fw	1174	ACCATAGCGGTGGCATGT	3794
Liprin-α4b exon 28	rev	1175	GGAGAGCATGTGTCCGTAGAG	4056

Table3.8: Oligonucleotides used to insert multiple cloning site (MCS) or HA-tag into a pCMV vector.

Oligo	#	5´-SEQUENCE-3´	Vector
MCS fw	1024	AATTGGCGCGCCGGTACCGGATCCATCGATTTAA TTAAGAATTCGCGATCGCT	pCMV5
MCS rev	1025	GATCAGCGATCGCGAATTCTTAATTAAATCGATGG ATCCGGTACCGGCGCGCC	pCMV5
HA N-term. fw	1427	CATGTACCCATACGATGTTCCAGATTACGCTCCCG GTCCCGGGTAC	pCMV5-MCS
HA N-term. rev	1428	CCGGGACCGGGAGCGTAATCTGGAACATCGTATG GGTACATGGTAC	pCMV5-MCS

2.3.3. Sequencing primer

Table 3.9: Sequencing Primers

Template		#	5´-SEQUENCE-3´	Position (bp)
pAMU6	fw	1637(B)	TACGATACAAGGCTGTTAGAGAG	
pCMV5	fw	pCMVF	CCAAAATGTCGTAATAACCCCG	822
pCMV5	rev	pCMVR	AGGACACCTAGTCAGACAAAATGATG	1076
pGEX-KG	fw	319	GGGCTGGCAAGCCACGTTTGGTG	869
pGEX-KG	rev	320	CCGGGAGCTGCATGTGTCAGAGG	1056
GFP	fw	GF-fw	CATGGTCCTGCTGGAGTTCGTG	
Liprin-α1	fw	1007	ACCACAAAGCCTTGGATGAG	509
Liprin-α1	fw	997	ATAGACAGGCAGGCGAGAGA	772
Liprin-α1	fw	998	GCCTGTCTGACACTGTGGAT	1419
Liprin-α1	fw	1084	TTGGACAATCTTGGTCGTTTT	2077
Liprin-α1	fw	1085	GGGAGGACAAGCTGAGAAAA	2646
Liprin-α1	fw	999	TAGAGCTCTGGGTTGGGATG	2762
Liprin-α1	fw	1000	TCTGGCTTTGGACGAGACTT	3438
Liprin-α2	fw	1038	CCCTACCTCAGGACATCGAA	239
Liprin-α2	fw	990	AAGAATGACGGTGGTCAAGC	456
Liprin-α2	fw	991	GTGGGAGAGGTGGAACAAGA	892
Liprin-α2	fw	1086	TGGAGAAGCGTTACCTGAGTG	1028
Liprin-α2	fw	992	ATGGCTGCTTTGGAAGAGAA	1462
Liprin-α2	fw	994	GAGACTTCTCCTCCCCCAAC	2314
Liprin-α2	fw	995	TGCCATCATGTCAGCGTTAT	2784
Liprin-α2	fw	996	TCGGGAATATGCAAACAACA	3366
Liprin-α2	fw	1087	GCCTTTGTGAAGACTGAATCC	3870
Liprin-α3	fw	1088	ATCGCTCTGCCTCAGGAGTT	226
Liprin-α3	fw	1089	GAGCTGGAGGAAGCTCTGG	709
Liprin-α3	fw	1090	CAGCTGGAGGAGAAGAACCA	1213
Liprin-α3	fw	1091	GAGAGCTGGATGGCTCAGAT	1715
Liprin-α3	fw	1008	CTGCCCGTCTTGAGAGGAT	2162
Liprin-α3	fw	1092	GCCATTCAGGAGATGGTGTC	2689

Template		#	5´-SEQUENCE-3´	Position (bp)
Liprin-α3	fw	1093	TGGCTCTGGATGAAACCTTC	3215
Liprin-α4	fw	1009	CAGGTGTCTCCAGTGAGGTG	425
Liprin-α4	fw	1003	TGACTGAGCTGGAGGAGGAC	767
Liprin-α4	fw	1004	ACCGGTTGCTTAGTGAGTCC	1283
Liprin-α4	fw	1005	AGATTGAGACCCGTGTGACC	1811
Liprin-α4	fw	1010	GACCCACGAAGAGATGGAAA	2739
Liprin-α4	fw	1006	GGATCACCTCACCAAGAAGG	2925
Liprin-α4	fw	1094	ACCATAGCGGTGGCATGTT	3389
Liprin-α4	fw	1095	TGGACTAATTGGCCTTCTGG	3967
Liprin-α4	fw	1096	GGCTTCCCCTTTAGTGACTC	4438

2.3.4. Site directed mutagenesis

Table 3.10: Primers for site directed mutagenesis

Template		#	5´-SEQUENCE-3´	Domain/ aa exchange
pCMV-MCS-N-term. Liprin-α2	fw	1415	GAACGGTTAACAGCTGACTCTTCCCG GGTGGG	RBD 294 L->D
pCMV-MCS-N-term. Liprin-α2	rev	1416	CCCACCCGGGAAGAGTCAGCTGTTAA CCGTTC	
pCMV-MCS-N-term. RIMα1	fw	1423	CCTGTATAGCCAAAAAGAAGGCAAGA ATTGCACGGAAAACT	C2B 1454 T->A
pCMV-MCS-N-term. RIMα1	rev	1424	AGTTTTCCGTGCAATTCTTGCCTTCTT TTTGGCTATACAGG	
pCMV-MCS-N-term. RIMα1	fw	1425	CTCTAGATCCTTTGTATCAGGCGTCC CTGGTTTTTGATGAAA	C2B 1467 Q->A
pCMV-MCS-N-term. RIMα1	rev	1426	TTTCATCAAAAACCAGGGACGCCTGA TACAAAGGATCTAGAG	

2.3.5. shRNA constructs

Table 3.11: Oligos for shRNA constructs

Target		#	Oligo	Vector
Liprin-α1	fw	1469	GATCTCGAAAGATTAGCAGAAGAAATTCAAGAGAT TTCTTCTGCTAATCTTTCTTTTTTGGAAA	pAMU6
Liprin-α1	rev	1469	AGCTTTTCAAAAAGAAAGATTAGCAGAAGAAATCT CTTGAATTTCTTCTGCTAATCTTTCCGA	pAMU6
Liprin-α2	fw	1468	GATCTCGACCAACTTGTCGTGACTATTCAAGAGAT AGTCACGACAAGTTGGTCTTTTTTGGAAA	pAMU6
Liprin-α2	rev	1468	AGCTTTTCAAAAAAGACCAACTTGTCGTGACTATC TCTTGAATAGTCACGACAAGTTGGTCCGA	pAMU6
Liprin-α2	fw	1652	GATCTCGCTCAGGCTAGCTATCCAATTCAAGAGAT TGGATAGCTAGCCTGAGCTTTTTTGGAAA	pAMU6
Liprin-α2	rev	1653	AGCTTTTCAAAAA GCTCAGGCTAGCTATCCAA TCTCTTGAATTGGATAGCTAGCCTGAGCGA	pAMU6
Liprin-α2	fw	1654	GATCTCGGACAGAAGGCTGAAGAAATTCAAGAGA TTTCTTCAGCCTTCTGTCCTTTTTTGGAAA	pAMU6
Liprin-α2	rev	1655	AGCTTTTCAAAAAGGACAGAAGGCTGAAGAAATCT CTTGAATTTCTTCAGCCTTCTGTCCGA	pAMU6
Liprin-α2	fw	1656	GATCTCGCCAAGATTCTCTCCACAAAGTTCAAGAG ACTTTGTGGAGAGAATCTTGGCTTTTTTGGAAA	pAMU6
Liprin-α2	rev	1657	AGCTTTTCAAAAAGCCAAGATTCTCTCCACAAAGT CTCTTGAACTTTGTGGAGAGAATCTTGGCGA	pAMU6
Liprin-α2	fw	1658	GATCTCGCTATCCAAGAGATGGTTTCTTTCAAGAG AAGAAACCATCTCTTGGATAGCTTTTTTGGAAA	pAMU6
Liprin-α2	rev	1659	AGCTTTTCAAAAAGCTATCCAAGAGATGGTTTCT TCTCTTGAAAGAAACCATCTCTTGGATAGCGA	pAMU6
Liprin-α3	fw	1642	GATCTCGACCACAATAAGCGACTGTCATTCAAGAGATG ACAGTCGCTTATTGTGGTCTTTTTTGGAAA	pAMU6
Liprin-α3	rev	1643	AGCTTTTCAAAAAGACCACAATAAGCGACTGTCATCTC TTGAATGACAGTCGCTTATTGTGGTCGA	pAMU6
Liprin-α3	fw	1644	GATCTCGGTTACAGCTTCACCTCAAAGTTCAAGAGACT TTGAGGTGAAGCTGTAACCTTTTTTGGAAA	pAMU6
Liprin-α3	rev	1645	AGCTTTTCAAAAAGGTTACAGCTTCACCTCAAAGTCTCT TGAACTTTGAGGTGAAGCTGTAACCGA	pAMU6
Liprin-α3	fw	1646	GATCTCGAGCATCAAGTCGTCCATATTCAAGAGATATG GACGACTTGATGCTCTTTTTTGGAAA	pAMU6
Liprin-α3	rev	1647	AGCTTTTCAAAAAGAGCATCAAGTCGTCCATA TCTCTTGAA TATGGACGACTTGATGCTCGA	pAMU6

2.4 Vectors and vector construction

2.4.1. Multiple cloning site (MCS)

pGEX-KG:

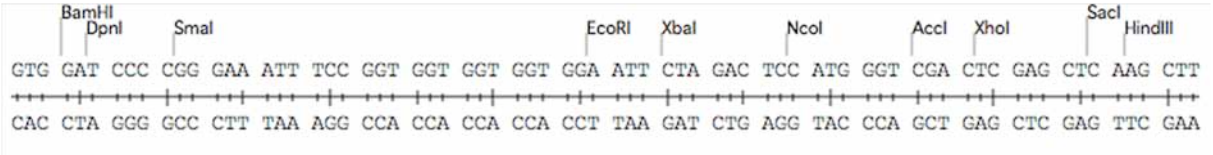

pCMVMCS:

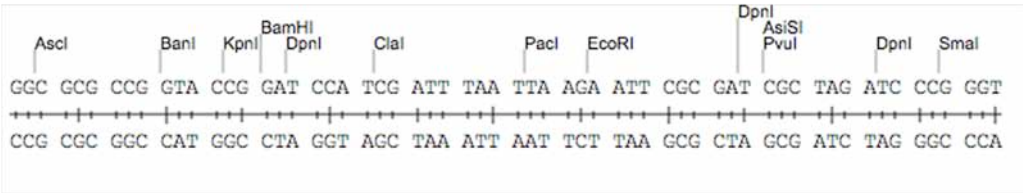

2.4.2. Generated constructs

Name	Insert	Template	Vector	Enzyme template/ vector
Topo constructs				
pCDNA 3.1 TOPO Liprin-α1	Liprin-α1 (mouse)	cDNA	pcDNA 3.1-TOPO	-
pCDNA 3.1 TOPO Liprin-α2	Liprin-α2 (mouse)	cDNA	pcDNA 3.1-TOPO	-
pCDNA 3.1 TOPO Liprin-α3	Liprin-α3 (mouse)	cDNA	pcDNA 3.1-TOPO	-
pCDNA 3.1 TOPO Liprin-α4a	Liprin-α4 (mouse)	cDNA	pcDNA 3.1-TOPO	-
pCDNA 3.1 TOPO Liprin-α4b	Liprin-α4 (mouse)	cDNA	pcDNA 3.1-TOPO	-
pCMV N-term. GFP Liprin-α2	Liprin-α2 (mouse)	pCDNA 3.1 TOPO Liprin-α2	pCMV N-term. GFP	BglII-PacI/ BamHI-PacI
pCDNA N-term. GFP Liprin-α1a	Liprin-a1a	pCDNA 3.1 TOPO Liprin-α1	pcDNA6.2 N-termGFP TOPO	-
pCDNA N-term. GFP Liprin-α1b C-term.	Liprin-a1b C-term.	cDNA	NT-GFP Fusion TOPO TA	-
pCDNA N-term. GFP Liprin-α4b	Liprin-a4b	pCDNA 3.1 TOPO Liprin-α4b	pcDNA6.2 N-termGFP TOPO	-
Vectors				
pCMV MSC	Oligo	Oligo	pCMV5	-/EcoRI-BamHI
PCMVMCS GFP N-term.	EGFP	EGFP	pCMVMCS	KpnI
pCMV MSC HA	HA tag	HA oligo	pCMVMCS	-/KpnI
PCMVMCS paGFP N-term.	paGFP	paGFP	pCMVMCS	KpnI
GFP fusion constructs				
pCMV N-term. GFP Liprin-α2	Liprin-α2 (mouse)	pCDNA 3.1 TOPO Liprin-α2	pCMV N-term. GFP	BglII-PacI/ BamHI-PacI
pCMV N-term. GFP Liprin-α2 sdm	sdm RBD	pCMV N-term. GFP Liprin-α2	-	-
pCMVMCS N-term. GFP Liprin-α2 N-term. half	Liprin-α2 N-term. half	pCDNA 3.1 TOPO Liprin-α2	pCMVMCS N-term. GFP	BglII-PacI/ BamHI-PacI

Name	Insert	Template	Vector	Enzyme template/ vector
pCMVMCS N-term. GFP Liprin-α2 C-term. half	Liprin-α2 C-term. half	pCDNA 3.1 TOPO Liprin-α2	pCMVMCS N-term. GFP	BglII-PacI/ BamHI-PacI
pCMVMCS N-term. GFP Liprin-α3 CC domain	Liprin-α3 CC domain	pCDNA 3.1 TOPO Liprin-α3	pCMVMCS N-term. GFP	BglII-PacI/ BamHI-PacI
HA fusion constructs				
pCMVHA Liprin-α2 RBD	Liprin-α2 RBD	pCDNA 3.1 TOPO Liprin-α2	pCMVHA	BglII-PacI/ BamHI-PacI
pCMVHA RIM1α C2B	RIM1α C2B	pCMV YFP-RIM1α	pCMVHA	BglII-PacI/ BamHI-PacI
pCMVHA RIM1α C2Bsdm1	RIM1α C2Bsdm1	pCMV GFP-RIM1α sdm1	pCMVHA	BglII-PacI/ BamHI-PacI
pCMVHA RIM1α C2Bsdm2	RIM1α C2Bsdm2	pCMV GFP-RIM1α sdm2	pCMVHA	BglII-PacI/ BamHI-PacI
fl RIM1α constructs				
pCMV-cherry RIM1α	cherry	cherry	pCMV RIM1α	ERI/XhoI
pCMV-GFP RIM1α	GFP	GFP	pCMV RIM1α	ERI/XhoI
pCMV-paGFP RIM1α	paGFP	paGFP	pCMV RIM1α	ERI/XhoI
pCMV GFP-RIM1α sdm1	sdm	pCMV-GFP RIM1α	-	-
pCMV GFP-RIM1α sdm2	sdm	pCMV-GFP RIM1α	-	-
pGEX constructs				
pGEX Liprin-α1 peptid	oligo	-	pGEX	BamHI/HindIII
pGEX Liprin-α2 peptid	oligo	-	pGEX	BamHI/HindIII
pGEX Liprin-α3 peptid	oligo	-	pGEX	BamHI/HindIII
pGEX Liprin-α4 peptid	oligo	-	pGEX	BamHI/HindIII
pGEX Liprin-α2 RBD	RBD	pCMV N-term. GFP Liprin-α2	pGEX	BamHI/HindIII
pGEX Liprin-α2 RBDsdm	RBDsmd	pCMV N-term. GFP Liprin-α2 sdm	pGEX	BamHI/HindIII
shRNA constructs				
pAMU6-Liprinα1shRNA 1469	Oligo	-	pAMU6	BamHI-HindIII/ BglII-HindIII
pAMU6 Liprinα2shRNA 1468	Oligo	-	pAMU6	BamHI-HindIII/ BglII-HindIII
pAMU6 Liprinα2shRNA 1652	Oligo	-	pAMU6	BamHI-HindIII/ BglII- HindIII
pAMU6 Liprinα2shRNA 1654	Oligo	-	pAMU6	BamHI-HindIII/ BglII-HindIII
pAMU6 Liprinα2shRNA 1656	Oligo	-	pAMU6	BamHI-HindIII/ BglII-HindIII

Name	Insert	Template	Vector	Enzyme template/ vector
pAMU6 Liprinα2shRNA 1658	Oligo	-	pAMU6	BamHI-HindIII/ BglII-HindIII
pAMU6 Liprinα3shRNA 1642	Oligo	-	pAMU6	BamHI-HindIII/ BglII-HindIII
pAMU6 Liprinα3shRNA 1644	Oligo	-	pAMU6	BamHI-HindIII/ BglII-HindIII
pAMU6 Liprinα3shRNA 1646	Oligo	-	pAMU6	BamHI-HindIII/ BglII-HindIII

Table 3.12: List of all constructs

Plasmids obtained from other labs:

pGEX GRIP (aa343-809) construct: Prof. H. Hirling (Geneva, Switzerland)

pCMV YFP-RIM1α, pCMV RIM1α: Gyorgy Lonart (EVMS, Norfolk, USA)

SV2cherry: Noam Ziv (Haifa, Israel)

3 Methods

All methods were performed following standard procedures (Current Protocols in Molecular Biology) if not noted otherwise.

3.1 Bioinformatics

3.1.1. Sequence analysis

The National Center for Biotechnology Information (NCBI) (http://www.nlm.nih.gov/), the ENSEMBL (http://www.ensembl.org/), UCSC (http://genome.ucsc.edu/index.html) and the TIGR gene indices (http://www.tig.org/) databases were searched using homology BLAST with standard settings. Searches for splice variants were conducted using EST databases. Multiple alignments were performed using T-coffee (http://tcoffee.vital-it.ch/cgibin/Tcoffee/tcoffee_cgi/index.cgi), ClustalW (http://www.ebi.ac.uk.clustalw/index.html) and Dialign (http://bibiserv.techfak.uni-bielefeld.de/dialign/) (Morgenstern, 2004). Boxshade was used to create alignment figures (http://bioweb.pasteur.fr/seqanal/interfaces/boxshade.html). Phylogenetic analyses were conducted with Phyml Online (http://atgc.lirmm.fr/phyml/) using standard settings with 100 bootstraps and the WAG substitution model for sequence evolution (Whelan and Goldman, 2001).

Sequence data for the cDNA sequences of Liprins-α was deposited with the DDBJ/EMBL/GenBank Data Libraries under Accession No. EU568869 (Liprin-α1), EU568870 (Liprin-α2), EU568871 (Liprin-α3), EU568872 (Liprin-α4).

3.2 Molecular biological methods

3.2.1. RNA extraction and cDNA synthesis

Total RNA was extracted from whole brains of different developmental stages, various tissues, and brain regions using the RNeasy Lipid Tissue Kit following manufacturers instructions. Samples were stored at -80°C. Reverse transcription was carried out using 5μg of total RNA and the Superscript RT III kit with oligo dT primers for full length cloning of Liprins-α. 1μg of total RNA and the iScript cDNA synthesis kit were used as template for PCR reactions to detect alternative spliced exons. For real-time PCR the QuantiTect reverse transcription kit was employed, using 1 μg RNA. cDNA samples were stored at -20°C.

3.2.2. PCR

Standard PCR protocol:

Step	Temperatur	time	cycle
1	95°C	4 min	
2	95°C	30 sec	
3	55°C	45 sec	
4	72°C	xkb x 1min	35 cycles step 2-4
9	4°C	∞	

Touch down PCR protocol:

Step	Temperatur	time	cycle
1	95°C	4 min	
2	95°C	30 sec	
3	67°C	30 sec	-0.5°C every cycle
4	72°C	8 min	20 cycles step 2-4
5	95°C	30 sec	
6	50°C	30 sec	
7	72°C	8 min	15 cycles step 5-7
8	72°C	10 min	
9	4°C	∞	

General amplification procedure:

For all amplifications from plasmid DNA *pfu* DNA polymerase and the standard PCR protocol were used, except for the full-length amplification of Liprin-α2, for which a touch down PCR was performed.

Detection of alternative splicing:

Alternative splicing of exons was detected via PCR using *Taq* polymerase (GoTaq). PCR conditions were optimized for each primer pair and the resulting fragments were analyzed on 2.5% agarose gels and visualized by ethidium bromid staining. Several independent primer pairs were used to analyze each alternatively spliced exon. Primers used in the analysis are listed in table 3.7.

Amplification of full length Liprins-α from cDNA:

Full length Liprin-α1-4 were amplified using the Fermentas Long PCR Enzyme Mix. Primers used for the amplification are listed in table 3.3. Standard conditions were used and 2.5% DMSO was added to the PCR mix.

3.2.3. Real-time PCR

Validated real-time PCR primer pairs for Liprins-α1-4 were purchased from Qiagen QT01594712 (Liprin-α1), QT01616839 (Liprin-α2), QT01577415 (Liprin-α3), QT01596756 (Liprin-α4). Real-time PCR was performed using the SYBR Green PCR kit following the manufacturers instructions. Each sample was assayed in triplicates and in two independent experiments using an ABI Prism 9700HT sequence detection system. Relative quantification of target gene expression and PCR efficiency were performed using HPRT as internal reference genes. The expression levels of the genes was calculated using the formula (ProbeCT) − (ActinCT) = z; Probeexpr = 2−z.

3.2.4. Vector construction

For cloning DNA fragments were amplified from plasmid DNA via PCR, purified (DNA Clean and Concentration kit) and cut with the respective restriction enzymes. Subsequently, the PCR reaction was separated on an agarose gel and the band of interest was cut out and purified (Zymoclean Gel DNA recovery kit). The vector was cut with the respective restriction enzymes, dephosphorylated and then purified with phenol-chloroform followed by precipitation of the DNA. Then the ligation reaction was carried out at 37°C for 1 h.

3.2.5. Site directed mutagenesis

Primers were designed with the help of the QuickChange Primer Designe Program (http//www.stratagen.com/qcprimerdesign). Mutations were introduced using the QuickChange II XL Site-Directed Mutagenesis Kit using standard conditions as recommended by the manufacturer. For introduction of point mutations into Liprin-α2 a touch down PCR was performed.

3.2.6. Sequencing

The PCR reaction for sequencing of plasmid DNA was performed using the BigDye Terminator v3.1 cycle sequencing kit and template specific primers (Table 3.9). The

sequencing PCR reactions were purified through a gel filtration spin column (DyEx 2.0 spin kit) and sequencing was carried out using a capillary sequencer. Subsequent analysis of the sequencing results was carried out using Lasergene 8 software SeqMan.

3.3 Biochemical methods

3.3.1. Peptid-antibody generation

Specific antibodies against Liprin-α1 (α1), Liprin-α2 (α2), Liprin-α3 (α3), and Liprin-α4 (α4) were raised in rabbits against the following peptides: (α1) CSHGSGSPSQPDADSHFE; (α2) SSYHNDARSSLSAC; (α3) RGRPPSSYSRSLPGSC; (α4) DPLGPPHGADAEANFEC. A cysteine was added N- or C-terminally for coupling. The localization of the peptides is shown in Suppl. Fig. 2. Antibodies were affinity purified using the immunizing peptides according to standard procedures. Generation and purification was performed by Pineda antibody service (http://www.pineda-abservice.de/).

3.3.2. Western Blotting

Preperation of protein extracts:

Tissue was lysed in 1xPBS with 2% SDS, 10mM EDTA pH 8.0 and Complete Protease Inhibitor Cocktail Tablets and HEK-293T cells over expressing Liprins-α were lysed in PBS with 1% Triton X-100 and Complete Protease Inhibitor Cocktail Tablets.

Electrophoreses and blotting:

5x loading buffer was added to the samples, which were heated to 95°C for 5 minutes for denaturation. For all immunoblots performed to analyse expression in tissues, 50 µg protein was loaded on 10% SDS-polyacrylamide gels. Proteins were separated by size during electrophoresis and subsequently transferred to nitrocellulose membrane. Membranes were preincubated for one hour at room temperature (RT) in blocking solution (2% cold water fish gelatin or 10% milk in PBS), and then incubated with the primary antibodies for 1 hour at RT. Secondary antibodies were IR-labeled (Odyssey) and used at a 1:20.000 dilution or horseradish peroxidase labeled and used at 1:3000. The IR-labeled secondary antibodies were visualized with an infrared imaging System

(Odyssey, Li-cor) and HRP coupled secondary antibodies were visualized by Amersham ECL Plus Western Blotting Detection Reagents using the HyperFilm. Quantitative analysis of immunoblots was performed using the AIDA software.

3.3.3. Protein purification from bacteria

GST-fusion proteins were overexpressed in *Echeria coli BL21*. After induction with IPTG cultures were grown for 5h at 37°C. For purification bacteria were resuspended in PBS containing Complete Protease Inhibitor Cocktail Tablets and lyzed by incubation with lysozyme and subsequent sonification. GST-fusion proteins were bound to glutathione-agarose beads through incubation for 1h followed by washing. If necessary, elution was performed with 10 mM gluthatione in PBS. For analysis, proteins were loaded on a SDS-PAGE gel and visualized using Coomassie.

3.3.4. Pull down assay

For the pull-down assay, the GST-GRIP, GST-Liprin-α2 RBD (RIM binding domain), GST-Liprin-α2 RBD sdm and GST-RIM1α C2B fusion proteins were expressed in *Echeria coli BL21* and bound to glutathione-agarose beads. Transfection of HEK-293T cells with the expression plasmids for GFP-Liprin-α1a, GFP-Liprin-α1b C-term., Liprin-α4a, GFP-Liprin-α4b, HA-Liprin-α2 RBD, RIM1α C2B, RIM1α C2B sdm1 and RIM1α C2B sdm2 were performed with Lipofectamine 2000 (GRIP interactions) or Ca^{2+}-phosphate transfection (Liprin-α2-RIM1α interaction). To test binding of the alternatively spliced C-terminus of Liprin-α1 and -α4 to GRIP cells were harvested 3 days after transfection and lysed in buffer L1 (20 mM HEPES/KOH, pH 7.4, 2 mM EDTA, 2 mM EGTA, 0.1 mM DTT, 0.1 M KCl, 1% Triton X-100, Complete Protease Inhibitor Cocktail Tablets) for 1 h at 4 °C. All other assays were performed in buffer L2 (50 mM HEPES, pH 7.4, 80 mM NaCl, 1% Trion X-100, Complete Protease Inhibitor Cocktail Tablets). The extracts were subsequently incubated with GST and GST- fusion proteins on agarose beads equilibrated in buffer L1/L2 for 3h. After washing bound proteins were analyzed by western blotting. Liprin-α1a and -α1b were detected with an anti-GFP antibody while Liprin-4αa and -4αb were detected with a pan-Liprin-α antibody (4396). HA-tagged proteins were detected by an anti-HA antibody.

3.4 Cell culture

3.4.1. HEK-293 cell culture

HEK-293T and AAV-293 cells were maintained in DMEM, 10% FCS and penicillin/streptomycin (100 units/ml penicillin and 100 mg/ml streptavidin). Cells were passaged every 2-3 days and plated in a 1:10 dilution. All cell lines were cultured in humidified incubators supplied with 5% CO2 at 37°C.

3.4.2. Transfection of HEK-293 cells

For heterologous expression human embryonic kidney-293 cells (HEK 293T or AAV-293) were transfected using Lipofectamine 2000.

For the overexpression of poteins used in pull down assays to test point mutations and their effect on the Liprin-α2-RIM1α interaction 10 cm plates were transfected using the Ca^{2+}-phosphate method. Cells were transfected at approximatly 70% confluency. Before transfection the medium was exchanged for IMDM containing 5% FCS. DNA and $CaCl_2$ were mixed and HBS was added while vortexing. The precipitate was directly added to the cells and left to incubate over night. The next day the cells were washed one time with PBS and then kept in DMEM with 10% FCS and Pen/Strep until they were harvested after three days.

Plasmid	20 µg
2,5M $CaCl_2$	30 µl
H_2O	x µl
Σ	300 µl
+	
1xHBS	300 µl

3.4.3. Primary cell culture

Solutions:

- Borate buffer containing 0.1 mg/ml Poly-L-Lysin
- HBSS containing 20% FCS

- Digestion solution:
  0.8 g NaCl
  0.037 g KCl
  0.099 g Na_2HPO_4
  0.6 g Hepes
  in dd H_2O
  adjust pH to 7.2

- Dissociation solution:
  100 ml HBSS containing 0.295g $MgSO_4$-$7H_2O$

- BME:
  500 ml BME containing
  1% FCS
  2 % B-27
  1% Glucose 45 %
  1.2 ml L-Glutamine (200mM)

Coverslip and well pretreatment:

To allow optimal adhesion of the neurons on the coverslips or wells they were pretreated as follows. Coverslips were baked over night at 240 ºC. 24 wells with or 6 wells without sterile coverslips were then coated overnight by incubation with poly-L-Lysin (0.1 mg/ml in borate buffer) at 37ºC. Wells were subsequently washed three times with sterile distilled water and several hours later two additional washing steps followed.

Preparation of primary neurons:

The pregnant rat or mouse was sacrificed, and the uterus containing the embryos (E16-E19) was removed. The embryo heads were dissected in HBSS/20% FCS and placed in a Petri dish with ice-cold dissection medium. The cortex and the hippocampus of every pup were isolated and separately collected in a Petri dish. The cortex was cut in approx. 1 mm thick pieces. The tissue was washed six times

in HBSS/20% FCS, trypsin solution (3mg trypsin in 0.5 ml digestion solution per pup) was added to the tissue and both were transferred into a 3.5 mm dish and incubated for 10 minutes at 37 ºC. The tissue was then transferred into a 15 ml Falcon tube and washed three times with HBSS/20% FCS. The tissue was resuspended in 2 ml dissociation solution by repetitive tituration (20-50 x) using a blue tip. 3 ml HBSS/20% FCS were added and the solution was centrifuged for 10 min at 1000 rpm.

The supernatant was transferred into a new Falcon tube and 2 ml BME were added. Tituration was repeated. Per pup 2 ml BME medium is added, the cells were counted using a Neubauer chamber and seeded (see table below). After two hours the medium was replaced with fresh BME.

Cells were kept at 37°C and 5% CO_2 for up to four weeks. Once a week half of the BME per well was exchanged for fresh medium.

Cell numbers seeded:

Well	Cell number
24 well (low density)	30.000
24 well (high density)	60.000
6 well (high density)	300.000

3.4.4. Transfection of neurons

Primary cortical and hippocampal neurons were transfected using a protocol for hippocampal neurons based on DNA/Ca^{2+}-phosphate coprecipitation as descibed by Kohrmann et al. (Kohrmann et al., 1999). Neurons were transiently transfected at DIV3-10. The original culture medium was exchanged for MEM and kept in the incubator for the time of the transfection procedure. Per 24 well 1.5 μg endotoxin free DNA were used. $CaCl_2$, DNA and BES buffer were vortexed for 20 sec. Then the precipitate was added to the neurons and incubated at 2.5% CO_2 for 30-40 min. Subsequently, cells were washed twice with HBS and three times with BME and then the original medium was added back to the wells.

3.5 Immunochemical methods

3.5.1. Immunocytochemistry

Primary cortical and hippocampal neurons DIV4 and DIV14-21 as well as glial cells DIV21 were fixed with 4% paraformaldehyde (PFA) for 15 min, washed in PBS and incubated over night with primary antibodies at 4°C in blocking solution 1 (10% normal goat serum, 5% sucrose, 0.2% BSA, 0.3% Triton X-100 in PBS). After washing in PBS, cells were incubated with secondary antibodies in blocking solution 2 (5% sucrose, 0.3% Triton X-100, 0.2% BSA in PBS) at room temperature in the dark. Cover glasses were mounted in Mowiol.

3.5.2. Immunohistochemistry

Freshly dissected brain regions and retinae were immersion fixed in 4% PFA for 15-30 min. Tissue was cryoprotected by immersion in increasing concentrations of sucrose in PBS (10%, 20%, 30%) at 4°C and subsequently embedded in freezing medium (Tissue-Tek). 12 μm (brain) and 16 μm (retina) sections were cut on a microtome (Microm). The sections were blocked for 1 hour in blocking solution (10% normal goat serum, 0.5% Triton X-100 in PBS) and incubated in the primary antibodies in 3% normal goat serum, 0.5% Triton X-100 in PBS) over night at room temperature. After extensive washing in PBS, sections were incubated with secondary antibodies coupled to Alexa594 or Cy3 and Alexa488 for 1 hour at room temperature in the dark. Slices were mounted in Vectashield hard set mounting medium.

3.6 Imaging

3.6.1. Light microscopy

For light microscopic analysis labeled sections were imaged with a fluorescent microscope (Zeiss Axio Observer 1A). For high magnification cells and sections were examined with a confocal laser scanning microscope (Leica TCS and Zeiss LSM710).

3.6.2. Time lapse imaging

FRAP and FRAPA time lapse imaging experiments were performed as described in (Tsuriel et al., 2006; Tsuriel et al., 2009).

Neurons expressing the fusion proteins were placed in a laminar flow chamber and maintained at 33–35°C in a physiological solution. After collecting baseline images, three to five fluorescent puncta per axon area, using multiple axonal areas per experiment, were selectively bleached by high-intensity 488 nm laser light for FRAP experiments or phoptactivated by a 405 nm diode laser for FRAPA experiments. Fluorescence recovery was monitored by collecting image stacks (two to three sections) at rates of one image every 10 min for 2-16 h for FRAP experiments and at rates of one image every 1 h for FRAPA experiments.

3.7 rAAV virus

3.7.1. rAAV virus production

For rAAV virus production AAV-293 cells were seeded onto 10 cm plates and transfected at ca. 70% confluency using the Ca^{2+}-phosphate transfection method. Before transfection the medium was exchanged for IMDM containing 5% FCS. DNA and $CaCl_2$ are mixed and HBS was added while vortexing. The precipitate was directly added to the cells and left to incubate over night. The next day the cells were washed one time with PBS and then kept in DMEM with 10% FCS and Pen/Strep until harvested after three days. The cells were harvested in 1 ml DMEM and frozen at -80°C. To disrupt the cell walls harvested cells were thawed and frozen for four times. To investigate the efficiency of the crude extract containing viral particles 1μl, 0.1μ and 0.01μl were tested on a 24 well of primary neurons.

Plasmid	6.6 μg
PFdelta6	13.3 μg
pNLrep	3.2 μg
pH21	3.3 μg
2,5M $CaCl_2$	176 μl
H_2O	x μl
Σ	1600 μl
+	
1xHBS	1600 μl

3.7.2. shRNA experiments using rAAV viruses

The rAAV virus system was used to transduce neurons with plasmids containing shRNAs. To get the most effective knock-down the virus was added to the primary neurons on DIV1-2. To evaluate the knock down 6-wells were used for western blotting and 24-wells were used for immunocytochemistry. For immunoblotting neurons were checked for transduction efficiency at DIV7 and if 100% transduction was achieved the cells were harvested at DIV14. For immunocytochemistry a dilution of the virus that allowed the transduction of only a few cells was determined. Neurons were fixed and immunostained at DIV14.

4 Abbreviations

AMPA	α-amino-3-hydroxy-5-methyl-4-isoxazolepropionic acid
APC	Anaphase promoting complex
AZ	Active zone
CaMKII	Ca^{2+}/calmodulin-dependent protein kinase II
CASK	Calcium/calmodulin-dependent serine protein kinase
DG	Dentate gyrus
ELKS	Name stems from the proteins high content in glutamate (E), leucine (L), lysine (K), and serine (S)
EM	Elektron micropgraph
FRAP	Fluorescent recovery after photobleaching
FRAPA	Fluorescent recovery after photoactivation
GC	Cerebellar granule cell layer
GFP	Green fluorescent protein
GIT1	G protein-coupled receptor kinase-interacting protein 1
GRIP1	Glutamate receptor-interacting protein 1
h	Hour
HBS	HEPES buffered saline
HBSS	Hanks buffered salt solution
HC	Hippocampus
HEK 293T	Human embryonic kidney cell line 293T
ICC	Immunocytochemistry
IHC	Immunohistochemistry
INL	Inner nuclear layer
IPL	Inner plexiform layer
IR	Infrared
Kb	Kilo base
kDa	Kilo Dalton
KIF1A	Kinesin family member 1A
l	Liter
LAR	Leukocyte common antigen-related
LH	Liprin homology domain
MAGUK	Membrane-associated guanylate kinase
MCS	Multiple cloning site
min	Minute
ML	Molecular layer
ml	Mililiter
mM	Milimolar
mRNA	Messenger RNA
ng	Nanogram
NGS	Normal goat serum
NMJ	Neuro muscular junction
OB	Olfactory bulb
Oligo	Oligonucleotide

OPL	Outer plexiform layer
paGFP	photoactivatable GFP
PL	Polymorphic layer
P0	Postnatal day 0
PAGE	Polyacrylamide gel electrophoresis
PBS	Phosphate buffered saline
PC	Purkinje cells
PCR	Polymerase chain reaction
PDZ	PDZ-protein binding domain
PFA	Paraformaldehyde
PKA	Protein kinase A
PSD	Postsynaptic density
RIM	Rab interacting molecule
RNA	Ribonucleic acid
RT	Room temperature
RT-PCR	Reverse transcription PCR
RSY-1	regulator of synaptogenesis-1
SAM	Sterile-α-motif
SDS	Sodium dodecyl sulfate
SL	Stratum lucidum
SM	Stratum moleculare
SP	Stratum pyramidale
SV	Synaptic vesicle
SV2	Synaptic vesicle protein 2
SYD-1	synapse- defective 1
SYD-2	synapse- defective 2
µl	Microliter
WB	Wester blot

5 Results

5.1 Analysis of the genomic organization of the mouse and human Liprin-α family and their alternative splicing

Liprins-α exhibit a striking degree of conservation, with 40% amino acid identity between the human Liprin-α1 and worm SYD-2. All Liprin-α proteins share a common domain organization as they are composed of an N-terminal region predicted to form coiled-coil structures and three C-terminal SAM (sterile-α-motif) domains that constitute the LH (Liprin homology) region (Pulido et al., 1995; Serra-Pages et al., 1995; Serra-Pages et al., 1998). Recent studies have begun to shed light on the neuronal functions of Liprins-α (Spangler and Hoogenraad, 2007; Stryker and Johnson, 2007a) and have provided first evidence for potential functional differences between the four isoforms (Hoogenraad et al., 2007). However, so far the sequence, structures, and alternative splicing of *Liprin-α* genes have not been comparatively and thoroughly analyzed.

5.1.1. The structure of human and mouse Liprin-α genes

We characterized the exon/intron structure of human and mouse *Liprin-α* genes and analyzed the alternative splicing pattern of each *Liprin-α* gene in both human and mouse using bioinformatics and RT-PCR. For each *Liprin-α* a search for mRNA sequences and expressed sequence tags (ESTs) was performed. Furthermore, the identified cDNAs of mouse were cloned and verified by sequencing.

The properties of the human and mouse *Liprin-α* genes are summarized in Table 5.1, the genomic structure of the human and mouse genes is depicted in Fig. 5.1, and the sizes of the exons and the sequences of the exon-intron junctions are shown in Suppl. Tables 1-8. The four *Liprin-α* genes are dispersed in the human and mouse genome, but exhibit highly conserved exon-intron structures, suggesting that they are the result of a relatively recent gene duplication. The number of exons differs between the Liprins-α, due to additional exons as well as distinct numbers of alternatively spliced exons. The individual genes are highly conserved between the mouse and human genomes with mostly identical placement of the exons and sizes of the introns (Fig. 5.1).

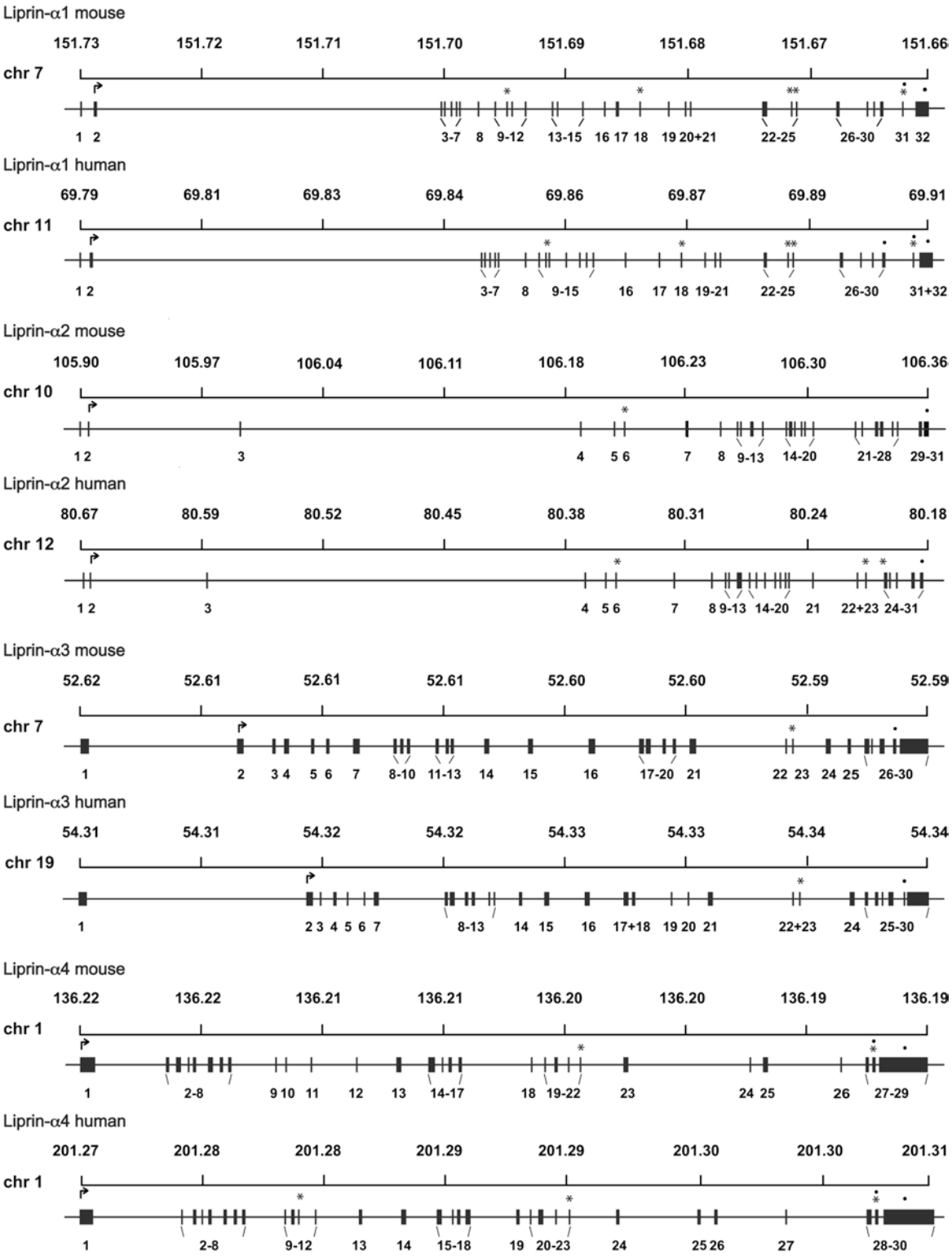

Fig. 5.1: Comparison of the human and mouse *Liprin-α* gene structures.
The organization of the exon/intron structure for the individual human and mouse *Liprin-α1, Liprin-α2, Liprin-α3,* and *Liprin-α4* genes was determined by bioinformatic analysis of genomic and mRNA data bases and by RT-PCR. Exons are represented by numbered solid boxes. An arrow above an exon indicates the start of translation and a dot marks a stop codon. Alternatively spliced exons are labeled with an asterisk. The rulers above each gene diagram depict the positions in the USCD genome sequences.

The human and mouse *Liprin-α2* genes are large with sizes of approximately 500 kb, while the *Liprin-α3* and *Liprin-α4* genes are relatively small, approximately 30 kb and 40 kb, respectively (Table 5.1, Fig. 5.1). The human and mouse *Liprin-α1* genes are of intermediate size, 114 kb (human) and 77 kb (mouse). It is notable that in *Liprin-α1* and *Liprin-α2* the exon containing the translation start site is separated from the remaining clustered exons by a large intron, around half the size of the complete genes. In the case of *Liprin-α2* this intron contains an additional exon (Exon 3), which is not present in any of the other *Liprin-α* genes.

Tabel 5.1: Chromosomal locations and sizes of Liprin-α genes

Gene (symbol)	Human location	Size (kb)	Protein names	Gene ID	Mouse location	Size (kb)	Protein names	Gene ID
Liprin-α 1 (PPFIA1) (PTPRF interacting protein alpha 1)	11q13.3	114.041	Liprin-α1 LIP.1 LIP1 MGC26800	8500	7F5	76.975	Liprin-α1 LIP.1 LIP1 CO30014K08Rik	233977
Liprin-α 2 (PPFIA2) (PTPRF interacting protein alpha 2)	12q21.31	500.523	Liprin-α2 MGC132572 FLJ41378	8499	10D1	463.108	Liprin-α2 E130120L08Rik	327814
Liprin-α3 (PPFIA3) (PTPRF interacting protein alpha 3)	19q13.33	31.620	Liprin-α3 KIAA0654 LPNA3	8541	7B4	27.805	Liprin-α3 2410127E16Rik	76787
Liprin-α4 (PPFIA4) (PTPRF interacting protein alpha 4)	1q32.1	40.138	Liprin-α4 KIAA0897	8497	1E4	36.146	Liprin-α4 1110008G13Rik	68507

5.1.2. Liprin-α genes in human and mouse display distinct alternative splicing

Even though the overall gene structure of the *Liprin-α* genes is highly conserved, database analysis and RT-PCR revealed striking variations in alternative splice patterns among the four *Liprin-α* isoforms and between human and mouse orthologs. *Liprin-α1*, composed of 32 exons in human and mouse, is the family member with the highest degree of alternative splicing (Suppl. Table 9 and 10). We identified 5 alternatively spliced cassette exons (exons 10, 18, 24, 25, and 31) in the human and mouse genes encoding *Liprin-α1.* Exon 10 is only found in *Liprin-α1* and is inserted within the ELKS binding regions (Ko et al., 2003a). In contrast, exons 18, 24, and 25 are located between characterized domains: the only ten amino acids encompassing exon 18 between the coiled-coil region and the first SAM-domain and the small exons 24 and 25, with a size of 22 and 10 amino acids, respectively, between the first and second SAM-domain (Fig. 5.2). Moreover, in human and mouse, exon 26 includes an alternative splice acceptor site, leading to the deletion or insertion of a short 3-residue sequence (Suppl. Tables 1, 2). The human *Liprin-α1* gene contains an alternative splice donor site for exon 30 that is not found in the rat or mouse genome. The use of this site results in an exon with an in-frame stop codon (Fig. 5.3A).

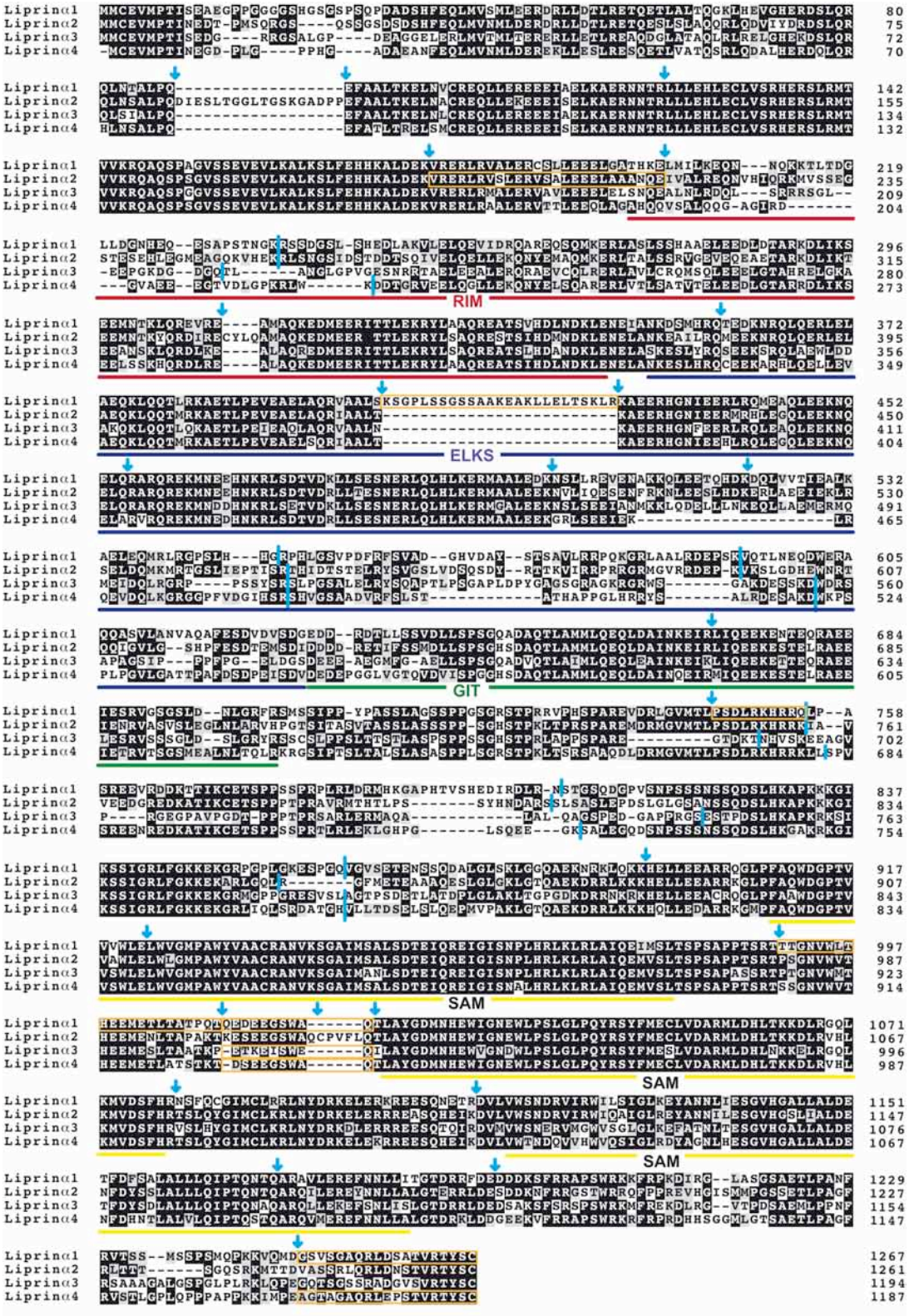

Fig. 5.2: Protein domain and exon-intron structure of mouse Liprins-α1-4.
The sequence alignment of mouse Liprins-α1-4 shows their highly similar overall organization and high sequence conservation. Black boxes indicate identical amino acid residues and grey boxes similar residues. Protein interaction domains are underlined: red, RIM interaction domain; blue, ELKS interaction domain; green, GIT interaction domain; yellow, the three SAM-domains. Light blue arrows mark conserved exon borders and light blue lines indicate diverging exon borders. Alternatively spliced exons are highlighted by orange boxes.

The encoded protein does not contain the conserved C-terminal PDZ-binding motif through which Liprins-α interact with GRIP (Wyszynski et al., 2002). The exclusion of cassette exon 31, which is found in the human and mouse genome, also generates a transcript coding for a protein without the C-terminal PDZ-binding motif (Fig. 5.3A, Suppl. Tables 1, 2). Therefore, alternative splicing of the C-terminal exons results in Liprin-α1 proteins with three (human) or two (mouse) distinct C-termini (Fig. 5.3, Fig. 5.4A).

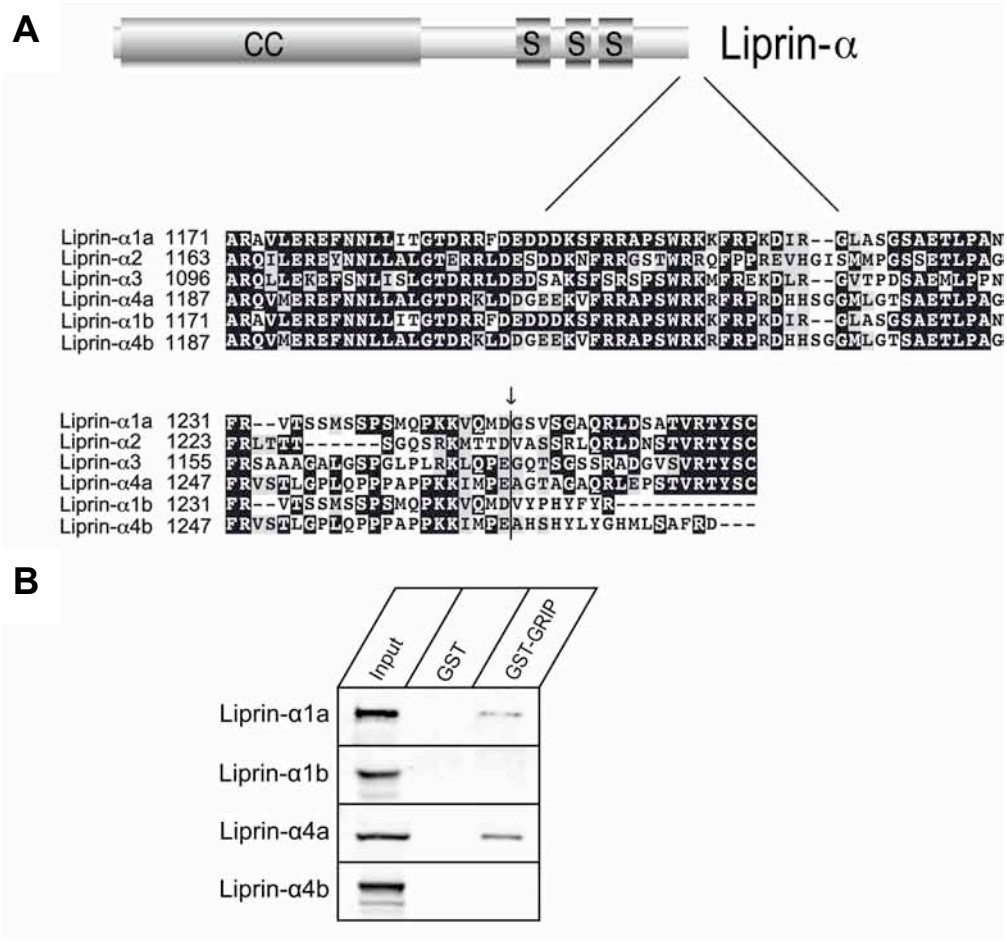

Fig. 5.3: Liprins-α share the same modular organization but are diversified via alternative splicing.

(A), The cartoon shows the conserved modular organization of Liprins-α1-4. Alternative splicing of Liprin-α1 and -α4 results in variants with diverging C-termini. The alignment was performed using the mouse Liprin-α sequences. Variants Liprin-α1a and -α4a contain the conserved PDZ-interaction motif, whereas this motif is absent in the variants Liprin-α1b and -α4b. The arrow and line labels the last exon boarder. Sequences were aligned using T-coffee. Boxshade was used to create the alignment figure. Black boxes indicate identical amino acid residues and grey marks similar residues. CC, coiled-coil domains, S, SAM domains. (B), Characterization of the interaction of GRIP1 with the different C-terminal variants of Liprin-α1 and 4. HEK-293T cell lysates transiently transfected with C-terminal variants of Liprin-α1 and -α4 were pulled down by GST-GRIP-PDZ6 or GST, and analyzed by immunoblotting with antibodies against GFP or pan-Liprin-α. Only the a variants, which contain the consensus PDZ-binding motif (-VRTYSC) specifically bind to GST-GRIP.

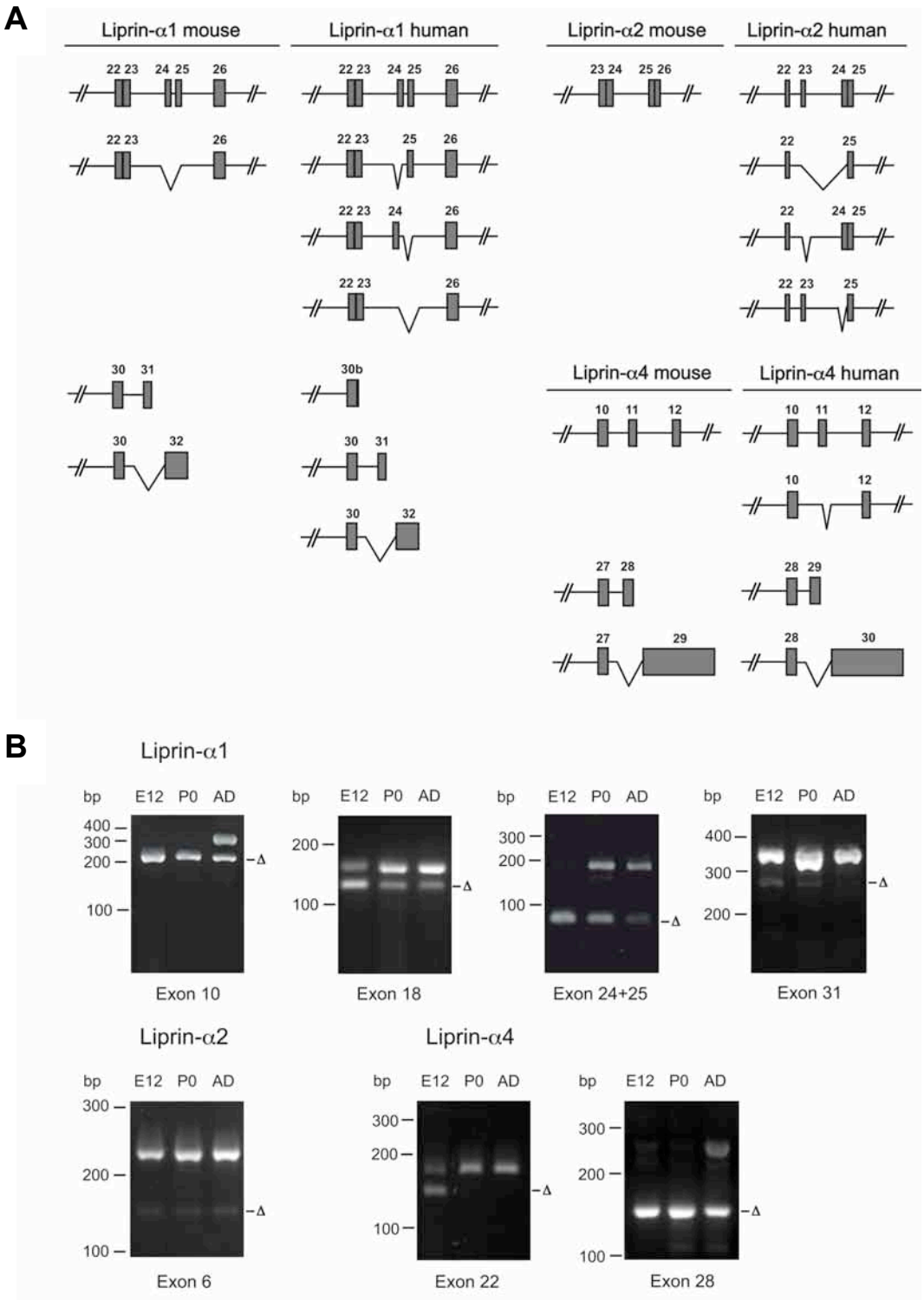

Fig. 5.4: Alternative Splicing is regulated during development.
(A), Mouse and human orthologs of Liprins-α exhibit diverging alternatively spliced exons. The diagram depicts the potential splice patterns for the mouse and human Liprins-α orthologs. Exons are represented by numbered grey boxes. (B), RT-PCR analysis of alternatively spliced transcripts of mouse Liprin-α1, -α2, and -α4 at different time points during development. E12, prenatal day 12; P0, day of birth; AD, adult. Primers flanking the exon of interest were used for the RT-PCR and the resulting fragments were resolved on an agarose gel. cDNA was transcribed from mouse whole brain total RNA. A DNA size marker is indicated at the left. The upper band corresponds to the PCR product including the examined exon, whereas the lower band (marked by a Δ) represents the product without the exon.

The gene encoding *Liprin-α2* consists of 32 exons in both human and mouse genomes (Suppl. Tables 3, 4). Alternative splicing occurs for exon 6 in human and mouse, leading to the presence or the lack of a sequence in the transcript immediately downstream the RIM-interaction domain (Fig. 5.2). Analysis of human transcripts revealed additional splice variants where exon 23 and 24, which are localized in the linker region between the first and second SAM-domains, were either present or absent in combination or independently (Fig. 5.4A, Suppl. Table 9). All mouse transcripts observed in extensive searches of databases and by RT-PCR of various mouse mRNAs contained exon 23 and 24 (Fig. 5.4A, Suppl. Table 10). Exons 9, 20, and 26 of the mouse *Liprin-α2* gene contain alternative splice acceptor sites resulting in the insertion or deletion of 1, 4, or 6 amino acids, respectively (Suppl. Tables 3, 4). The human and mouse genes that encode *Liprin-α3* comprise 30 exons (Suppl. Tables 5, 6). After comparison of genomic and cDNA sequences, alternative splicing was only identified upstream of the second SAM-domain for exon 23 (Suppl. Tables 9 and 10, Fig. 2).

Liprin-α4 is encoded by 30 exons in humans and by 29 exons in mice (Suppl. Tables 7, 8). The difference in exon number between human and mouse Liprin-α4 orthologs is due to human exon 11, which is not found in the mouse and rat genome. Alternative exon usage generates six human and four mouse Liprin-α4 transcripts. As in the other Liprins-α, except Liprin-α2, splicing occurs directly upstream of the second SAM-domain, where exon 22 either is included or deleted (Fig. 5.2, Fig. 5.4A, Suppl. Tables 9 and 10). Interestingly, we identified a novel C-terminal exon of *Liprin-α4* including an in-frame stop codon. Insertion of this exon (29 in human or 28 in mouse) results in Liprin-α4 transcripts , which code for a protein that contains the C-terminal PDZ-binding motif present in the remaining Liprins–α. The non-conserved C-terminal sequence (-MLSAFRD) is generated by transcripts missing exon 29 or 28, in human or mouse respectively (Fig. 5.3A, 5.4). Liprin-α1 and Liprin-α4 variants without the conserved VRTYSC C-terminal sequence are predicted to not interact with the adaptor protein GRIP. To test this hypothesis we performed GST pull-down assays using GST-GRIP (aa343-809) and HEK-293T cell lysates transfected with the variants of mouse Liprin-α1 and Liprin-α4 (Fig. 5.3B). GST-GRIP, but not GST alone, selectively pulled down Liprin-α1a and Liprin-α4a, the variants which contain the PDZ-binding motif, but not Liprin-α1b (-VYPHYFYR) and Liprin-α4b (-MLSAFRD) (Fig. 5.3B).

In summary, it is notable that alternative splicing of Liprin-α4 as is the case for Liprin-α1 can lead to proteins with diverging C-termini and thereby to the deletion or insertion of a protein interaction motif.

5.1.3. Alternative splicing of Liprins-α is regulated developmentally

To determine if alternative splice events of the mouse *Liprin-α* genes are regulated in a developmental- or region-specific manner we designed primers to detect the alternate transcripts and performed RT-PCR analyses (Fig. 5.4B, Suppl. Tables 9 and 10). The results showed that mouse *Liprin-α* alternative transcripts are expressed ubiquitously throughout the brain (data not shown). However, most alternatively spliced exons of *Liprin-α* mRNAs exhibited a developmental regulation (Fig. 5.4B). The Liprin-α1 transcripts including exon 10 can only be detected in mRNA of adult brain. Whereas transcripts lacking Liprin-α1 exon 18 are more abundant at E 12.5, this ratio reverses at P0 through adulthood. Liprin-α1 transcripts containing exons 24 and 25 are barely detectable at E 12.5 but are strongly expressed in the adult brain. In the case of Liprin-α4 the splice variant in which exon 22 is absent is only found early in development. Interestingly, the novel C-terminal Liprin-α4 exon 28 is only found at high levels in the adult mouse brain.

5.1.4. Liprin-α proteins are highly evolutionary conserved

A phylogenetic comparison of human and mouse Liprin-α full-length sequences classifies Liprin-α2 and -α4 as more closely related to each other than to Liprin-α1 and Liprin-α3, which is the most distant family member (Fig. 5.5A). While in invertebrates there is only one Liprin-α, starting in the clade of the Euteleostomes as early as in the *Danio rerio* four Liprins-α are found. All Liprin-α proteins share a common domain structure with a N-terminal coiled-coil region, three C-terminal SAM-domains and a conserved seven amino acid sequence at the C-terminus, which functions as a PDZ interaction motif. The four human and mouse family members share an extremely high degree of amino acid identity, ranging for the full-length proteins from 58%-66%. Their significant overall conservation with regard to amino acid identity and similarity is apparent in the alignment of their sequences (Fig. 5.2 and Suppl. Fig 1). In addition, this alignment highlights the striking similarity of the three C-terminal SAM-domains and their conserved PDZ interaction motif at the C-terminus. Surprisingly, whereas the Liprin-α SAM-domains not only exhibit a

remarkable conservation between the family members but also across species (the first SAM-domain of mouse Liprin-α2 is approximately 96% similar to *C. elegans SYD-2* and 97% to *Drosophila* Dliprin), the PDZ interaction motif is not present in the *C. elegans* and *Drosophila* Liprin-α homologs (Fig. 5.5B and Suppl. Fig. 1).

A

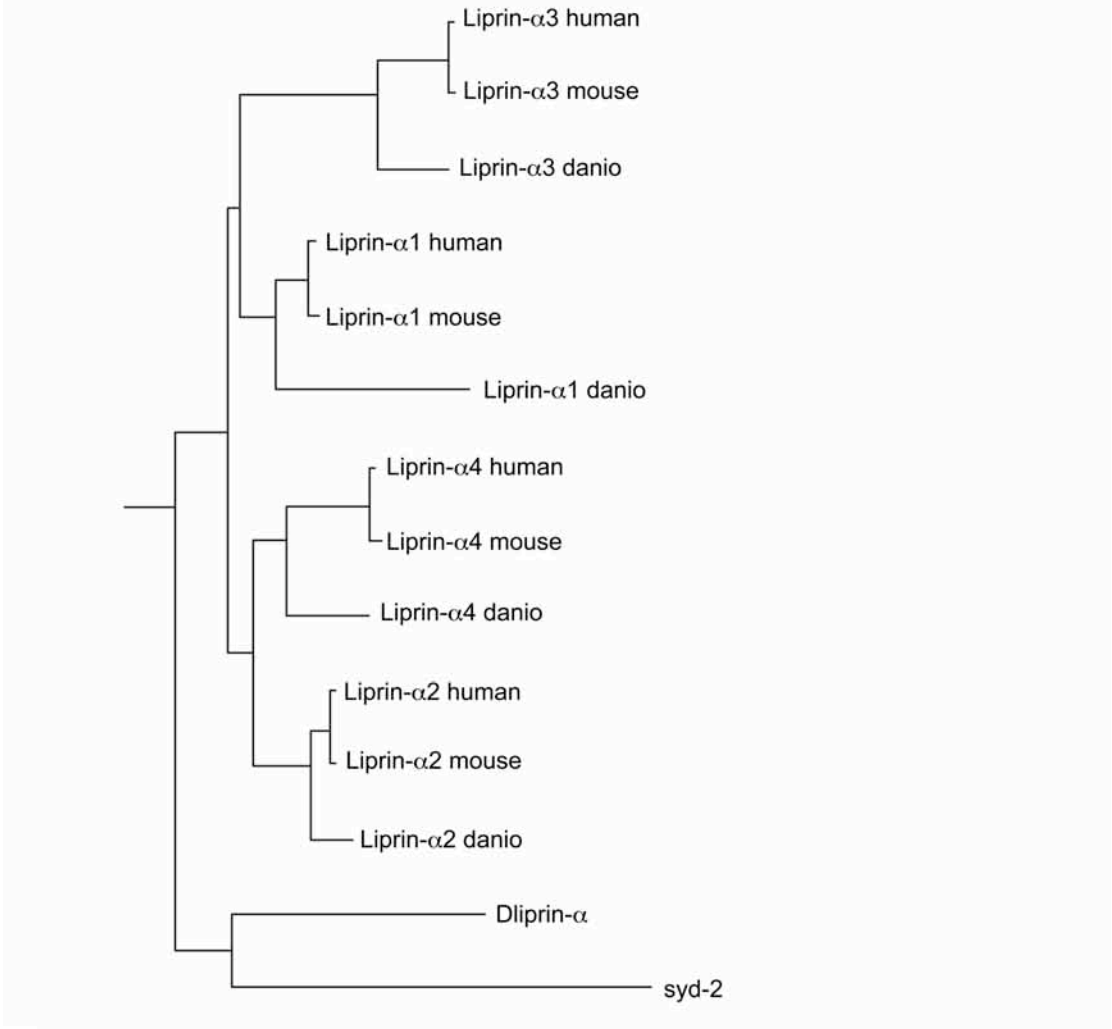

B

Fig. 5.5: Evolution of the *Liprin-α* gene family.
(A), The phylogenetic tree was generated based on a T-coffee alignment of the appropriate sequences using PhyML online (http://atgc.lirmm.fr/phyml/). Branch lengths are proportional to the amount of inferred evolutionary changes. (B), Liprin-α structural domains are highly conserved from *C. elegans* to human as shown here by an alignment of the first SAM domain of *C. elegans* SYD-2, *Drosophila* Dliprin and mouse Liprins-α1-4. Sequences were aligned using T-coffee. Boxshade was used to create the alignment figure. Black boxes indicate identical amino acid residues and grey marks similar residues.

Comparison of Liprin-α proteins from *C. elegans*, *Drosophila* and mouse furthermore identifies a region of very high conservation in the N-terminus of the proteins, upstream of the RIM binding domain (Suppl. Fig. 1). This sequence constitutes the beginning of a predicted coiled-coil region and does not exhibit any significant homology with any other protein in the databases (the closest match is the myosin heavy chain 10 with less than 30% identity). The Liprin-α binding sites for RIM, ELKS, and GIT have been mapped within the coiled-coil region (Ko et al., 2003a). Surprisingly, the interaction domains for RIM and ELKS do not exhibit the high degree of homology observed for large parts of Liprin-α proteins but are rather composed of a highly conserved sequence stretch and an area of low conservation (Fig. 5.2).

5.2 Analysis of the cellular and subcellular expression pattern of Liprin-α1-4

The bioinformatic analysis revealed a strong evolutionary conservation and striking sequence homology of the Liprins-α but also differences in alternative splicing that can translate into functional differences by influencing protein interactions. In addition, recent evidence from other studies suggests that despite their structural conservation the mammalian Liprin-α isoforms are differentially regulated, implying that they might exert diverging next to common functions (Hoogenraad et al., 2007). A distinct regional and/or subcellular localization could point to further diverging functions within the Liprin-α family.

5.2.1. Expression of Liprin-α transcripts

To access the expression pattern of the four Liprin-α isoforms on the mRNA level we performed quantitative real-time PCR using rat cDNA of different brain regions and adult organs and specific primer sets. These had been previously evaluated for their specificity because of the high degree of sequence homology between the four Liprin-α isoforms. Liprin-α2 and Liprin-α3 are synthesized at high levels in the brain and are only found at low levels in other tissues (Fig. 5.6A).

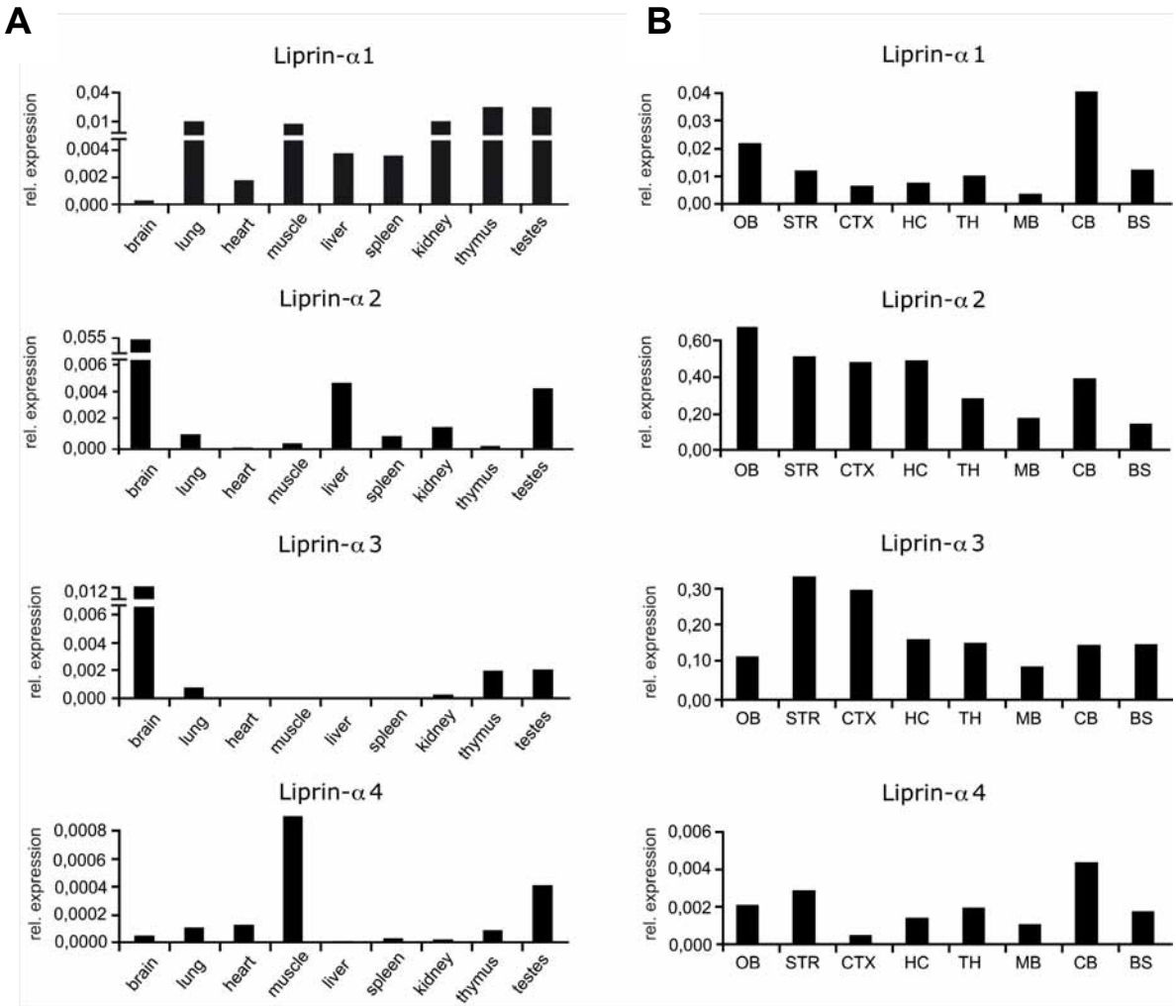

Fig. 5.6: Relative expression profiles of rat Liprin-α1-4 in different tissues and brain regions of the adult rat.
(A), Expression of Liprins-α1-4 in selected tissues analyzed by quantitative real-time PCR. Bars represent relative mRNA levels normalized to HPRT as internal reference gene. (B), Analysis of expression as in (A) in various brain regions. OB, olfactory bulb; STR, striatum; CTX, cortex; HC, hippocampus; TH, thalamus; MB, midbrain; CB, cerebellum; BS, brain stem.

Liprin-α1 mRNA in contrast was detected ubiquitously, with the lowest level of expression in the brain. Liprin-α4 was most prominently expressed in muscle and testes but is also present in brain, lung, heart, and thymus; however, the overall level of expression was very low. Liprin-α2 and Liprin-α3 exhibited a strong ubiquitous expression throughout the brain. Liprin-α2 mRNA levels are highest in the rostral brain regions, e.g. the olfactory bulb, striatum, cortex, and hippocampus, and lowest in the brain stem, whereas Liprin-α3 is most prominently found in the striatum and cortex. Liprin-α1 and Liprin-α4 were also detected in all brain regions analyzed, albeit at much lower levels (Fig. 5.6B). Both isoforms were most strongly expressed in the cerebellum and only at low levels in the cortex.

5.2.2. Generation of isoform specific antibodies

To characterize the expression patterns of Liprin-α 1-4 proteins, we raised isoform specific antibodies (Suppl. Fig. 2). Due to the strong homology of the four isoforms verifing their isoform specificity was critical. Using immunoblotting we could show that all antibodies only detected a single isoform, i.e. were isoform specific (Fig. 5.7).

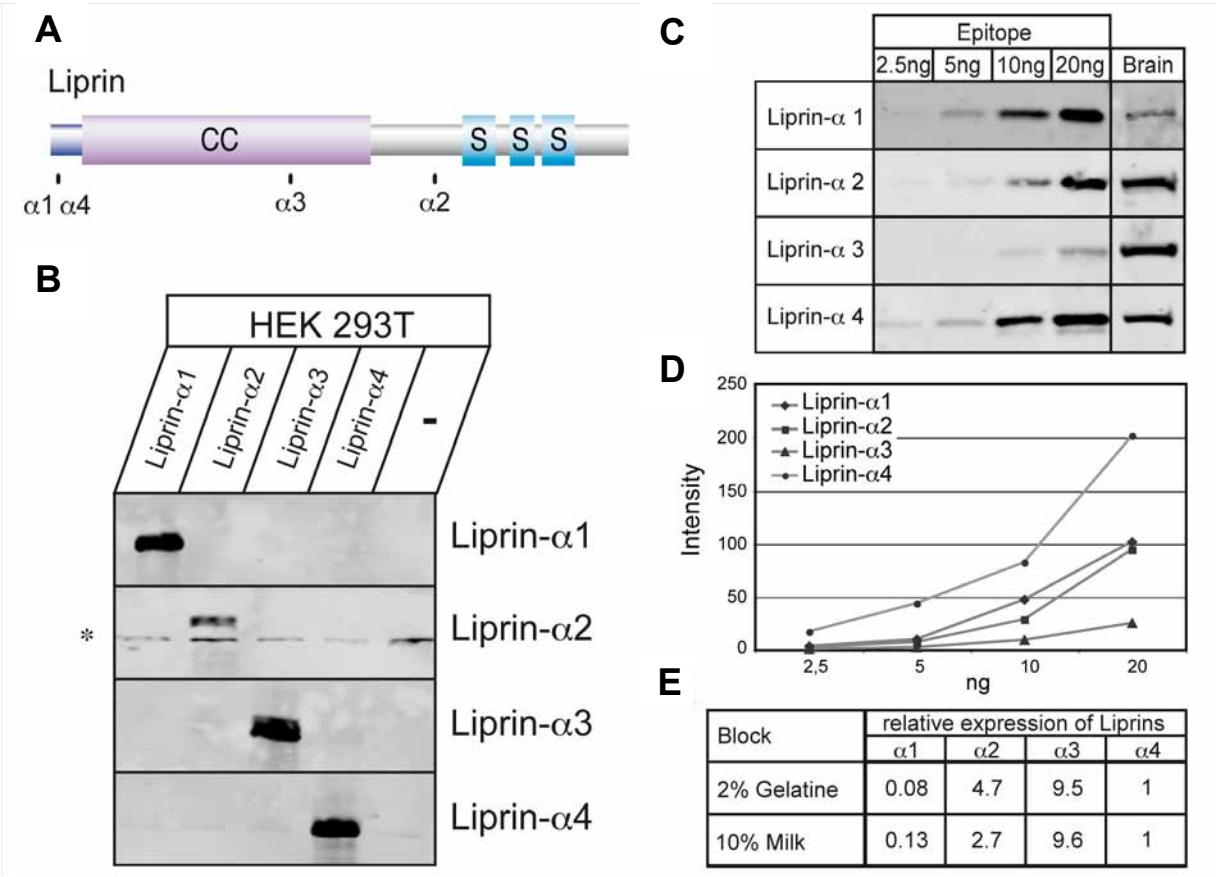

Block	relative expression of Liprins			
	α1	α2	α3	α4
2% Gelatine	0.08	4.7	9.5	1
10% Milk	0.13	2.7	9.6	1

Fig. 5.7: Characterization of isoform specific antibodies
(A), Cartoon depicting the modular organization of Liprins-α. *CC*, coiled coil domain; *S*, SAM (sterile alpha motif) domain. Localization of peptides is indicated. (B), HEK-293T cells were transfected with expression constructs encoding full-length mouse Liprin-α1-4. Total cell lysates were prepared, and equal lysate fractions were analyzed by immunoblotting. The asterisk marks an unspecific signal. (C), Determination of antibody affinity. Defined amounts of GST-peptide fusion proteins as well as whole brain lysate (50μg) were analyzed by immunoblotting with antibodies against Liprin-α1-4. The contrast was increased for the Liprin-α1 antibody labeling to allow visibility of the signal in the total brain protein lysate. (D), The Liprin-α antibody signals of the immunoblot shown in C were analyzed using the software AIDA and the signal intensity was plotted against the amount of peptide loaded in ng. (E), Liprin-α3 is the most abundant isoform in the brain. The relative expression of the four Liprin-α isoforms was calculated by comparing the intensity values of each isoform detected in whole brain lysate. Intensity values of two lanes were averaged for the calculations. Quantification was performed using immunoblots blocked with either 2% gelatin or 10% milk.

To examine the relative abundance of the four isoforms in brain we determined the affinity of the antibodies. The results from this quantification suggest that in the adult mouse brain Liprin-α3 is the family member with the highest and Liprin-α1 the one with the lowest abundance (Liprin-α3 > Liprin-α2 > Liprin-α4 > Liprin-α1) (Fig. 5.7C-E).

5.2.3. Spatiotemporal expression pattern of Liprin-α 1-4

Immunoblot analysis revealed that Liprin-1α is the only isoform detected in all tissues tested, being most strongly expressed in brain, lung and testes (Fig. 5.8A). Liprin-α3 and -α4 expression is restricted to the brain, whereas Liprin-α2 is detected at very low levels also in testes in addition to a prominent expression in brain. In accordance with the mRNA data, all Liprin-α proteins are present in all brain regions tested (Fig. 5.8B).

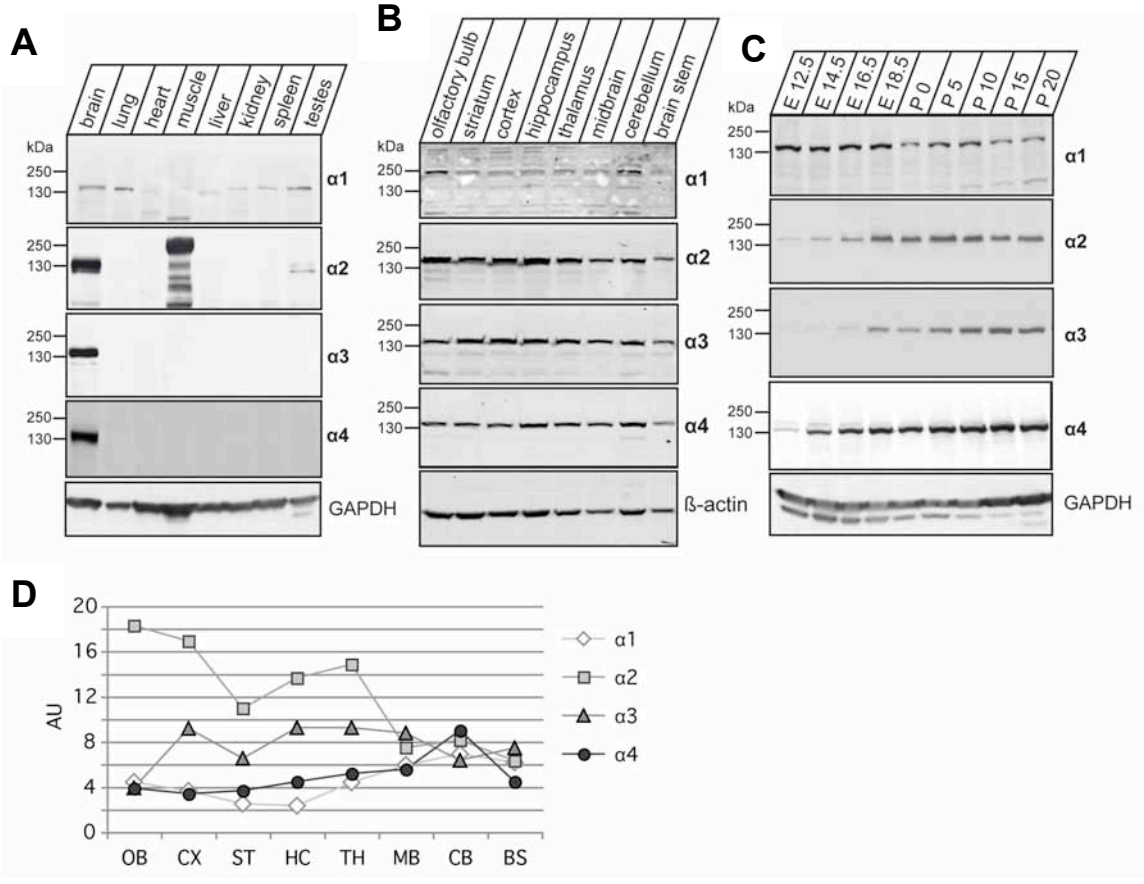

Fig. 5.8: Liprin-α1-4 exhibit distinct spatiotemporal expression profiles.
(A-C), Immunoblot analysis of the expression of Liprin-α1-4 in various tissues (A), brain regions (B) and during brain development (C). GAPDH or ß-actin antibodies were used as loading controls. (D), For the different brain regions the relative intensity values of Liprin-α signal compared to ß-actin were calculated and plotted in a graph, AU: arbitrary units. For Liprin-α1 all values were multiplied by 10. Immunoblots were analyzed using the software AIDA. OB, olfactory bulb; CX, cortex; ST, striatum; HC, hippocampus; TH, thalamus; MB, midbrain; CB, cerebellum; BS, brain stem.

Here, Liprin-α1 is most strongly expressed in the olfactory bulb and the cerebellum. Liprin-α2 and -α3 levels are highest in the forebrain and decline towards midbrain and brain stem (Fig. 5.8B). In direct comparison, Liprin-α2, is present at higher levels within the olfactory bulb, where Liprin-α3 is only weakly expressed. Liprin-α4 protein levels are highest in the cerebellum.

To gain insight into the function of Liprin-α in brain development, we determined their ontogenetic protein expression profile in mouse brain (Fig. 5.8C). All Liprins-α are already expressed at early embryonic stages (E12.5). We found that levels of Liprin-α2, -α3 and -α4 increase during development and peak around day E18.5 in the case of Liprin-α2 and -α4 and around P10 for Liprin-α3 (Fig. 5.8C). Strikingly, Liprin-α1 exhibits an inverse time course of expression, being most prominently expressed at early embryonic stages of development and at lower levels after birth. These results demonstrate that Liprin-α proteins are coexpressed throughout the brain as well as during development and therefore have the potential to function in the same protein complexes. Intriguingly Liprin-α1 exhibits a distinct spatial and temporal expression profile indicative for a potentially diverging functional role.

5.2.4. Distribution of Liprin-α1-4 in the cerebellum and hippocampus

To resolve the distribution of Liprin-α1-4 at the cellular level we performed immunohistochemistry with the newly generated isoform specific antibodies (Fig. 5.9). Confocal immunofluorescence microscopy revealed that in the molecular layer of the cerebellum the strongest immunoreactivity is observed for Liprin-α4 (Fig. 5.9A). The signal shows a high degree of overlap with the labeling for synaptophysin indicating a synaptic localization. A similar distribution pattern albeit at lower intensity was found for Liprin-α1. Labeling with antibodies against Liprin-α2 resulted in a strong staining of the granule and purkinje cell layers, where the Liprin-α3 antibody resulted a comparable distribution but a weaker signal. In the cerebellar molecular layer immunoreactivity for both Liprin-α2 and -α3 was observed in the soma of dispersed cells, most likely of interneurons of the stellate or basket cell type.

In the CA3 region of the hippocampus all four Liprin-α isoforms show co-staining with synaptophysin in stratum lucidum (SL), though to a varying degree (Fig. 5.9B).

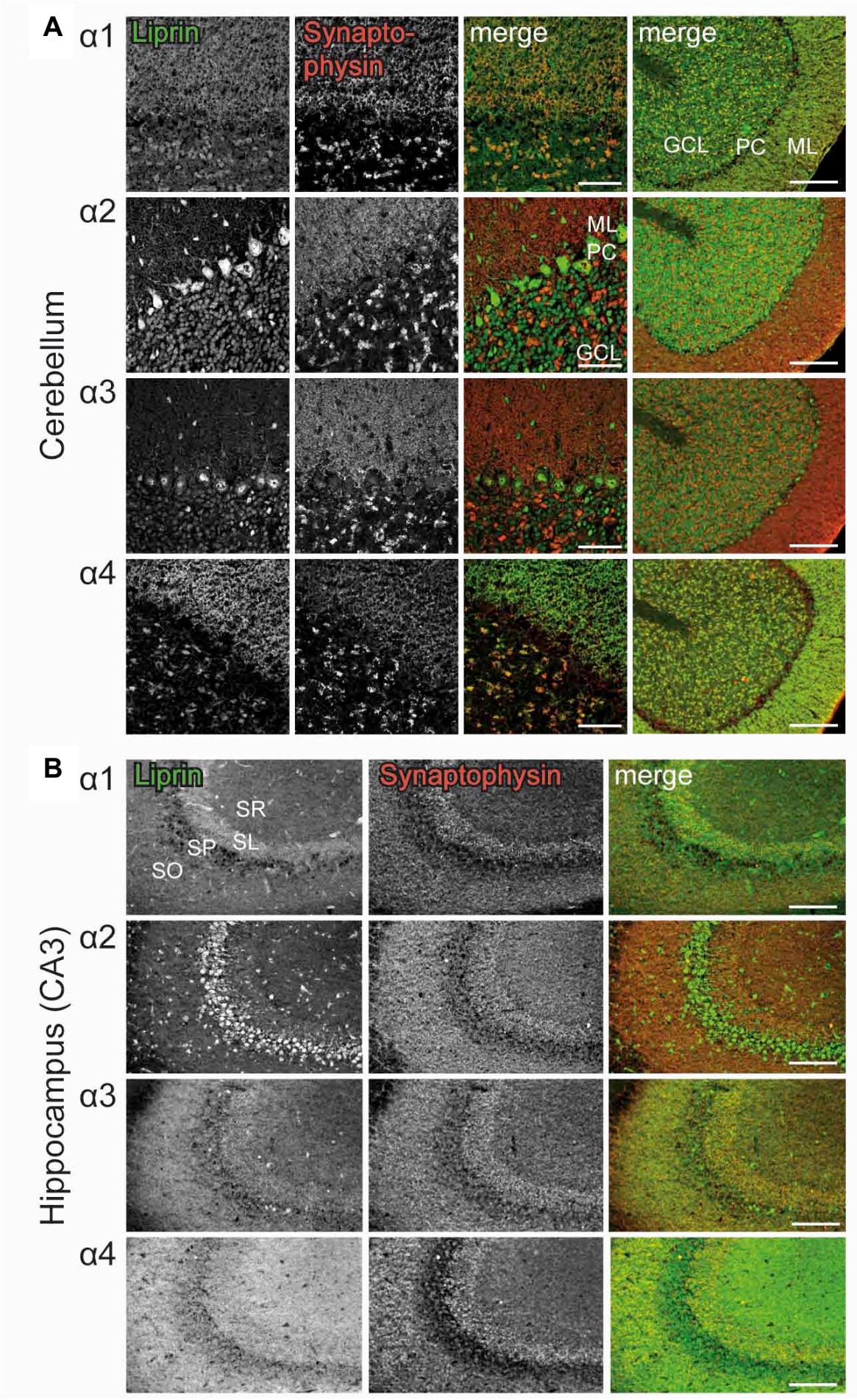
A
α1
Liprin
Synapto-
physin
merge
merge
GCL
PC
ML
α2
ML
PC
GCL
α3
α4
Cerebellum
B
α1
Liprin
SR
SP
SL
SO
Synaptophysin
merge
α2
α3
α4
Hippocampus (CA3)

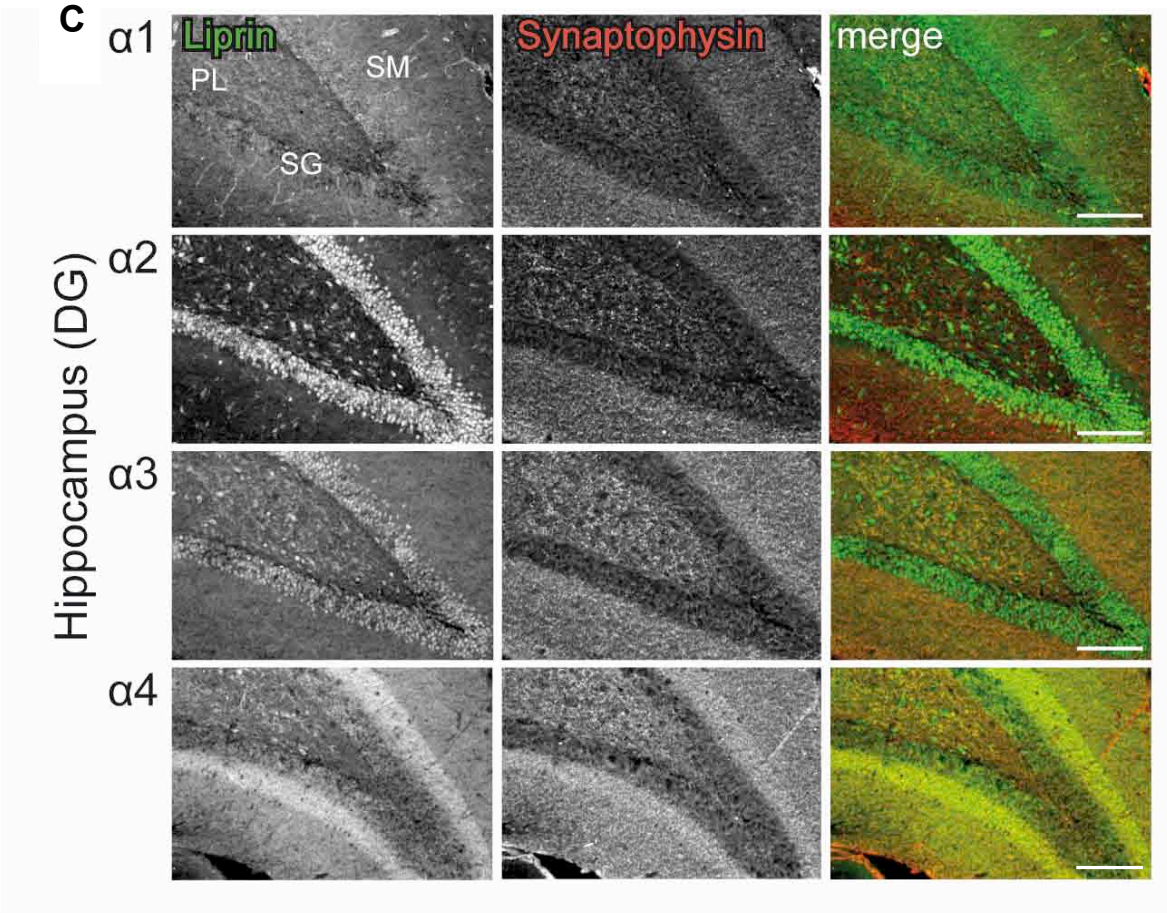

Fig. 5.9: Immunohistochemical localization of Liprin-α1-4 in the cerebellum and hippocampus.
Confocal scanning micrographs of sagittal cryo-sections of adult rat cerebellum and hippocampus were double labeled with antibodies against Liprin-α1-4 and synaptophysin. (A), In the cerebellum, Liprin-α4 is the isoform showing the strongest immunoreactivity in the molecular layer and exhibiting a synaptic expression pattern, similar to the weaker Liprin-α1 while Liprin-α2 and -α3 show a strong staining in the granule and purkinje cell layer. GCL: granule cell layer, PC: purkinje cell layer, ML: molecular layer. (B), In the hippocampal CA3 region of the hippocampus all four Liprin-α isoforms show co-labeling with synaptophysin in stratum lucidum, though to a varying degree. *SO*, stratum oriens; *SP*, stratum pyramidale; *SL*, stratum lucidum; *SR*, stratum radiatum. (C), In the dentate gyrus (DG) Liprin-α4 shows strong staining in the stratum moleculare while Liprin-α1, -α2 and -α3 can only be weakly detected. Interestingly Liprin-α2, -α3 and -α4 label putative interneurons in the hilus. *SG*, stratum granulosum; *PL*, polymorphic layer; *SM*, stratum moleculare. Scale bar: 200μm; higher magnification in A scale bar 50μm.

While Liprin-α1 was most prominently expressed in the SL mossy fibres, Liprin-α2 expression was more strongly detected in the cell bodies in the stratum pyramidale (SP), and Liprin-α3 and -α4 showed only very weak signals. In the dentate gyrus (DG) on the contrary (Fig. 5.9C), Liprin-α4 shows strong staining in the stratum moleculare (SM), where Liprin-α1, -α2 and -α3 proteins can only be weakly detected. Liprin-α2 and -α3 are most strongly expressed in the DG stratum granulosum and together with Liprin-α4 they are present in putative interneurons in

the hilus (PL).

5.2.5. Differential localization of Liprin-α1-4 in the retina

Double staining of retinal sections with Liprin-α1-4 and CtBP2 antibodies revealed that Liprin-α isoforms are distributed differentially in the retina (Fig. 5.10). The patterns are overlapping but show a distinct distribution of Liprins-α in synaptic and extrasynaptic regions. CtBP2 antibodies label the presynaptic cytomatrix protein RIBEYE at the active zones of ribbon synapses in the two synaptic layers of the retina - the inner and outer plexiform layers (IPL, OPL) and the transcriptional co-repressor CtBP2 in nuclei of the inner nuclear layer (INL) and are therefore a useful marker for synaptic orientation in the retina. The Liprin-α1 antibody labeled both retinal synaptic layers arguing for a synaptic localization of Liprin-α1. In the outer plexiform layer the staining is most likely postsynaptic since Liprin-α1 staining is oriented towards the inner retina with respect to the presynaptic RIBEYE/CtBP2 immunoreactivity in the OPL. In addition, a cell type spanning the whole inner retina from the ganglion cell layer to the outer plexiform layer is labeled by the Liprin-α1 antibody, a pattern in accordance with Müller glia cell labeling. Likewise Liprin-α2 exhibits a mainly synaptic localization with the most prominent labeling in two sublayers of the highly stratified IPL. Furthermore, somata in the INL were labeled, a region containing the cell bodies of amacrine and bipolar cells. Liprin-α3 showed an even more widespread distribution. Interestingly, no enrichment of immunolabeling was seen in the ribbon synapses of the OPL. However, synaptic staining was obvious in the IPL in addition to a prominent somatic staining in the inner and outer nuclear layers. In contrast to the OPL that contains only ribbon synapses, the IPL contains ribbon and conventional synapses.

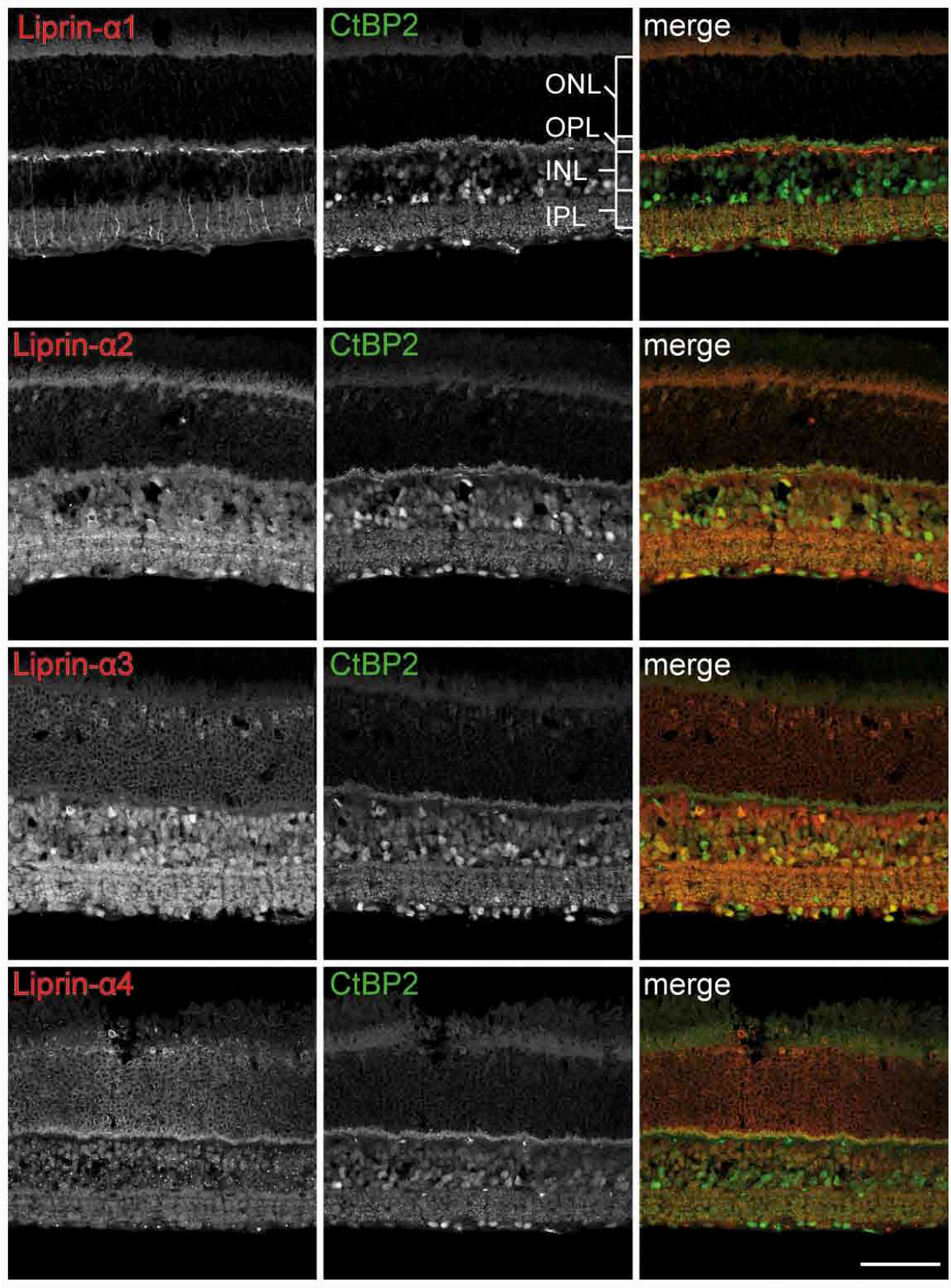

Fig. 5.10: Differential but overlapping expression of Liprin-α1-4 in the retina.
Confocal microscopy images of vertical mouse retina sections labeled with antibodies against Liprin-α1-4 and CtBP2. *ONL*, outer nuclear layer; *OPL*, outer plexiform layer; *INL*, inner nuclear layer; *IPL*, inner plexiform layer. Scale bar: 50μm**.** Performed by S. tom Dieck.

Thus, the different immunolabeling of OPL and IPL could arise from the absence of Liprin-α3 from ribbon synapses. The Liprin-α4 antibody homogeneously labeled photoreceptor somata in the ONL. Faint labeling of Liprin-α4 was also seen in the synaptic layers. In contrast to Liprin-α1 the diffuse label in the OPL seems to surround and partially colocalizes with the RIBEYE/CtBP2 staining suggesting a presynaptic localization of Liprin-α4 at photoreceptor ribbon synapses. Immunohistochemistry of retinae from Bassoon knockout mice that allow to differentiate between ribbon- or arciform density associated proteins (tom Dieck et al., 2005) did not reveal a differential distribution for Liprin-α1-4 (data not shown).

5.2.6. Subcellular localization of Liprin-α1-4 in neurons

Liprin-α2 has been described to be present at pre- and postsynaptic sites by immuno-electron microscopy using an antibody against the highly homologous N-terminal domain (Wyszynski et al., 2002). To investigate the distribution of individual Liprin-α proteins in neurons we performed double immunostainings of DIV14-21 cortical and hippocampal neurons for the Liprin-α isoforms and several pre- and postsynaptic marker proteins (Fig. 5.11). All four Liprin-α family members can be detected in primary cortical and hippocampal neurons (Fig. 5.11A). Liprins-α are present in dendrites and axons and could also be detected in the soma to a varying degree. Liprin-α2 and -α3, the predominantly expressed isoforms in the brain, exhibited a mostly punctate staining pattern. Significant colocalization was observed in double immunolabelings with the presynaptic markers Bassoon (Fig. 5.11A) as well as with the postsynaptic marker PSD-95 (Fig.5.11.B). Liprin-α1 and -α4 could only be detected at low levels in a punctate pattern with some of the signal being diffuse. Double immunolabeling with primary neurons with antibodies against Liprin-α1-4 and GAD67, a marker for inhibitory neurons, revealed that all four isoforms are present in GABAergic cells (Fig. 5.11C).

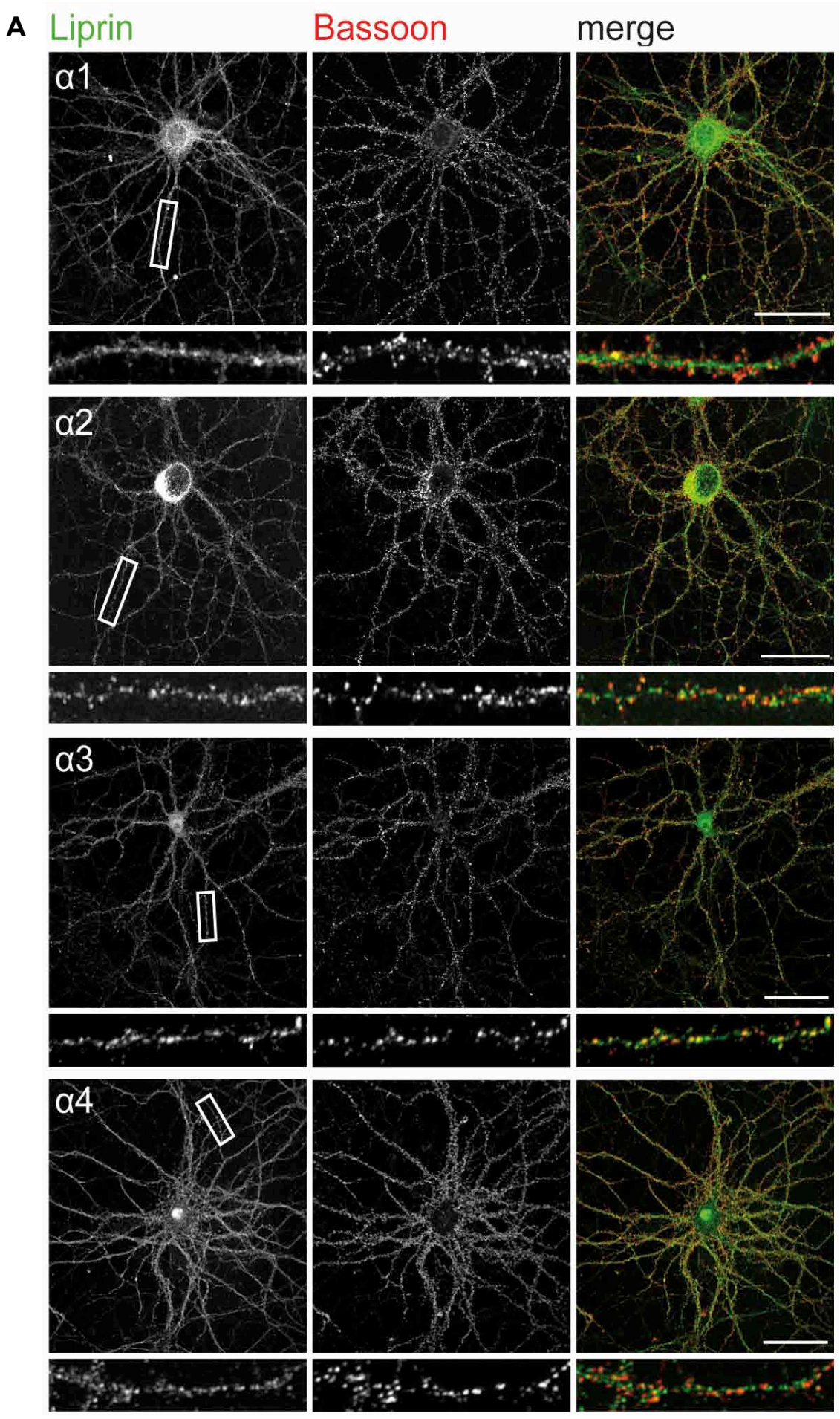
A
Liprin
Bassoon
merge
α1
α2
α3
α4

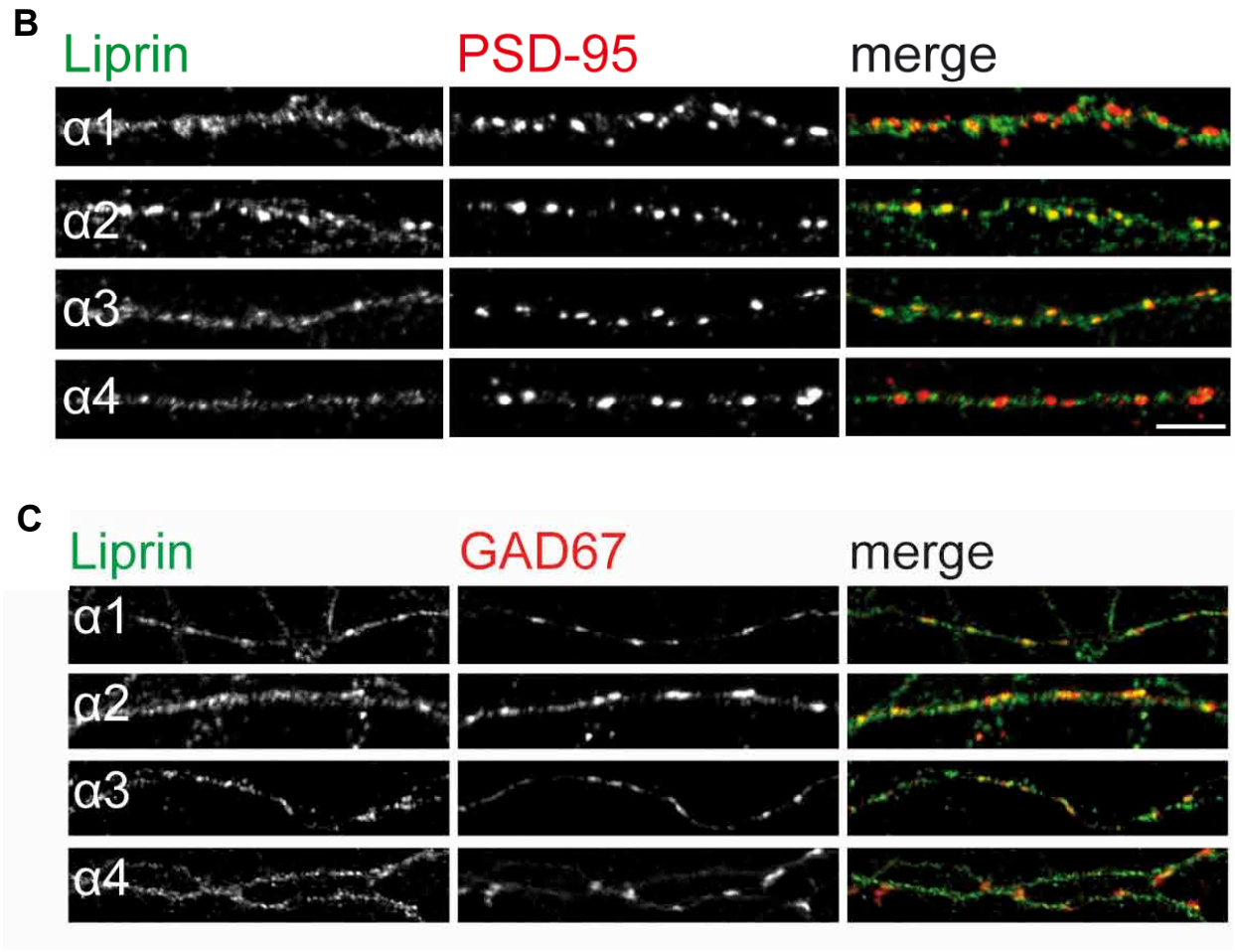

Fig. 5.11: Subcellular localization of Liprin-α1-4 in primary neurons.
Immunocytochemistry of primary neurons DIV14-21. Presynaptic active zones were labeled by Bassoon (A), the PSD was labled by PSD-95 (B) and inhibitory neurons by GAD67 (C). Scale bar: (A), 50μm, (B) 5μm.

5.2.7. Liprin-α1-3 accumulate at the leading edge of growth cones

Liprins-α have been suggested to play a critical role in synaptogenesis and active zone formation. Therefore, we examined which Liprin-α family members are present in outgrowing axons and where they are located within the growth cone. Immunolabeling of hippocampal neurons at DIV4 revealed that all four Liprin-α isoforms are present in growth cones (Fig. 5.12). Liprin-α2 and -α3 show a strong accumulation at the edge of the peripheral region of the growth cone. This distribution pattern is also observed for Liprin-α1, albeit less pronounced. In contrast, Liprin-α4 is found only weakly throughout the growth cone in a punctate manner. We performed double immunolabelings with two active zone proteins, RIM1α and Bassoon (Fig. 5.12A and B, respectively). The staining patterns of RIM1α and Liprin-α1, -α2, and -α3 show a substantial degree of overlap at the leading edge of the growth cone (Fig. 5.12A). Bassoon exhibits a distinct punctate pattern of

distribution throughout the growth cone and is not enriched at the leading edge (Fig. 5.12A). Only a minor degree of colocalization was observed with the four Liprin-α isoforms.

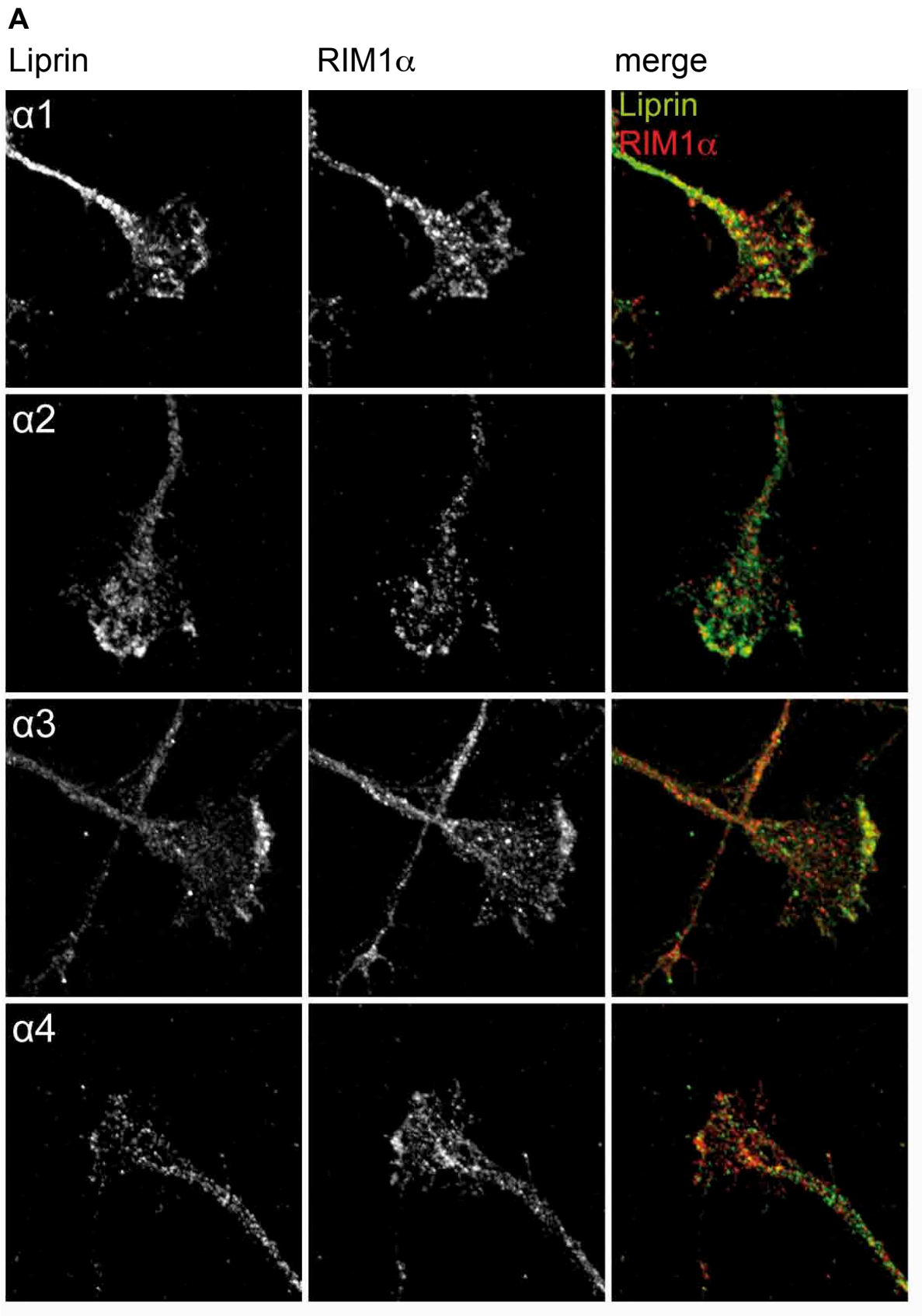

B

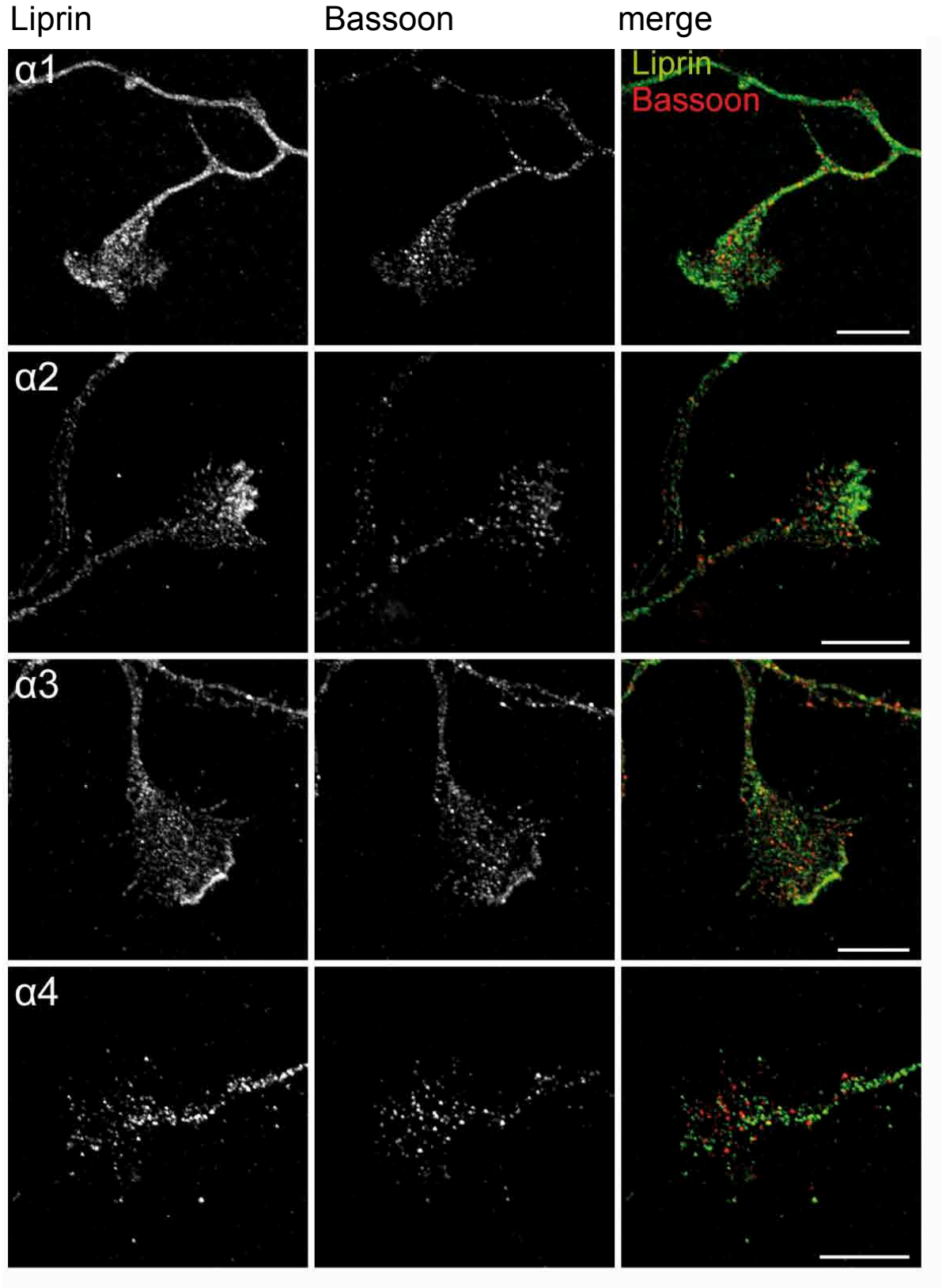

Fig.5.12: Distribution of Liprin-α1-4 in neuronal growth cones.
Liprin-α1, -α2 and -α3 accumulate along the leading edge of the growth cone while Liprin-a4 shows an evenly distributed punctate pattern. Primary neuronal cultures were analyzed at DIV4 by confocal microscopy after double immunolabeling for Liprin-α1-4 and RIM (A) or Bassoon (B). Scale bar: 10μm.

5.2.8. Liprin-α1 is the predominant Liprin-α isoform in glial cells

A comparative transcriptome study of neurons, astrocytes and oligodendrocytes suggested that Liprin-α1 is the most abundant Liprin-α isoform in glial cells while Liprin-α2, -α3 and -α4 were only detected at very low levels (Cahoy et al., 2008). The results of our immunolabeling of cultured astrocytes confirmed this observation as we found Liprin-α1 to be present in this cell type at high levels whereas the signals for the other three isoforms were close to background (Fig. 5.13A). Interestingly, Liprin-α1 in astrocytes, identified by double labeling with an antibody against GFAP, was mainly localized at distinct areas near the edge of processes.

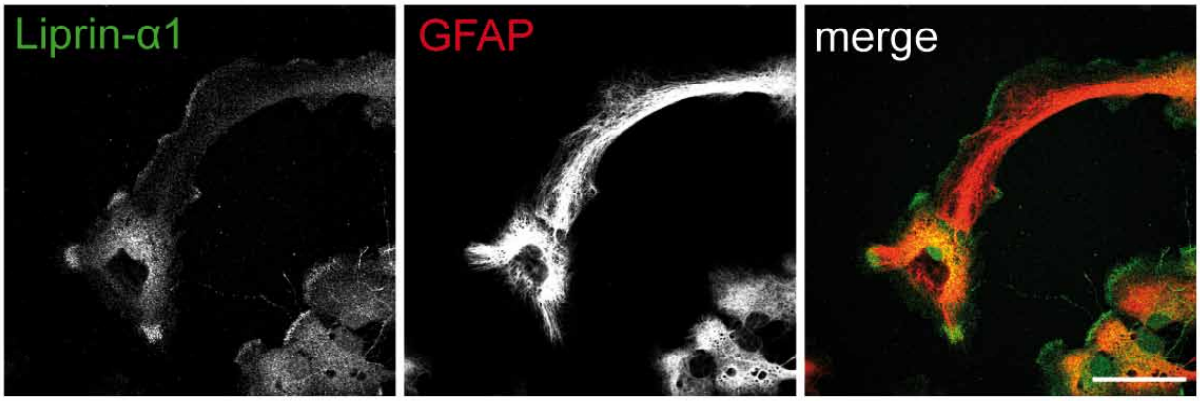

Fig. 5.13: Liprin-α1 is the predominant Liprin-α in glial cells and is mainly localized in clusters at the rim.
Immunocytochemistry of primary glia DIV14-21. Astrocytes were colabeled with an antibody against GFAP. Scale bar: 50μm.

5.3 Analysis of Liprin-α2 localization and dynamics in primary neurons using overexpression

Liprins-α have been described as integral components of the protein network at the presynaptic active zone where they interact with many different active zone proteins, e.g. RIM1α a protein that links SVs to Ca^{2+}-channels and plays an important role in SV priming (Coppola et al., 2001; Kiyonaka et al., 2007; Mittelstaedt et al., 2010). However, as shown in chapter 5.2 Liprins-α are not like RIM1α purely presynaptic proteins but also present throughout dendrites and at the popstsynaptic density. Liprins-α share a highly conserved domain structure but so far it is unclear which domain and binding partners are critical for the association of Liprins-α to the CAZ (cytomatrix at the active zone) and how Liprins-α are targeted to the synapse.

5.3.1. GFP-Liprin-α2 is located at focal clusters in the presynaptic bouton

To study the dynamic properties of Liprin-α2 we generated a plasmid expressing a N-terminal fusion protein of the fluorescent reporter GFP and Liprin-α2. As tags can affect localization we first verified correct targeting in primary neurons by comparing the distribution of the overexpressed fusion protein to the endogenous Liprin-α2.

The N-terminal GFP-Liprin-α2 fusion protein transfected into primary hippocampal neurons can be detected in axons and dendrites while its interaction partner at the active zone, GFP-RIM1α, is only present in the axon (Fig.5.14A). Both proteins show an enrichment at boutons along the axon. This result is in accordance with observations from immunostainings with the respective antibodies. When GFP-Liprin-α2 and cherry-RIM1α are cotransfected a very strong colocalization at synaptic boutons is detected (Fig. 5.14B). This suggests that the cotransfection of the interaction partners increases their synaptic localization as it has been shown for Liprins-α and ELKS (Ko et al., 2003a). To study the distribution of GFP-Liprin-α2 at the bouton we labled the presynaptic bouton, that is filled with synaptic vesicles, by cotransfecting the synaptic vesicle transmembrane protein SV2A. High magnification micrographs revealed that GFP-Liprin-α2 is not ubiquitiously distributed throughout the presynaptic bouton but appears to be clustered in subcompartments along the membrane.

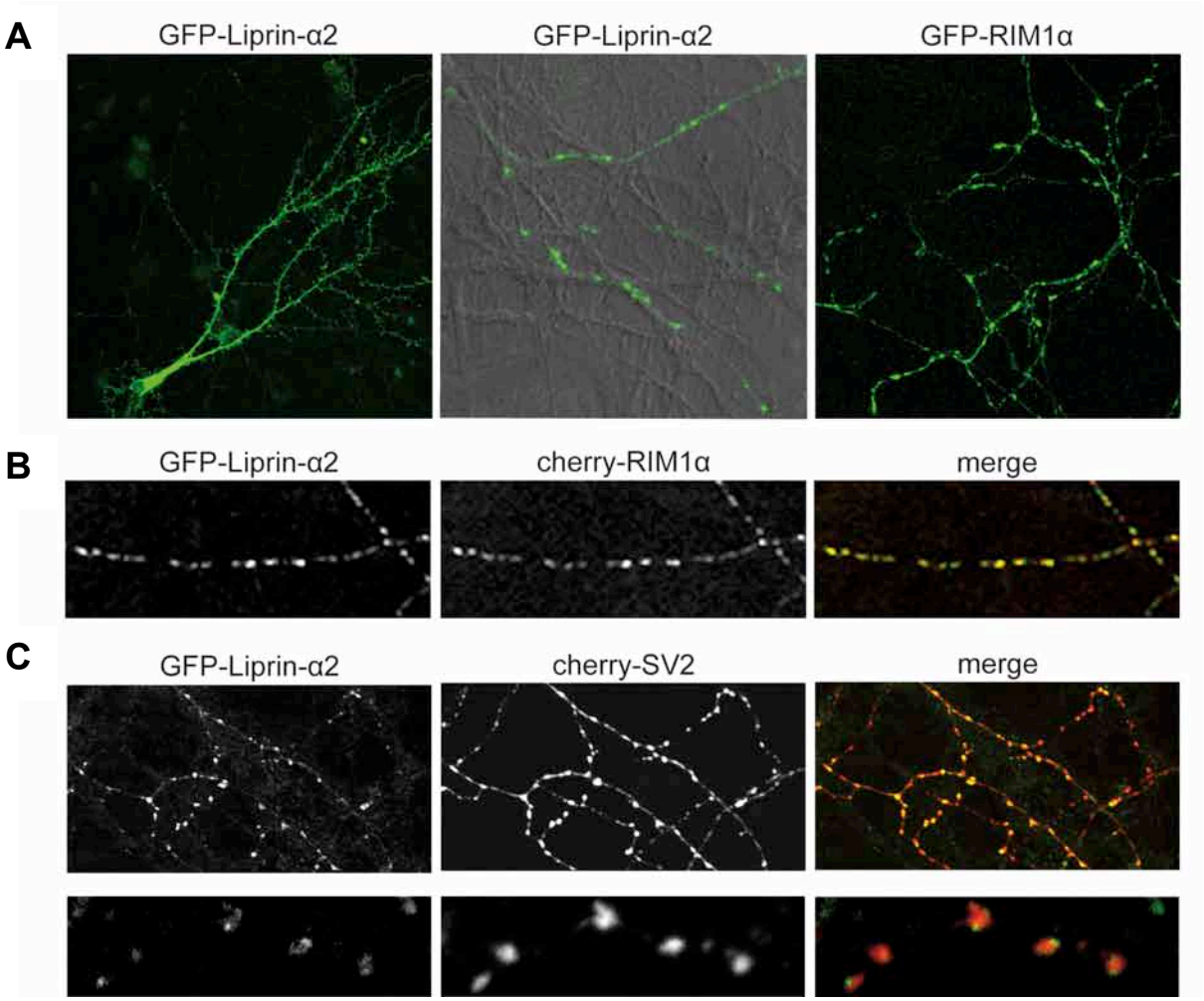

Fig. 5.14: Overexpression of GFP-Liprin-α2 in primary hippocampal neurons.
Cells were tranfected DIV3-6 and fixed for imaging at DIV14.
(A) GFP-Liprin-α2 is present throughout the neuron while RIM1α expression is restricted to the axon. (B) Coexpressed GFP-Liprin-α2 and cherry-RIM1α strongly colocalize at synaptic boutons. (C) Coexpression of GFP-Liprin-α2 and cherry-SV2, a synaptic vesicle protein, shows that GFP-Liprin-α2 is restricted to focal clusters at the bouton.

5.3.2. Localization of Liprin-α deletion mutants

The domain structure of Liprins-α is highly evolutionary conserved and binding partners have been identified for most regions. However, little is known about how these domains and their interaction partners relate to the targeting of Liprins-α and to their described functional role, e.g. in dendritic branching. To gain insight into the functional role of the coiled-coil domain in the N-terminal half and the three SAM-domains followed by the PDZ binding motif in the C-terminal half we generated deletion contstructs coding for GFP fusion proteins. GFP-deletion variants were first expressed in NG108 cells to test for their expression and stability. In NG108 cells the full-length GFP-Liprin-α2 as well as the fusion proteins containing the coiled-coil domain, which mediates dimerization, showed a punctate accumulation throughout

the cell. The GFP-SAM-domains and GFP transfected as a control were ubiquitously distributed. Next, primary neurons were analysed at DIV7, when the axons are already well developed but dendrites are just growing out, and at DIV14, when cultured neurons are mature, for analysis of the cell morphology. For Liprin-α1 it was shown that overexpression of the N-terminal half at DIV13 leads to decreased arborisation of the dendritic tree at DIV17 (Hoogenraad et al., 2007). Here, no obvious changes in arborisation in neurons transfected with deletion constructs of Liprin-α2 were observed at both time points. No unique targeting domain could be identified all deletion mutants were present in dendrites and axons and no diverging distribution was detected.

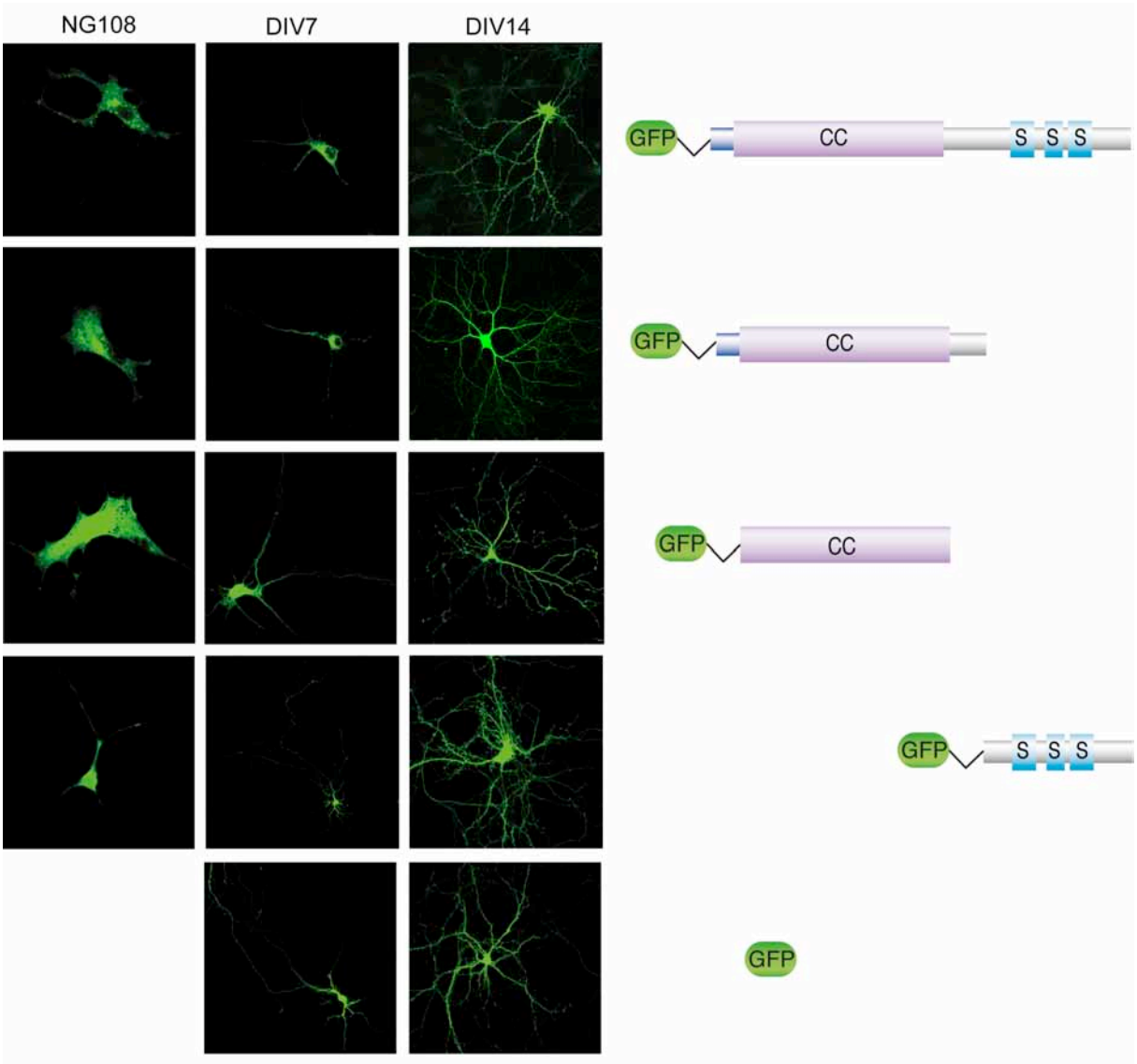

Fig.5.15: Effect of overexpression of deletion constructs on cell morphology. Full-length GFP-Liprin-α2 as well as the N-terminal and C-terminal part of Liprin-α2 tagged with GFP were transfected in NG108 cells as well as in DIV3-4 hippocampal neurons. As control GFP was transfected. Cells were fixed for imaging at DIV 7 and DIV14.

5.3.3. *Dynamics of RIM1α and Liprin-α2 at the presynaptic bouton*

In recent years the dynamics of several presynaptic proteins were elucidated. Depending on the localization of proteins either on a synaptic vesicle or integrated into the CAZ and on their functional role, the dwell time at the presynaptic bouton can range from minutes to hours. For synaptic vesicle proteins like synapsin the exchange time constant at the presynaptic bouton is in the minute range while the large scaffolding protein Bassoon has an exchange time constant that exceeds 8 hours (Tsuriel et al., 2006; Tsuriel et al., 2009). To gain insight into the stability and exchange rates of Liprin-α2 and its interaction partner RIM1α we used two approaches, fluorescence recovery after photobleaching (FRAP) and fluorescence recovery after photoactivation (FRAPA), where a photoactivatable GFP (paGFP) is employed, recorded by time-lapse confocal microscopy (Fig. 5.16).

Individual putative presynaptic sites of transfected rat hippocampal neurons are selected. In FRAPA experiments CFP was cotransfected to enable selection of putative presynaptic sites since paGFP is hardly visible before activation. After collecting baseline images multiple sites were selectively bleached or activated and the loss and reincorporation was monitored at rates of every 10 minutes for FRAP experiments and every 1h for FRAPA experiments. To verifiy that the bleaching or photoactivation procedure does not affect the functionality of the synapse high KCl stimulation was used to label all boutons in the fields of view with the fluorescent functional endocytosis marker N-(3-triethylammoniumpropyl)-4-(p-dibutylaminos-tyryl) pyridinium, dibromide (FM4–64, 15 lM) (Fig. 5.16C).

The two different approaches have different advantages and disadvantages. The EGFP used in FRAP experiments allows a high sampling rate but errors arising from photo-bleaching lead to an underestimation of recovery rates and are more significant near the end of the recovery phase. This is critical for correct estimations of slow exchange rates. In FRAPA, photobleaching is about twice as pronounced and leads to an overestimation of exchange rates and errors arising from photo-bleaching are extremely significant at the initial phase of recovery.

In initial experiments for RIM1α an exchange rate in the range of minutes was observed while Liprin-α2 showed much slower dynamics. Due to these observations, FRAPA experiments were performed to access the exchange rate of Liprin-α2 (Fig. 5.16 B) and FRAP experiments to analyse RIM1α dynamics (Fig. 5.16 D).

A

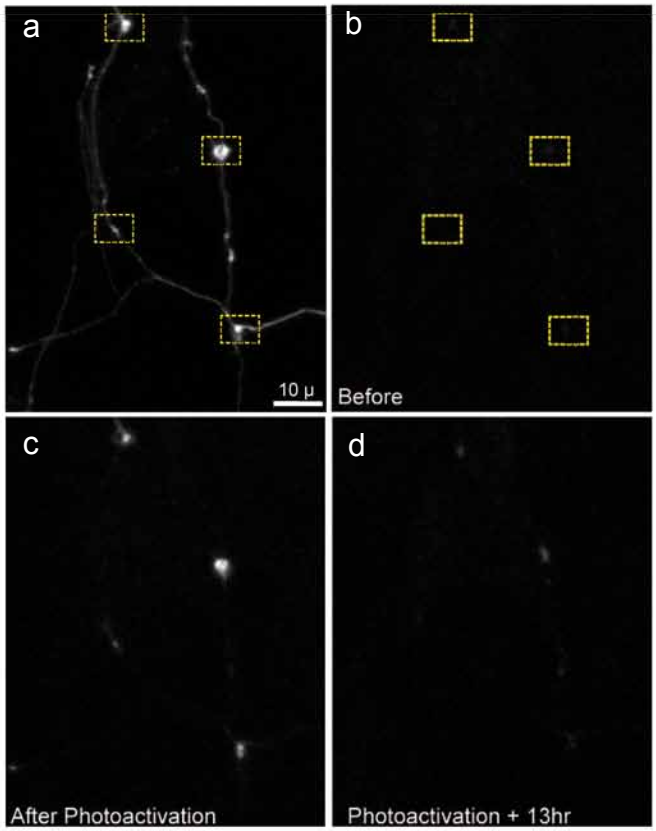
a
b
10 µ
Before
c
d
After Photoactivation
Photoactivation + 13hr

B

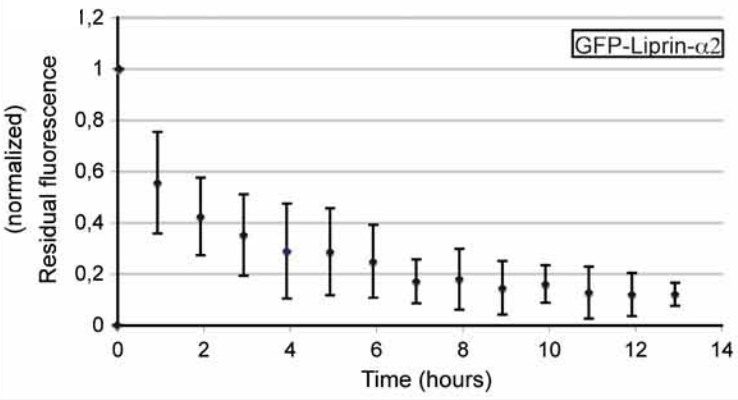
GFP-Liprin-α2
Residual fluorescence
(normalized)
1,2
1
0,8
0,6
0,4
0,2
0
0
2
4
6
8
10
12
14
Time (hours)

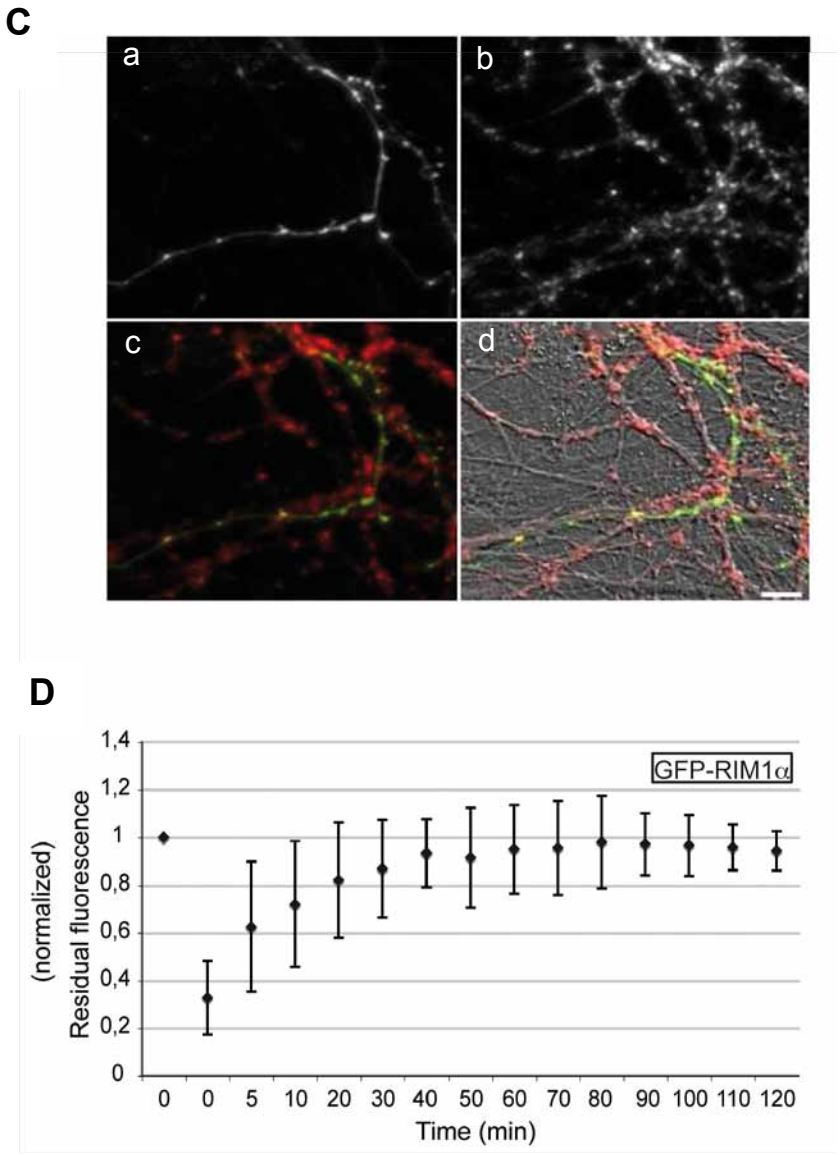

Fig.5.16: Dynamics of RIM1α and Liprin-α2 at the presynaptic bouton.
(A), Fluorescent recovery after photoactivation (FRAPA) of paGFP-Liprin-α2. Neurons were cotransfected with paGFP-Liprin-α2 and CFP to allow selection of putative pre-synaptic boutons for photo-activation. Axon expressing CFP (a) as well as paGFP-Liprin-α2, here shown befor activation (b) and at timepoint 0 (c), directly after photo-activation. 13 h after photoactivation there is still paGFP-Liprin-α2 detectible at some boutons (d). (B) Dynamics of paGFP-Liprin-α2 at the presynaptic bouton are relatively slow. Primary rat cortical cultures were transfected with paGFP-Liprin-α2 at DIV10 and imaged at DIV22. The residual fluorescence of photoactivated paGFP-Liprin at presynaptic boutons was imaged every hour. The average residual fluorescence of 10 sites was plotted against time. (C) Fluorescent recovery after photobleaching (FRAP) of GFP-RIM1α followed by a FM uptake assay. Rat primary cortical cultures were transfected with GFP-RIM1α at DIV10 and imaged at DIV22 (a). As a control of functionality of the synapses imaged neurons were loaded with FM-64 at the end of the experiment (b). (c), overlay of a and b, (d) overlay of a, b and a DIC image. (D) Dynamics of GFP-RIM1α at the presynaptic bouton are relatively fast. The recovery of fluorescence of GFP-RIM1α after photobleaching was imaged every 10 minutes. The average residual fluorescence of four sites was plotted against time. Scale bar: 10μm (A) 7,5 μm (B).

For Liprin-α2, a scaffolding protein thought to be critical for active zone composition, a relatively slow exchange rate was observed. In the first three hours the residual fluorescence went down to about 40%. Even 7 h following photoactivation, when no further decrease in fluorescence was detected, residual fluorescence was observed at some boutons. It is likely that the recovery has two phases due to a slow and a fast exchange pool of proteins. RIM1α showed a much faster exchange rate, with an almost complete recovery of fluorescence 40 min after bleaching.

5.4 Disruption of Liprin-α function

Little is known about the diverging and overlapping functional roles of the four highly homologous Liprin-α isoforms in the mammalian brain. Many putative interaction partners have been identified and so far it is assumed that all interactions are common to all isoforms. Our analysis of the gene structure and alternative splicing showed that Liprins-α can be differentially regulated by alternative splicing in a development dependent manner. This could potentially change their affinity to specific interaction partners. The characterization of the expression patterns of the four Liprin-α isoforms revealed that Liprins-α show a distinct but overlapping distribution with Liprin-α2 and -α3 being the most abundant isoforms present at most synapses. To further investigate the functional roles of the Liprin-α2 and -α3 isoforms in neurons two approaches were chosen, a loss of function experiment and the interference with specific interactions.

5.4.1. Identification of shRNAs

To analyze the effect of the lack of single Liprin-α isoforms on neuronal morphology as well as synapse formation and maintenance we chose to use an shRNA approach. We first tested four shRNAs for each isoform by cotransfecting shRNAs and the target Liprin-α in HEK-293T cells. The quantitative analysis of the immunoblot of HEK-293T cells three days after transfection yielded one shRNA for Liprin-α1 and -α2 which showed a significant knock down of the respective protein (data not shown). Since we wanted to focus on Liprin-α2 and -α3 seven additional shRNAs targeting these two most abundant expressed isoforms in the b rain were analyzed. To directly test the ability of the new shRNAs as well as the before identified candidate shRNA against Liprin-α2 to downregulate the endogenous protein primary neuronal cultures were transduced using rAAV viruses. Viral particals

were added to primary cortical cultures on DIV0-1 and cells were harvested for immunoblotting on DIV12-14. The immunblots were quantified using the AIDA software. For the quantification of the knock-down the levels of Liprin-α were normalized to α-tubulin and cells transduced with shRNAs were compared to cells transduced with the empty vector. Two shRNAs, one for each isoform, were found to be efficient in the down regulation of the Liprin-α protein levels. The knock-down efficiency was 80% for Liprin-α2 (shRNA 1469) and 80-85% for Liprin-α3 (shRNA 1644), respectively (Fig. 5.17A, B). The other shRNAs tested did not show a sufficient down regulation of the target protein.

As a first test to examine if the knock-down of Liprin-α3, the most abundant Liprin-α isoform leads to a drastic change in neuron morphology, as for example observed for its interaction partner GRIP1 (Hoogenraad et al., 2005), viral particles were added at DIV1 to primary neurons which were analyzed at DIV5 and DIV14. A first analysis of the effect of the down regulation of Liprin-α3 showed no obvious impact on the morphology of the neurons (Fig. 5.17C). At DIV5, when axons are already well developed but dendrites are just growing out, no change in axon development was observed. In adult cortical neurons at DIV14 no change in dendrite or spine morphology was detected and axon morphology seemed unchanged.

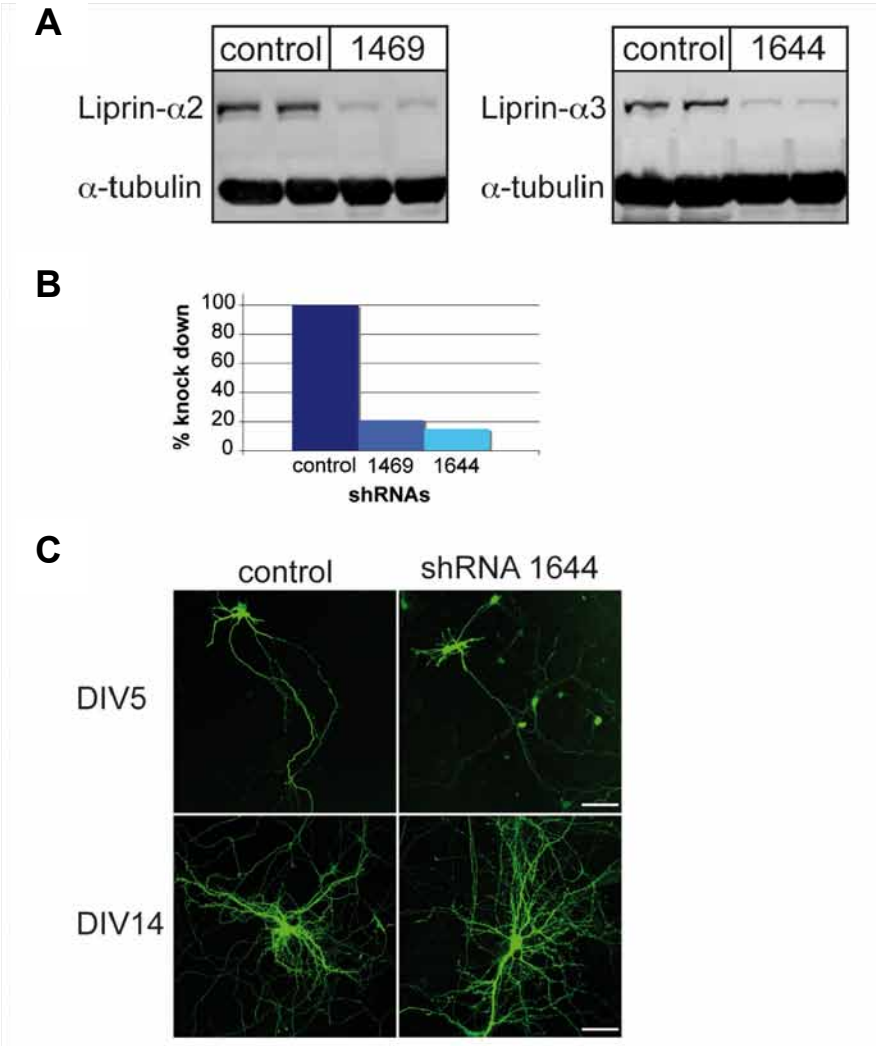

Fig. 5.17: Identification of shRNAs to specifically knock down Liprin-α2 and α3 (A), The knock-down efficiency of shRNAs was analyzed by immunoblotting of lysates of DIV13-14 old cortical primary neurons treated on DIV0-1 with rAAV virus containing a shRNA plasmid or empty vector as control. (B), The Liprin-α antibody signals of the immunoblots shown in (A) were quantified using the AIDA software with α-tubulin as an internal control. (C), Cortical primary neurons treated with rAAV Virus containing a shRNA plasmid or the empty vector as control on DIV1 were fixed and imaged with a confocal laser scanning microsope on DIV5 and DIV14. Scale bar: 50μm.

5.4.2. Identification of point mutations to disrupt specific interactions

To study the role of individual binding partners for Liprin-α function specific interactions need to be disrupted. Therefore, point mutations should be inserted in the interaction domains of Liprin-α or its binding partners to lower the binding affinity. As no structural data for Liprins-α are available to date, the Liprin-α tertiary structure was modeled based on existing structures (in collaboration with Carsten Reissner, Institute for Anatomy, University Münster). This model was used to identify point mutations that were predicted to disrupt the interaction between Liprin-α2 and RIM1α

as well as Liprin-α homodimerization.These analyses provided one point mutation in the coiled-coil domain of Liprin-α (L294D) that was predicted to disrupt Rim1α binding as well as homodimerization of Liprins-α and a mutation in the RIM1α C2B domain (T1454Q) that was predicted to disrupt the RIM1α-Liprin-α2 interaction. The mutations were introduced in the Liprin-α2 and RIM1α sequence by site directed mutagenesis. Subsequently the ability of these point mutations to disrupting the interaction was tested in pull down assays.

In the pull down assay to test the effect of the mutation in the RIM1A C2B domain on the binding to Liprin-α2 the mapped interaction domains for the RIM1α-Liprin-α binding were used. Since the Liprin-α2 coiled-coil domain was relatively instable without the GST it was purified from bacteria as a GST-fusion protein and the RIM1α C2B domain was overexpressed in HEK-293T cells as a HA-tagged protein. In this assay the mutation in the RIM1α C2B domain successfully disrupted the binding to the Liprin-α coiled-coil domain (Fig. 5.18 A).

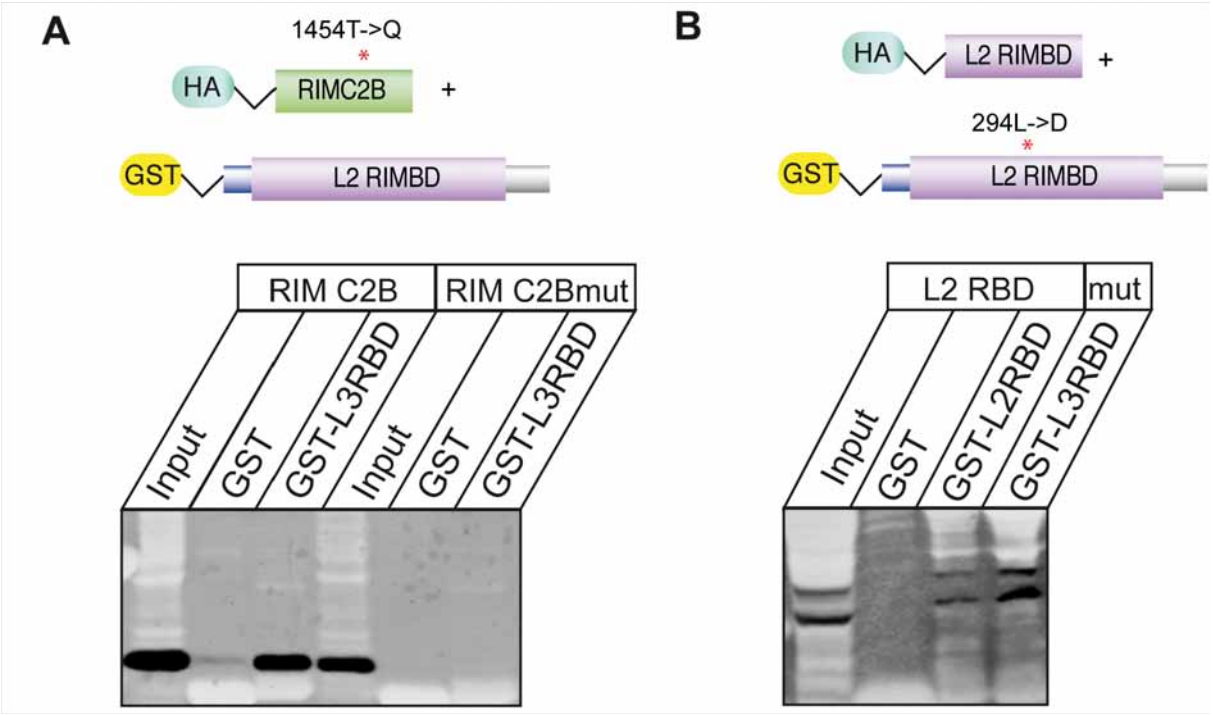

Fig. 5.18: Identification of point mutations to disrupt the Liprin-α2 interaction
(A), (B), Schematic drawings depict the constructs used in each pull down assay. The interaction domains of Liprin-α and RIM1α are depicted with the respective tag. The point mutation is indicated with a red asterisk and the exchanged amino acid is noted above. For the pull down assay GST-fusion proteins were purified and incubated with the binding partner overexpressed in HEK-293 cells. Binding was analyzed by immunoblotting using an anti-HA antibody. RBD: RIM binding domain, *: mutation

To test the effect of the mutation in the Liprin-α2 leucin-zipper motif of the coiled-coil domain on the homodimerization a pull down with the coiled-coil domain of Liprin-α was performed. Here the same domain was once purified from bacteria as a GST-fusion protein and also overexpressed in HEK-293T cells with a HA-tag. In this assay the mutation in the coiled-coil domain did not have an influence on the Liprin-α homodimerization (Fig. 5.18B).

6 Discussion

6.1 Liprins-α share a similar genomic organization but are differentially regulated by alternative splicing

In recent years studies in *C. elegans* and *Drosophila* have identified the Liprin-α family of scaffolding proteins as a key player in synapse development and maintenance as well as in intracellular transport (Spangler and Hoogenraad, 2007; Stryker and Johnson, 2007b). So far, relatively little is known about the mammalian Liprin-α orthologs. To gain insight into the overlapping and diverging properties of the Liprin-α protein family in mammals we carried out a comparative characterization of the human and mouse Liprin-α gene structure and their regulation by alternative splicing.

6.1.1. Phylogenetic analysis

The phylogenetic analysis of the Liprin-α family revealed that in accordance with their presumably fundamental functional role Liprin-α homologs are present throughout all invertebrate and vertebrate genomes. Whereas *C. elegans* and *Drosophila* each express one single Liprin-α gene, Liprins-α were diversified early during evolution into a family consisting of four genes as present in *danio rerio,* mouse or human. Liprin-α proteins exhibit a remarkable degree of overall amino acid identity and similarity within the human and mouse families and are highly conserved from *C. elegans* to human in several regions. However, these regions of striking similarity between species as well as between isoforms only partially coincide with the experimentally mapped sites of protein interaction. The SAM-domains and adjacent linker sequences constitute the regions with the highest degree of homology. In contrast, the RIM and ELKS binding domains are composed of highly homologous and quite diverging sequences. The region of the RIM interaction site is preceded by a sequence that is highly conserved from *C. elegans* to humans. No function or binding partner for this region has been described to date. In contrast, a novel site of protein interaction has only been added later during evolution. The C-terminal PDZ consensus binding site is not present in *C. elegans* and *Drosophila* but found in *Danio rerio* and higher mammals (Suppl. Fig. 1). This is surprising as the only known binding partner for this motif, GRIP, is also expressed in *C. elegans* and *Drosophila*.

6.1.2. Exon-intron structure of human and mouse Liprins-α

The diversification of *Liprin-α* genes into a complex gene family has led to multiple shared properties in their exon-intron structure but has also resulted in various differences in their genomic organization. On the one hand, the size and composition of their exons is very similar and the splice acceptor/donor site phases are conserved among all four genes. On the other hand, the size of the genes varies from very large, with approximately 500 kb for Liprin-α2, to small, with approximately 30 kb for Liprin-α3. In Liprin-α1 and Liprin-α2, the second exon containing the translation start site is separated from the remaining clustered exons by an intron half the size of the whole gene. In the case of Liprin-α2 an additional short exon that is found in all Liprin-α2 transcripts is present in this large intron. This exon represents the only constitutive exon that is solely found in one Liprin-α isoform. Its presence in the Liprin-α2 proteins interrupts the N-terminal region of high homology between the isoforms with unknown functional consequences. In addition, whereas in *Liprin-α1*, -*α2*, and -*α3* the first exon contains only untranslated sequence, in *Liprin-α4* all exons are comprised of protein-coding sequence. Therefore, while Liprin-α2 and Liprin-α4 proteins are the closest family members on the amino acid level, their gene size and structures are quite different.

The high degree of sequence conservation at the protein level between the human and mouse *Liprin-α* orthologs is also reflected in the similarity of their genomic organization. The lengths of the introns are highly comparable for the human and mouse *Liprin-α* orthologs and identical for their exons. However, major differences were found in the splice patterns of Liprin-α1, -α2, and -α4 transcripts for the human and mouse orthologs. We have identified six sites of alternative splicing in *Liprin-α* genes in human and five in mice. Whereas in many synaptic protein families sites of alternative splicing are conserved between family members, e.g. RIMs (Wang and Sudhof, 2003), RIM-BPs (Mittelstaedt and Schoch, 2007), and Neurexins (Tabuchi and Sudhof, 2002), only one of these splice sites was used in all human Liprin-α isoforms and none of them in all mouse Liprin-α isoforms. In the case of the observed difference between the human and mouse Liprin-α1 and Liprin-α4 variants the divergence in alternative spliced exons was due to the fact that the alternatively spliced sequence of the human Liprin-α is not present in the mouse genome. Further

studies will be required to address the biological relevance of human and mouse splice variants to synapse development and membrane organization.

6.1.3. Alternative splicing is developmentally regulated

It is striking that despite the similarities in their genomic organization and their strong homology at the protein level Liprins-α are differentially regulated at the post-transcriptional level. Liprin-α1, the turnover of which is regulated by synaptic activity through APC and CaMKII (Hoogenraad et al., 2007), is the isoform most prone to functional variability that could arise from alternative splicing. One Liprin-α1 splice product contains an insertion in the ELKS binding domain; in a second splice product a short sequence in the linker between the coiled-coil region and the SAM-domains is either present or absent; and a third splice variant alters the distance between the first and second SAM-domain. However, the most remarkable alteration is caused by alternative splicing of the C-terminal exons, which results in transcripts encoding proteins with three (human) or two (mouse) C-termini. Diverging C-termini have already been described for the human Liprin-α1 (Serra-Pages et al., 1995). We now report that in the mouse Liprin-α1 gene alternative splicing generates transcripts with alternate C-termini and that this new splice pattern can be found in human transcripts, too. Therefore, three human C-terminal splice variants are expressed. Liprin-α4 had been described as the only Liprin-α isoform that did not contain the C-terminal PDZ interaction motif (Katoh, 2003). In this analysis we have identified a Liprin-α4 transcript variant in human and mouse that encodes the conserved seven amino acid stretch present in the other Liprin-α isoforms. This C-terminal PDZ interaction motif mediates the binding of Liprins-α to the adaptor protein GRIP. Thereby, alternative splicing at the C-terminus directly affects the interaction of Liprin-α1 and -α4 with GRIP. No GRIP-binding deficient variants exist of Liprin-α2 and -α3, which are the most abundant Liprin-α isoforms at later stages of development and in mature neurons. Also, in the case of Liprin-α1 the isoform most prominently expressed throughout development contains the PDZ-interaction motif. Only for the Liprin-α isoform with the lowest abundance, Liprin-α4, is the GRIP-binding deficient variant the major transcript expressed. GRIP binds to the PDZ-binding motif at the C-terminus of GluR2. By neuronal overexpression of C-terminal GluR2 point and deletion mutants, in which GRIP binding was abolished, it was shown that this region is essential for the surface accumulation of the GluR2

receptors in neurons (Osten et al., 2000). These results suggested that GRIP is not required for normal targeting of GluR2 to the synaptic surface but contributes to the stabilization of AMPA receptors at the synaptic surface. Overexpression of the human-specific Liprin-α1 variant, which does not contain the PDZ-interaction motif and therefore can not bind to GRIP, lead to a reduced number of AMPA receptor clusters along dendrites and a diffuse localization of AMPA receptors in the soma and dendrites (Wyszynski et al., 2002). Therefore, Liprin-α seems to act as a targeting molecule to recruit GRIP and associated proteins to postsynaptic sites or that Liprin-α plays a role in trafficking or transport of the GRIP complex. Due to the multiple interactions of Liprin-α with several components of the postsynaptic specialization, like LAR-RPTPs, GIT1, CASK, and CaMKII, the Liprin-α-GRIP complex may be required for the retention of AMPA receptors, containing the GluR2 subunit, at the surface membrane or could be involved in the regulation of AMPA receptor internalization. AMPA receptors are critically involved in synaptic function and plasticity and therefore mechanisms that regulate targeting and surface expression of the receptors play an important role in these processes (Isaac et al., 2007). In the adult brain Liprin-α isoforms, that can not interact with GRIP are only expressed at low levels. Increasing the level of the non-GRIP-binding Liprin-α variants could provide a mechanism by which neurons control the number of AMPA receptors targeted to the postsynaptic compartment and expressed at the postsynaptic surface. Future studies will be required to determine the signals that control these alternative splice events as well as their precise role.

Even though 206 SAM domains can be identified in human proteins and 178 in mouse, mainly single SAM-domains are found in the context of large multidomain proteins (Qiao and Bowie, 2005). Liprins-α contain three closely spaced tandem SAM-domains. In Liprin-α1, -α3, -α4, and in human but not mouse Liprin-α2 alternative splicing controls the distance between the first and second SAM-domain. In the proteins lacking the alternatively spliced exons the SAM-domains are only separated by 11 amino acids. Structural and biochemical studies are necessary to delineate the resulting functional implications. We furthermore show that usage of alternative exons in most cases is regulated throughout development. Synaptogenesis is associated with structural and functional alterations and several aspects of this process have been shown to be regulated by the complex alternative splicing of proteins, such as agrin, the protocadherins, neurexins, and neuroligins (Li

et al., 2007). Liprins-α on the other hand have been reported to play a role in photoreceptor axon targeting in *Drosophila* (Choe et al., 2006; Hofmeyer et al., 2006) and the development of excitatory synapses (Dunah et al., 2005). Accordingly, this analysis shows that alternative splicing constitutes a means by which Liprins-α can be modified in a developmental manner and by which the properties of the individual isoforms can be diversified independently.

6.2 Liprins-α display overlapping and diverging spatiotemporal and subcellular expression patterns

The single Liprin-α homolog in invertebrates is crucial for synapse formation and function. During evolution Liprin-α genes were diversified leading to four isoforms in mammals. Despite the high degree of homology increasing evidence suggests that the different Liprin-α isoforms can exhibit diverging functional and biochemical properties (Hoogenraad et al., 2007; Zurner and Schoch, 2009). Our analysis of the developmentally dependent alternative splicing of individual Liprin-α isoforms highlights one way in which single Liprins-α and their binding properties can be modified. The characterization of the expression pattern of the Liprin-α isoforms and thus the overlapping and distinct regional and/or subcellular localization of the Liprins-α could indicate further diverging functional roles.

6.2.1. mRNA expression profile of Liprin-α 1-4

Using real-time PCR to gain a first insight into the expression pattern of Liprins-α we observed greatly varying mRNA expression levels in all tissues and brain regions examined. Whereas Liprin-α2 and -α3 are predominantly found in the brain with a similar pattern of distribution, Liprin-α1 is the major isoform outside the nervous system. mRNA levels of Liprin-α4 are very low in all tissues tested, with the highest expression detected in muscle. However, all four Liprin-α isoforms are present in all brain regions even though their strength of expression varies greatly. Our results indicate that the promoters of the four Liprin-α genes are regulated independently. This is supported by evidence from two recent studies. A paper by Mattauch et al. showed that the human Liprin-α4 is strongly upregulated under hypoxia while the other Liprin-α isoforms are not significantly changed (Mattauch et al., 2010). The promoter of Liprin-α4 is directly activated by binding of the hypoxia-inducible factor 1α (HIF-1α). A study on the effects of pathophysiological activity on the expression of

active zone proteins using the Pilocarpine model of temporal lobe epilepsy showed that the four Liprins-α are diffentially regulated under these conditions. Liprin-α2 is strongly upregulated in the hippocampus 6 hours after status epilepticus while Liprin-α4 is downregulated after status epilepticus at all time points studied (Personal communication T. Mittelstaedt). The expression of Liprin-α1 and -α3 show no strong regulation under these conditions.

6.2.2. Protein expression profile of Liprin-α 1-4

To analyze the protein expression pattern of Liprin-α1-4 we generated isoform-specific antibodies. Using these antibodies we found that all four Liprins-α are expressed throughout the brain albeit with diverging abundance. Liprin-α2 and -α3 are the predominant isoforms in the brain with ubiquitously high expression levels, confirming previous results obtained by northern blotting as well as our quantitative real-time RT-PCR data (Serra-Pages et al., 1998; Zurner and Schoch, 2009). Liprin-α1 and -α4 show much lower overall expression levels evenly distributed throughout the brain, with stronger signals in areas of high cell density, like the cerebellar and the olfactory bulb granule cells. Divergent expression of Liprins-α is apparent in several distinct brain regions. In the cerebellum Liprin-α4, and to a lower extend Liprin-α1, are detected at high levels in the molecular layer on the protein level, indicating synaptic localization, while Liprin-α2 and -α3 protein is distinctly expressed in Purkinje Cells. Overlapping but distinct distribution patterns are also observed in the retina where immunolabeling against Liprin-α1 suggests a synaptic localization that in the OPL is most likely postsynaptic. In contrast to Liprin-α2 that is mainly found located at synapses, Liprin-α3 shows a more widespread distribution and may not be present at ribbon synapses. Liprin-α4 exhibits a faint labeling of the synaptic layers but in the OPL surrounds and colocalizes with RIBEYE/CtBP2 indicating a presynaptic localization. Interestingly, unlike other active zone enriched proteins, Liprins-α are not exclusively associated with one of the three defined compartments of the ribbon synapse, the ribbon-associated complex, the plasma membrane/arciform density-associated complex and the border area between these two complexes (tom Dieck et al., 2005). These results demonstrate that even though in most neuronal populations of the brain all four Liprin-α proteins are present each Liprin-α protein is characterized by a distinct expression profile.

6.2.3. Subcellular localization of Liprins-α

Whereas the *C. elegans* Liprin-α, SYD-2, has been described as a presynaptic protein (Zhen and Jin, 1999), Dliprin-α and the mammalian Liprins-α are present in axons and dendrites (Kaufmann et al., 2002; Wyszynski et al., 2002). However, it is still unknown if all Liprin-α proteins are found pre- and postsynaptically or if individual isoforms are targeted preferentially to one side of the synapse. Even though the resolution of confocal microscopy does not allow for an unequivocal identification of a pre- or postsynaptic localization, double immunolabelings of primary neurons show the highest degree of colocalization between pres- as well as postsynaptic markers and Liprin-α2 and -α3, whereas staining for Liprin-α1 and -α4 show less synaptic staining. Taken together, this data suggests that all four Liprin-α proteins are present in axons and dendrites but are differentially enriched at pre- and postsynaptic sites. Analyses using high-resolution techniques like immuno-electron microscopy and STED microscopy will be required to further resolve the distribution in detail.

6.2.4. Liprins-α are present in inhibitory neurons

Co-immunolabeling show, that all four Liprin-α proteins are expressed by excitatory and inhibitory cells. In primary neuronal cultures Liprin-α1-4 are present in cells that are immunopositive for GAD67, a marker for inhibitory presynapses. In the hilus of the hippocampus immunoreactivity of Liprin-α2, -α3 and -α4 coincides with the distribution of putative interneurons and in the cerebellum Liprin-α2 and -α3 are distinctly expressed by Purkinje Cells and detected in putative interneurons in the molecular layer. These results argue that there is not one Liprin-α molecule specific for the organization of protein complexes in inhibitory neurons as has been described for the neuroligin protein family where neuroligin 2 is the isoform selectively expressed by inhibitory cells (Varoqueaux et al., 2004).

6.2.5. Liprin-α1 displays a diverging spatial and temporal expression profile

Intriguingly, the spatial and temporal expression profile of Liprin-α1 stands out from the other three members of the Liprin-α protein family. Expression levels of Liprin-α1 protein during development were highest at the earliest time point tested (embryonic day 12.5) and decreased dramatically after birth. Furthermore, Liprin-α1 is the only isoform expressed ubiquitously outside of the brain and the main Liprin-α molecule in cultured glial cells where it is located in a restricted focal manner at the rim of the

cell. Liprin-α1 was found to colocalize with the receptor tyrosine phosphatase LAR at focal adhesions in non-neuronal tumor cell lines (Serra-Pages et al., 1995). Overexpression of Liprin-α1 enhanced cell spreading and the formation of lamellipodia and focal-adhesions at the cell edge while knock-down of Liprin-α1 inhibited cell spreading (Shen et al., 2007; Asperti et al., 2009). These findings together with the observed expression profile suggest that Liprin-α1 might play a role in organizing protein complexes that are involved in cell migration during brain development.

Table 6.1: Overview of the expression pattern of Liprin-α1-4.

	Organs		Brain		Synapse		Inter-neurons (ICC)	Glia (ICC)
	mRNA	protein	mRNA	protein	ICC	IHC		
Liprin-α1	+	+	+	+	+	+++	+	+
Liprin-α2	liver, testes	testes	+	+	+++	++	+	-
Liprin-α3	-	-	+	+	+++	++	+	-
Liprin-α4	muscle, testes	-	+	+	+	+++	+	-

The detected expression of Liprin-α isoforms using Real-time PCR (mRNA), immunoblotting (protein), immunhistochemistry (IHC) and immuncytochemistry (ICC) in the brain as well as tissues outside the brain. The signals detected at the synapse are graded + to +++.

6.2.6. Liprins-α expression pattern in growth cones

The analysis of Liprin-α expression in the growth cones of DIV4 neurons points in the direction of a similar functional role as Liprin-α1, -α2 and -α3 accumulate along the leading edge of the growth cone. The adhesion between growth cones and the extracellular matrix or adjacent cells is mediated via specific adhesion molecules, i. e. integrins, Ig cell adhesion molecules (IgCAMs), and cadherins (Bard et al., 2008). Liprin-α1 has been shown to play a role in the distribution and stabilization of β-integrins (Asperti et al., 2009) and is linked indirectly to cadherins via LAR (Dunah et al., 2005) and to PIX via GIT1 (Ko et al., 2003b). In addition, there is evidence from *Drosophila* that Dliprin-α in concert with LAR and N-cadherin is required for the regulation of photoreceptor targeting (Choe et al., 2006; Prakash et al., 2009). Furthermore, the levels of Liprin-α1, but not Liprin-α2, are tightly regulated at the synapse by synaptic activity and are directly correlated to dendritic arbor complexity (Hoogenraad et al., 2007). This raises the question if all Liprin-α isoforms can

function as regulators of cell spreading and motility or if this function is restricted to Liprin-α1.

6.3 Dynamics of Liprin-α2 at the presynaptic bouton

The level of active zone enriched proteins need to be sustained in the absence of obvious spatial or structural boundaries between the presynaptic bouton and the axon. At the same time alterations in the synapse composition are critical for synaptic plasticity. It has been hypothesized that while many proteins have a high flux some scaffolding proteins have a very slow turn over and thus form the basis for synaptic tenacity (Owald and Sigrist, 2009).

6.3.1. Localization of GFP-Liprin-α2

GFP-Liprin-α2 fusion proteins are ubiquitously present throughout the neuron in primary neurons but are enriched at putative presynaptic boutons along the axon. GFP-Liprin-α2 coexpressed with its interaction partner cherry-RIM1α show an increased accumulation at putative presynaptic boutons. Possibly the coexpression enhances the targeting of GFP-Liprin-α2 to the presynaptic bouton. A similar effect has been reported for the interaction between Liprin-α1 and ELKS (Ko et al., 2003a). Due to the low levels of presynaptic GFP-Liprin-α1 the observed effect of coexpression was very strong. GFP-Liprin-α2 is already enriched at the presynapse and thus a comparable effect would not be expected. About the interdependence of ELKS and Liprins-α in regard to their localization to the mammalian presynaptic AZ nothing is known. In *C. elegans* the absence of Liprin-α/SYD-2 leads to a disrupted localization of RIM/unc-10 while Liprin-α/SYD-2 localization is unchanged in RIM/unc-10 mutants (Dai et al., 2006).

GFP-Liprin-α2 shows a punctate localization at the presynaptic bouton. This could indicate that Liprin-α2 is restricted to certain subdomains of the active zone as it was observed for the Liprin-α homolog in *Drosophila* (Fouquet et al., 2009). At the NMJ Dliprin-α was shown to form distinct clusters at the edge of the active zone as labeled by Bassoon using STED microscopy. Further investigation using high-resolution microscopy, e.g. STED would be required to analyze the distribution of endogenous mammalian Liprin-α2.

So far no targeting sequence has been identified for Liprins-α. In contranst to the post synaptic density (PSD) where many proeins are targeted via PDZ interactions

no distinct motif is known for active zone proteins. So far the only protein studied is Bassoon, a protein highly enriched at the active zone. It was shown that a central coiled-coil domain is critical but not sufficient for the targeting of Bassoon to the active zone using deletion mutants (Dresbach et al., 2003). To investigate the role of the structural domains for the targeting of Liprin-α as well as for the morphology of the neuron we transfected GFP-tagged deletion mutants containing the N-terminal half, only the coiled-coil domain or the C-terminal half.

A decrease in arborisation of the dendritic tree at DIV17 was described for overexpression of the N-terminal half of Liprin-α1 at DIV13 (Hoogenraad et al., 2007). Here we transfected Liprin-α2 deletion constructs at DIV 3-5 and imaged neurons at DIV7 as well as DIV14. We could not detect any obvious effects of the deletion mutants on the dendritic branching of the neurons or on the targeting. A more detailed investigation would be necessary to identify the role of the domains for targeting of Liprin-α including e.g. time lapse imaging to study the trafficking of Liprins-α into the axon and dendrites.

6.3.2. Dynamics of Liprin-α2 and RIM1α at the presynapse

FRAPA experiments suggest that the scaffolding protein Liprin-α2 has a slow turn over at the presynapse while its interaction partner RIM1α shows faster dynamics in the performed FRAP experiments. In the FRAP experiment GFP-RIM1α signal had completely recovered 40 min after bleaching of the presynaptic bouton. A residual paGFP-Liprin-α2 signal could still be detected at some boutons after 8h in the FRAPA experiments while about 40% of the signal was lost from the presynaptic bouton after 3 h. This may seem contradictory at first as GFP-Liprin-α 2 has a higher proportion of cytoplasmic protein but possibly it could reflect the putative roles of these two active zone proteins. While Liprins-α are hypothesized to function as a scaffold and maintain the active zone structure and thus need to be robustly integrated in the proteinacous network at the active zone, RIM1α needs to be much more mobile to perform its role in priming of SVs. Most likely both proteins have two pools with different exchange rates, a slow pool reflecting the proteins integrated in the CAZ and a fast pool of unbound proteins as has been shown for three proteins, Basoon, Munc13 and synapsin I. These proteins also show very different dynamics (Fig. 6.1). For the large scaffolding protein Bassoon a time constant of >8h for the slow pool and a time constant of 5 min for the fast pool with a relation of 4:1 was

described (Tsuriel et al., 2009). In contrast much faster dynamics were reported for synapsin I, a molecule that is thought to link SV and the cytoskeleton. For synapsin I a time constant of the fast pool of 2.3 min and 87 min for the slow pool was observed (Tsuriel et al., 2006). Interestingly, the fraction of synapsin I belonging to the fast pool was activity dependent. About 30% of the protein belonged to the fast pool in unstimulated conditions while under stimulation the pool makes up about 50% of the protein. For Munc13, a protein involved in priming of synaptic vesicles, very similar time constants for the fast pool (3 min) as well as for the slow pool (80 min) were found (Kalla et al., 2006). To precisely define the time constants of Liprin-α2 and RIM1α and their possible dependence on activity more experiments would be required.

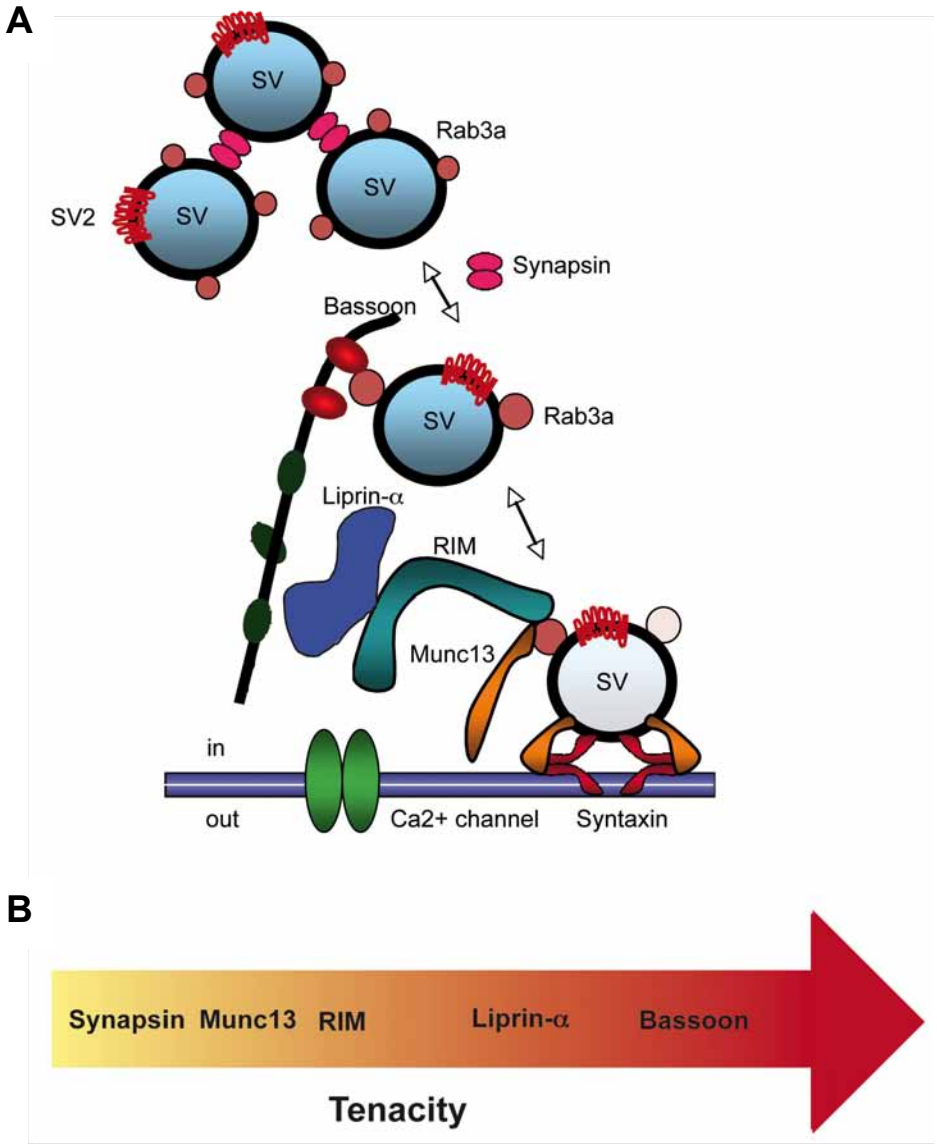

Figure 6.1: Relative tenacity of active zone and synaptic vesicle proteins
(A), Schematic drawing of SVs and selected AZ components. SV, synaptic vesicle. Modified from a figure by Noam Ziv. (B), Proteins are ordered from dynamic to stabil.

6.4 Disruption of Liprin-α function

We pursued two approaches to study the functional role of Liprins-α, shRNAs to investigate the consequences of the loss of single or multiple Liprins-α and point mutations to study the effect of the disruption of specific interactions.

So far, in contrast to *C. elegans* and *Drosophila*, there are no knockout mice for Liprins-α available. Our analysis of the expression of Liprins-α showed that all isoforms are present in all brain regions and in addition Liprin-α1 is also widely expressed outside the brain, e.g the lung and muscles, and is implicated to play a role in development. Therefore, it would be required to design conditional knockouts for all four isoforms and then cross quadruple knockouts to Cre-expressing mice. The analyses would require multiple generations of breeding which would be a very time consuming process. In addition, the knockout could be lethal early in development. We therefore decided to pursue an shRNA approach, which allows for studying the effect of a knock-down of single as well as combination of Liprin-α isoforms. Next to experiments in primary cell cultures using the rAAV virus as a method of shRNA introduction allows to study the effect of the knockdown *in vivo* by injecting the virus into either embryos or adult animals. Thus, this approach allows circumventing some of the problems of knockout animals like lethality, compensation or the cross breading of multiple mouse lines.

Here, we could identify shRNAs against Liprin-α2 and -α3, the two major Liprin-α isoforms in the brain. This tool allows testing the role of Liprins-α in different processes like synapse maturation or maintenance using assays like the synapse maturation assay established in the Dresbach lab (Wittenmayer et al., 2009). It would also be interesting to analyze the effect of the knock down on the dynamics of Liprin-α interaction partners using time-lapse imaging.

As a second approach we aimed to identify point mutations to disrupt the interaction of RIM1α and Liprin-α as well as the Liprin-α homodimerization. The advantage of point mutations in comparison to a knockout approach is that in a knockout animal the missing protein can potentially be substituted by another protein. This could prevent a phenotype. When a point mutation is introduced the protein is still present but not functional e.g. in respect to a specific interaction. A point mutation in Rim1α effectively disrupting the interaction between Liprin-α2 and RIM1α could be identified. Other studies showed that point mutations can be an effective tool to

delineate the role of specific interactions. Using a point mutation that disrupts the RIM1α-Munc13 interaction it was shown that RIM1α is critical for enrichment of Munc13 at the active zone (Andrews-Zwilling et al., 2006).

We intend to employ the identified point mutation e.g. to characterize the role of the RIM1α-Liprin-α interaction using time-lapse imaging. In addition, we plan to identify further point mutations that disrupt other interactions to be able to characterize the role of different interactions in Liprin-α function.

7 Acknowledgements

The realization of my PhD thesis would not have been possible without the help and support of others. Therefore, I wish to express my gratitude to all people who contributed to this work.

I am indebted to Prof. Susanne Schoch for offering me the opportunity to do my PhD in her lab and for being such an enthusiastic, patient and encouraging mentor.

I would like to thank my cooperation partners without whom parts of my project would not have been possible to realize.
Susanne tom Diek, Max Planck Institute for Brain Research, Department of Synaptic Plasticity, Frankfurt did the immunohistochemistry of the retina.
Carsten Reissner, Department of Anatomy, University Münster did the modeling of the tertiary structure of Liprin-α and based on this model the prediction of amino acids to disrupt specific interactions.
Noam Ziv, Rappaport Institute and the Department of Anatomy and Cell Biology, Technion, Faculty of Medicine, Haifa, Israel let me stay in his lab and taught me time-lapse imaging in combination with FRAP and FRAPA.
I would also like to thank Prof. Benjamin Kaupp, Caesar, Bonn for access to the laser scanning microscope.

Many thanks to the AG Schoch and AG Becker. Special thanks to Sarah Stellbogen, who did the rAAV virus production, cut the brain sections and supported my work in the last year, to Gudrun, Mario and Anne for the preparation of primary neuronal cultures, to Verena, Celine, Tobi and to Karen for her support, the discussions and for proof reading my thesis. I would also like to thank the AG Beck and AG Dietrich and here especially Elizabeth.

Many, many best thanks to my friends, especially to Kerstin, Michi and Saskia for sharing the last decade and to my family, particularly to Eva!

8 Appendix

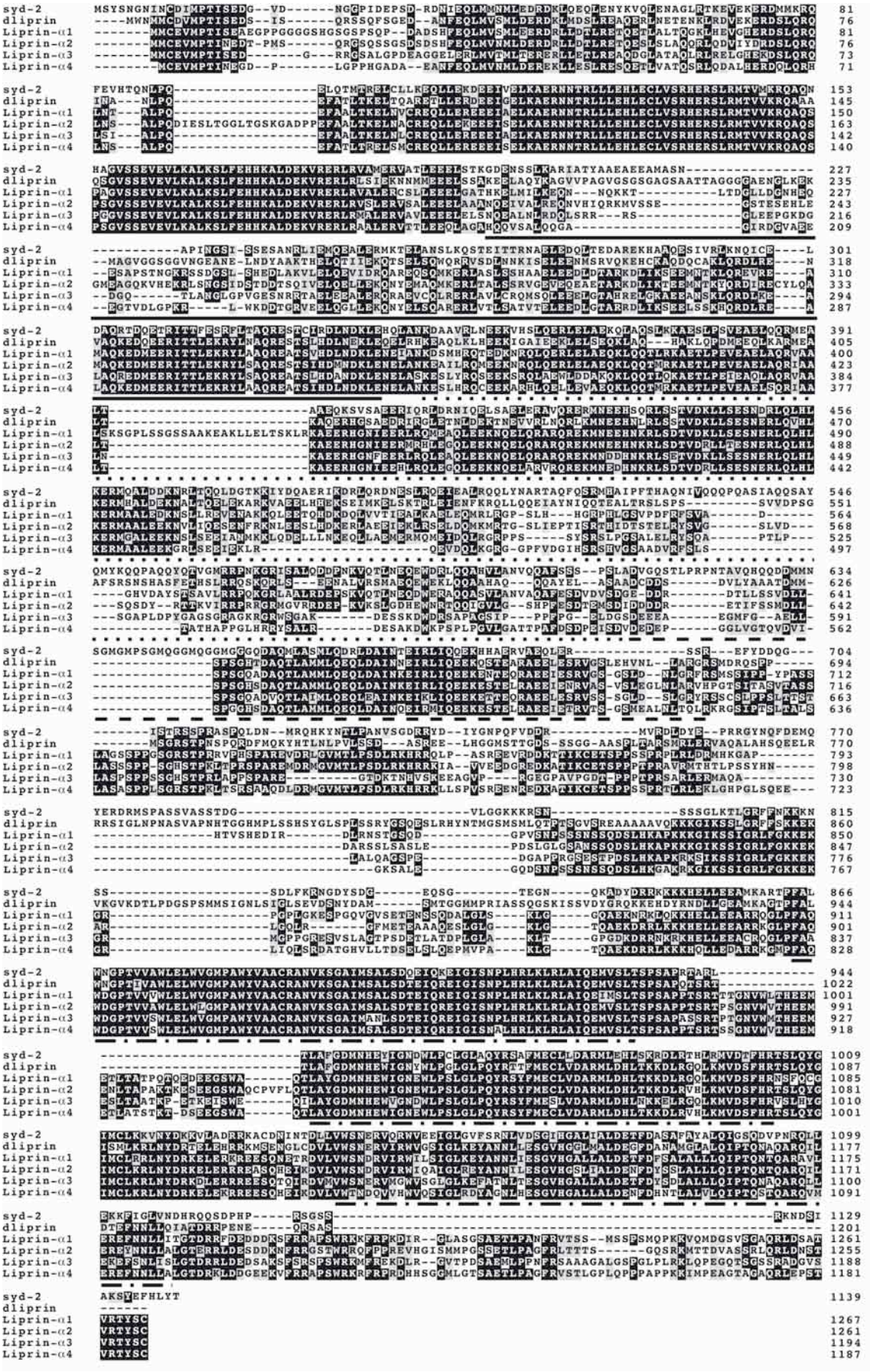

Suppl. Fig. 1: Alignment of *C. elegans* (SYD-2), *Drosophila* (Dliprin), and mouse Liprins-α1-4.
Sequences were aligned using T-coffee. Boxshade was used to create the alignment figure. Black boxes indicate identical amino acid residues and grey boxes mark similar residues.

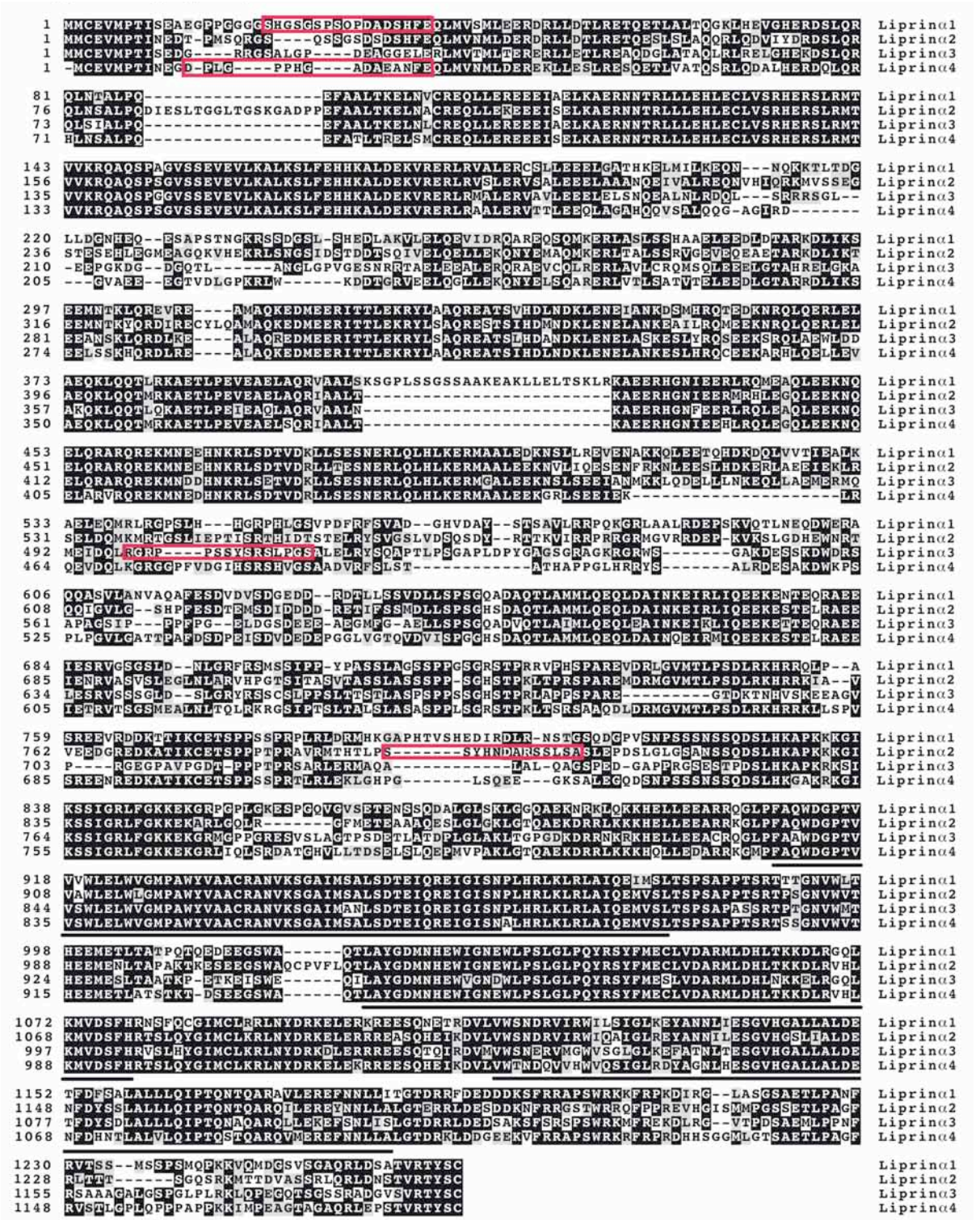

Suppl. Fig. 2: Alignment of the amino acid sequence of mouse Liprin-α1-4.
Red boxes highlight the locations of the peptide sequence used for the generation of the isoform-specific antibodies.

Suppl. Table 1

Exon-intron structure of the human *Liprin-α1 (PPFIA1)* gene

Exon	Nucleotide no.			Size	Flanking sequences			
1	69,794,471	-	69,794,668	198	agccgggccc	GCTCCTCCT	GCGAGCAAG	gtaagggagc
2	69,795,926	-	69,796,190	264	tcatttcaag	**ATG** ATG TGC	CTT CCA CAG	gtatgagtgc
3	69,848,156	-	69,848,257	102	gattttctag	GAG TTC GCA	AAC ACC AGG	gtgagtgtga
4	69,848,600	-	69,848,765	165	tttatttcag	CTG CTG TTA	GAT GAA AAG	gtgccatcag
5	69,849,254	-	69,849,328	75	ttattttcag	GTG AGA GAG	CAC AAA GAG	gtaagcttga
6	69,850,016	-	69,850,117	102	ttgctttcag	CTA ATG ATT	AGT GGA AAG	gcaagtctgt
7	69,850,351	-	69,850,572	222	cccctatcag	AGA TCT TCT	GTC CGT GAA	gtgagcaata
8	69,853,927	-	69,854,073	147	cctaatttag	GCC ATG GCC	CAT CGA CAG	gtaatggatt
9	69,855,714	-	69,855,848	135	cattttatag	ACT GAA GAT	CTT TCC AAG	gtagtgccat
10*	69,856,776	-	69,856,850	75	ggctttgtag	TCT GAC CTT	CTT AGG AAG	gtagaatggg
11	69,857,224	-	69,857,307	84	ctgctgacag	GCT GAA GAG	CTG CAG CGG	gtgagcatgc
12	69,859,317	-	69,859,448	132	cctgctttag	GCA AGG CAA	GAA GAT AAG	gtaagttaga
13	69,861,119	-	69,861,181	64	ctttttcag	AAC TCT CTT	CAC GAT AAG	gtactgaaat
14	69,862,128	-	69,862,207	79	ttttctgtag	GAT CAG CTT	CTT CAT CAT GG	gtatggtatt
15	69,862,925	-	69,863,060	136	catgtttcag	C CGA CCC CAC	CCT TCC AAG	gcaaggtctt
16	69,867,423	-	69,867,646	224	ttgtttatag	GTA CAA ACT	AAA GAG ATC AG	gtgtgtgcaa
17	69,871,943	-	69,872,174	232	tttattttag	G TTG ATT CAG	ATG ACC CTT	gtacgtatcc
18*	69,874,748	-	69,874,777	30	catctatcag	CCT AGT GAT	CGT AGA AAG	gtaaattgtt
19	69,878,055	-	69,878,206	152	caccctcag	TTG CCA CCT	GAC ATA AGG AA	gtaaggagcc
20	69,879,393	-	69,879,565	173	ttcctcgaag	C TCC ACA GGC	TTA GGA CAA G	gttggttggt
21	69,879,915	-	69,880,008	94	ttcctcacag	CT GGT GTT TCC	CTT CAA AAA AA	gtaagctttg
22	69,885,849	-	69,885,930	82	tcctttatag	G CAT GAA TTG	TGG CTA GAG	gtacatcctt
23	69,886,042	-	69,886,242	201	ccgcctccag	CTC TGG GTT	TCT AGA ACG	gtacgttcag
24*	69,889,127	-	69,889,189	63	gtcaccttag	ACC ACA GGA	CCG CAA ACG	gttagtcacg
25*	69,889,695	-	69,889,721	27	gtaaccccag	GAA GAT GAG	TGG GCT CAG	gttggagtct
26a	69,895,963	-	69,896,144	176	ttatgaaaag	CAG ACA CTC	AGT TTT CAC AG	gtaacttaat
26	69,895,966	-	69,896,144	173	tgaaaagcag	ACA CTC GCC	AGT TTT CAC AG	gtaacttaat
27	69,896,231	-	69,896,328	98	ttccaaatag	A AAC AGT TTC	GAA ATA AAA G	gttagtacat
28	69,898,672	-	69,898,847	176	tcttttgcag	AC GTG CTT GTT	AAC ACA CAG	gtgacgccaa
29	69,900,286	-	69,900,354	69	gttatttcag	GCT CGT GCT	TTT GAT GAA	gtaagttttt
30	69,901,784	-	69,901,949	166	aatttaccag	GAT GAT GAT	AGA TGG ACG	gtatgtgatg
30b	69,901,784	-	69,902,146	363	aatttaccag	GAT GAT GAT	**TGA** TGGGTC	aaaacacgct
31*	69,905,842	-	69,905,911	71	gttgaaacag	GCA ATG TAT	**TAA** AGTCTCCTGTTG **TGA** TTATGCAGCA...	gtgagtagag
32	69,906,757	-	69,908,511	1394	tattttccag	TTT ACC CAC	CACTGCTCA	caaaggtggc

Data are based on the analysis of human genome sequences in the NCBI, Ensembl and UCSC databases. Nucleotide numbers correspond to thoses of the assembled UCSC genome.
*Exons that are subject to alternative splicing.

Suppl. Table 2

Exon-intron structure of the mouse *Liprin-α1 (PPFIA1)* gene

Exon	Nucleotide no.			Size	Flanking sequences			
1	151,739,634	-	151,739,346	198	ccgacgcgcc	GGACGTCGG	CCGGCCAAG	gtgagggcgg
2	151,738,438	-	151,738,185	264	gccggccaag	**ATG** ATG TGC	CTT CCA CAG	gtatgcccat
3	151,706,966	-	151,706,865	102	cactctctag	GAG TTT GCT	AAC ACT AGG	gtcagtcact
4	151,706,694	-	151,706,530	165	tctgttgcag	CTG CTG TTG	GAT GAG AAG	gtacaatcac
5	151,705,955	-	151,705,881	75	tcacttgcag	GTA CGA GAG	CAC AAA GAG	gtaagcttgg
6	151,705,551	-	151,705,450	102	tcttttgtag	CTA ATG ATT	AAC GGC AAG	gcaagtcctt
7	151,705,272	-	151,705,054	222	tgcttttcag	AGA TCT TCT	GTC CGT GAA	gtgagtgcgg
8	151,703,651	-	151,703,505	147	tccaacacag	GCA ATG GCC	CAC CGA CAG	gtactggggt
9	151,702,025	-	151,701,891	135	ccctttctag	ACA GAA GAC	CTC TCC AAG	gtgcgcctgg
10*	151,700,851	-	151,700,778	75	tgctttatag	TCT GGT CCT	CTT AGG AAG	gtagaattgt
11	151,700,429	-	151,700,346	84	ttaccggcag	GCT GAG GAG	CTG CAG CGG	gtatgtatgg
12	151,699,282	-	151,699,251	132	tctgttttag	GCA AGG CAG	GAG GAC AAG	gtgagcagat
13	151,696,841	-	151,696,778	64	tcttttcag	AAT TCT CTA	CAT GAT AAG	gtacctcact
14	151,696,266	-	151,696,187	79	tgttttctag	GAC CAA CTT	CTC CAT CAT GG	gtatggcggt
15	151,694,169	-	151,694,034	136	catgtttcag	C CGA CCC CAT	CCC TCC AAG	gcaaggcctc
16	151,692,199	-	151,691,977	224	ttgttggtag	GTG CAG ACC	AAA GAG ATC AG	gtatatatct
17	151,691,039	-	151,690,808	232	tgtattttag	G CTG ATA CAA	ATG ACT CTG	gtaagtgggg
18*	151,688,801	-	151,688,772	30	catctgtcag	CCT AGT GAC	CGG AGA CAG	gtaaatcatt
19	151,686,308	-	151,686,157	152	ttgctctcag	TTG CCA GCT	GAC CTG AGG AA	gtaaggagcg
20	151,684,784	-	151,684,612	173	ttccttaaag	C TCC ACA GGC	CCA GGG CAA G	gttggtaggt
21	151,684,295	-	151,684,202	94	ttccttgtag	TT GGT GTT TCA	CTT CAG AAA AA	gtaagctgct
22	151,677,728	-	151,677,647	82	tccctcatag	G CAC GAG CTG	TGG TTA GAG	gtgagtcctc
23	151,677,557	-	151,677,357	201	tcatgtctag	CTC TGG GTT	TCC AGG ACG	gtaagtctcc
24*	151,675,164	-	151,675,102	63	ggtaccttag	ACC ACA GGA	CCA CAA ACG	gttagtcact
25*	151,674,625	-	151,674,596	30	gtaacatcag	GAA GAC GAG	TGG GCT CAG	gttggcatct
26a	151,671,110	-	151,670,938	176	ttactaaaag	CAG ACT CTA	AGC TTC CAC AG	gcaagtgctc
26	151,671,113	-	151,670,938	173	ctaaaagcag	ACT CTA GCA	AGC TTC CAC AG	gcaagtgctc
27	151,670,846	-	151,670,749	98	ttgtaaacag	A AAC AGT TTC	GAG ACA AGA G	gtgagttccc
28	151,668,340	-	151,668,165	176	tctcttgcag	AT GTG CTT GTG	AAT ACG CAG	gtgaccccag
29	151,667,684	-	151,667,616	69	actgttttag	GCT CGA GCT	TTT GAT GAG	gtaagtggat
30	151,667,155	-	151,666,990	166	ggtttgctag	GAT GAT GAC	AGA TGG ACG	gtatgtggtg
31*	151,665,002	-	151,664,932	71	gtggagacag	GTA GTG TGT	**TAG** AGCCTCCTGCTG AGA **TGA** CGT	gtgagtagag
32	151,663,894	-	151,662,660	1394	ttacttgcag	TTT ACC CAC	...CCTGCCAGTT	aagagtgctg

Data are based on the analysis of human genome sequences in the NCBI, Ensembl and UCSC databases. Nucleotide numbers correspond to thoses of the assembled UCSC genome.
*Exons that are subject to alternative splicing.

Suppl. Table 3

Exon-intron structure of the human *Liprin-α2 (PPFIA2)* gene

Exon	Nucleotide no.			Size	Flanking sequences			
1	80,676,564	-	80,676,310	254	ccgttgctag	GGAAATGGT	AGACATTAG	gtacagaagc
2	80,672,133	-	80,671,883	248	tttctttaag	CA ATG **ATG** TGT	CTG CCA CAG	gtatgcttcc
3	80,594,754	-	80,594,701	54	ccctttcag	GAT ATC GAA	GAT CCA CCG	gtaagttaga
4	80,375,776	-	80,375,675	102	acttttccag	GAA TTT GCT	AAC ACA AGA	gtaagtgtaa
5	80,363,630	-	80,363,466	165	aacccaatag	CTA TTA CTG	GAT GAA AAG	gtatagtatg
6	80,357,956	-	80,357,882	75	tttcttctag	GTA AGG GAG	AAT CAG GAG	gtaacctgcc
7	80,323,813	-	80,323,697	117	tattttgcag	ATT GTT GCC	CAT GAG AAG	gtatgacaca
8	80,302,154	-	80,301,933	222	atttctgcag	CGT TTG TCC	ATT AGG GAG	gtaagtgatt
9	80,293,852	-	80,293,706	147	ttaattgtag	GCC ATG GCA	CTG CGG CAG	gttcagtatc
10	80,292,678	-	80,292,544	135	cccatttcag	ATG GAA GAG	CTA ACC AAG	gtactgcact
11	80,287,104	-	80,287,021	84	ttcttaacag	GCT GAA GAG	CTT CAA AGA	gtatgtatat
12	80,286,766	-	80,286,635	132	aaaatgtaag	GCT AGG CAA	GAA GAA AAG	gtaaaacgat
13	80,285,080	-	80,285,018	63	ttttctttag	AAT GTT TTA	CAT GAT AAG	gtataatgga
14	80,280,694	-	80,280,603	92	gatttttag	GAA AGA TTA	ACA ATA CCA AG	gtaacattaa
15	80,276,127	-	80,275,992	136	ttttttccag	A ACT CAT CTA	GAG CCA AAG	gttaatcttt
16	80,271,249	-	80,271,029	221	caccattcag	GTG AAA TCT	AAA GAA ATC AG	gtaacttcaa
17	80,265,680	-	80,265,443	238	tatctttcag	G CTA ATT CAG	ATG ACA CTG	gtatggtgat
18*	80,262,603	-	80,262,574	30	ccaatcacag	CCA AGT GAT	CGG AGA AAG	gtacagtaaa
19	80,259,118	-	80,258,988	131	ttgcttctag	ATT GCA GTT	GAT GCT CGA AG	gtaagactct
20	80,257,244	-	80,257,090	155	tgttttgcag	T AGT TTA TCT	GGG CAG CTC C	gtaagtatgc
21	80,243,780	-	80,243,687	94	ctcttcacag	GA GGC TTT ATG	CTA AAG AAA AA	gtaggtttgg
22	80,217,292	-	80,217,211	85	tatacttcag	G CAT GAA CTT	TGG CTA GAG	gtaagagaat
23	80,212,945	-	80,212,745	201	tatctaacag	CTT TGG TTG	TCT CGA ACT	gtgagtcagt
24*	80,202,213	-	80,202,151	63	tcctcactag	CCT TCA GGC	GCA AAA ACG	gttagtctta
25*	80,200,949	-	80,200,920	30	gctaacacag	AAA GAA TCT	TGG GCC CAG	gtaggagatt
26a	80,199,360	-	80,199,167	194	acaattctag	TGT CCG GTT	AGT TTC CAT CG	gtaggtgttt
26	80,199,342	-	80,199,167	176	ttttctacag	ACC CTG GCT	AGT TTC CAT CG	gtaggtgttt
27	80,195,324	-	80,195,227	98	aaaaaaaaag	A ACA AGT TTA	GAA ATA AAA G	gtaatatatc
28	80,185,997	-	80,185,805	193	cttttcctag	AC TGT TTG GTG	AAC ACC CAG	gcaagtcact
29	80,184,925	-	80,184,862	64	acgtcaacag	GCA AGG CAG	CTG GAT GAA	gtaagtccac
30	80,181,300	-	80,181,141	160	gtactggcag	AGT GAT GAC	ACA ACA GAT G TGT **TGA** CCA...	gtacagtagt
31	80,179,950	-	80,179,859	92	ccatttgcag	TT GCT TCA TCA	TGACCTGCT	gtgagtagtt
32	80,177,570	-	80,175,914	1657	tatattttag	ATGGCGTCCT	ATATAGGAA	

Data are based on the analysis of human genome sequences in the NCBI, Ensembl and UCSC databases. Nucleotide numbers correspond to thoses of the assembled UCSC genome.
*Exons that are subject to alternative splicing.

Suppl. Table 4

Exon-intron structure of the mouse *Liprin-α2 (PPFIA2)* gene

Exon	Nucleotide no.			Size	Flanking sequences			
1	105,907,395	-	105,907,647	252	ccgttgctag	GGAAATGGT	AGACATTAG	gtacagaagc
2	105,911,687	-	105,911,938	251	tttctttaag	CA **ATG** ATG TGT	CTA CCT CAG	gtacgagtct
3	105,994,303	-	105,994,355	54	ccctttccag	GAC ATC GAA	GAT CCA CCG	gtaagttaga
4	106,180,543	-	106,180,644	102	ccacttctag	GAG TTT GCT	AAC ACA AGA	gtatgtatta
5	106,199,044	-	106,199,203	165	gatcccacag	CTG TTA CTG	GAT GAA AAG	gtatcgtaca
6*	106,204,530	-	106,204,604	75	tttcttctag	GTA AGG GAG	AAT CAG GAG	gtaacacacc
7	106,237,793	-	106,237,909	117	tatttttcag	ATT GTT GCC	CAT GAA AAG	gtatgatgca
8	106,256,392	-	106,256,623	222	cttcctgcag	CGT CTA TCC	ATC CGA GAG	gtaggtagct
9a	106,265,933	-	106,266,091	159	acctttacag	TGT TAT TTA	TTG CGG CAG	gttcagtatc
9	106,265,945	-	106,266,091	147	ttatttacag	GCC ATG GCT	TTG CGG CAG	gttcagtatc
10	106,267,622	-	106,267,756	135	cccatttcag	ATG GAA GAA	CTA ACA AAG	gtactgcact
11	106,272,752	-	106,272,835	84	tccttaacag	GCT GAA GAG	CTT CAA AGA	gtatgcatga
12	106,273,108	-	106,273,239	132	taactataag	GCT AGA CAA	GAA GAG AAG	gtacagtctc
13	106,274,336	-	106,274,399	63	ttttccatag	AAT GTT TTG	CAT GAT AAG	gtatcatgga
14	106,279,743	-	106,279,833	92	ttatttttag	GAA AGA TTA	ACT ATA TCA AG	gtaacattac
15	106,291,993	-	106,292,128	136	tgtttttcag	A ACT CAT ATA	GAA CCA AAG	gtgattgctt
16	106,294,465	-	106,294,685	221	cattattcag	GTG AAA TCC	AAA GAA ATA AG	gtatcgatac
17	106,295,217	-	106,295,454	238	tatcttctag	A CTA ATT CAA	ATG ACC CTG	gtatgattat
18	106,296,833	-	106,296,862	30	cccttaacag	CCA AGT GAT	CGG AGA AAG	gtaatgtaaa
19	106,300,309	-	106,300,440	131	ctatttctag	ATT GCA GTG	GAT GCC CGG AG	gtaaggctca
20a	106,302,303	-	106,302,457	155	tgttttgaag	C AGT TTA TCT	GGG CAG CTT C	gtaagtatgg
20	106,302,306	-	106,302,457	152	tttgaagcag	T TTA TCT GCC	GGG CAG CTT C	gtaagtatgg
21	106,306,935	-	106,307,028	94	ttctccacag	GA GGC TTC ATG	CTG AAG AAA AA	gtaggtttgg
22	106,330,487	-	106,330,569	82	tgtacttcag	G CAT GAA CTT	TGG CTG GAG	gtaagcaaaa
23	106,333,374	-	106,333,574	201	aatacaacag	CTC TGG CTG	TCG CGT ACT	gtgagtcaat
24	1063,406,99	-	106,340,761	63	ctctcattag	CCT TCA GGC	GCA AAA ACG	gttagtcttt
25	106,341,873	-	106,341,902	30	gctaacccag	AAA GAA TCT	TGG GCC CAG	gtaggaaact
26a	106,343,422	-	106,343,615	194	acaattccag	TGT CCG GTT	AGT TTC CAT CG	gtaggttgtg
26	106,343,440	-	106,341,902	176	ttttctacag	ACC CTG GCT	TGG GCC CAG	gtaggaaact
27	106,344,769	-	106,344,866	98	atgaaaatag	A ACA AGT TTA	GAA ATA AAA G	gtacatgccc
28	106,350,621	-	106,350,796	176	cttttcctag	AT GGT TTA GTG	AAC ACC CAG	gcaagcatgc
29	106,352,737	-	106,352,805	69	atgttaacag	GCA AGG CAG	CTG GAT GAA	gtaagttctt
30	106,364,759	-	106,364,918	160	gtactggcag	AGT GAC GAC	ACG ACA GAC G TGT **TGA** CAA...	gtacagtagt
31	106,366,110	-	106,366,201	92	tcatttgcag	TT GCT TCA TCA	TGACCTGCT	gtgagtagtt
32	106,368,179	-	106,370,502	2324	ccccttcag	ATGTCATCT	CTTTTGGCG	aataaaacaa

Data are based on the analysis of human genome sequences in the NCBI, Ensembl and UCSC databases. Nucleotide numbers correspond to thoses of the assembled UCSC genome. *Exons that are subject to alternative splicing.

Suppl. Table 5

Exon-intron structure of the human *Liprin-α3 (PPFIA3)* gene

Exon	Nucleotide no.			Size	Flanking sequences			
1	54,314,475	-	54,314,791	317	tgggggggaag	GTGGGATTT GCCCGCACCG	ACCAGGCAG	gtaagagccc
2	54,322,928	-	54,323,182	255	cgccccgcag	... GCC **ATG** ATG	CTG CCC CAG	gtctgggcgg
3	54,323,436	-	54,323,537	102	gtctggacag	GAG TTT GCA	AAC ACG CGG	gtgaggggtg
4	54,323,917	-	54,324,081	165	gtgcttgcag	CTC CTC CTG	GAT GAG AAG	gtatgagaat
5	54,324,449	-	54,324,523	75	cgatccccag	GTC CGG GAG	AAT CAG GAG	gtgtgggtgt
6	54,325,062	-	54,325,136	75	acacttccag	ACT CTG AAC	GAT GGG CAG	gtgagacatg
7	54,325,447	-	54,325,668	222	ctcactccag	ACT CTT GCC	CTC AAG GAG	gtgaggcccc
8	54,328,070	-	54,328,216	147	acctccgcag	GCG CTG GCG	TAT CGG CAG	gtgggggcgc
9	54,328,306	-	54,328,440	135	cctcccccag	AGT GAA GAG	CTC AAC AAG	gtgcggggag
10	54,328,865	-	54,328,948	84	catctcctag	GCC GAG GAA	CTG CAG CGG	gtgagggggc
11	54,329,103	-	54,329,234	132	ctttgcgcag	GCC CGG CAG	GAG GAG AAG	gtgcgccccc
12	54,329,708	-	54,329,770	63	gtctccacag	AAC TCC CTG	CTA AAC AAG	gtaggggggcc
13	54,329,905	-	54,329,984	80	cggccccag	GAG CAG CTC	TCC TAC TCC AG	gtgacagcag
14	54,330,848	-	54,330,992	145	atgcccacag	G TCT CTC CCT	CCC TCC AAG	gtcagcagct
15	54,331,793	-	54,331,980	188	acagggatag	GAT TGG GAG	AAG GAG ATC AA	gtgagccctg
16	54,333,274	-	54,333,496	223	ccctcctcag	G CTG ATC CAA	GAC AAG GCT	gtgagtgctc
17	54,334,737	-	54,334,900	164	ctgtcctcag	AAT CAT GTC	CCA CGG GGA AG	gtcagcaggg
18	54,335,030	-	54,335,157	128	tgctttcccag	T GAG GGC ACC	TCT TCT CTG G	gtgagtacct
19	54,336,489	-	54,336,582	94	ctgcctccag	CT GGA ACA CCC	AAC AAG AGG AA	gtgagtgtgt
20	54,337,103	-	54,337,184	82	acccttacag	G CAT GAA CTC	TGG CTG GAG	gtactggggc
21	54,337,873	-	54,338,073	201	tccgctgcag	CTG TGG GTG	TCC CGC ACT	gtgagtgtcc
22	54,341,012	-	54,341,074	63	tgcccctcag	TCC ACA GGA	ACC AAG CCC	gtgagtgccc
23*	54,341,235	-	54,341,261	27	aacgggtcag	GAG ACC AAG	TGG GAG CAG	gtagggggcg
24	54,343,152	-	54,343,327	176	atggccccag	ATC CTG GCA	AGC TTT CAC AG	gtgggggctg
25	54,343,735	-	54,343,831	98	tgctgctcag	G GTG AGT CTA	CAG ATC CGA G	gtgagtagag
26	54,344,0662	-	54,344,237	176	ccgtccccag	AC GTG ATG GTG	AAT GCA CAG	gtgagctgcc
27	54,344,326	-	54,344,394	69	ctctttccag	GCC CGG CAG	CTG GAC GAG	gtgggcgcgg
28	54,344,616	-	54,344,787	172	ctatacctag	GAC AGC GCC	CAG CCA GAA G TGC **TAG**	tgggggct
29	54,345,149	-	54,345,220	72	tctccctcca	GC CAG ACT TCT	TGCAGGCCTCCAG	gtgaggaccg
30	54,345,305	-	54,346,090	786	cgtcatgcag	GTGACCTCA	AACTGTTTC	aaaaagcttc

Data are based on the analysis of human genome sequences in the NCBI, Ensembl and UCSC databases. Nucleotide numbers correspond to thoses of the assembled UCSC genome.

*Exons that are subject to alternative splicing.

Suppl. Table 6

Exon-intron structure of the mouse *Liprin-α3 (PPFIA3)* gen

Exon	Nucleotide no.			Size	Flanking sequences			
1	52,622,296	-	52,621,29	268	cctggatctg	GCGACTGCG GCCGGCACCG...	GCGGACCAG	gtaggtaaga
2	52,617,192	-	52,616,935	255	gtacccgcag	**ATG** ATG TGC	CTG CCT CAG	gttgggcggg
3	52,616,007	-	52,615,906	102	gcctggacag	GAG TTT GCG	AAC ACC CGG	gtgagggccg
4	52,615,594	-	52,615,443	165	atccttccag	CTC CTT CTG	GAT GAG AAG	gtaggagagt
5	52,614,711	-	52,614,637	75	cggtctgcag	GTC CGG GAA	AAT CAG GAG	gtaggggcgg
6	52,614,232	-	52,614,158	75	actcttctag	GCC CTG AAC	GAT GGA CAG	gtgagagtct
7	52,613,350	-	52,613,129	222	ctctctccag	ACC CTT GCC	CTC AAG GAG	gtgaggcgga
8	52,612,057	-	52,611,911	147	acctcttcag	GCC CTG GCT	TAC AGA CAG	gtgaaagccc
9	52,611,814	-	52,611,680	135	tctctcccag	AGT GAA GAG	CTG AAC AAG	gtgacagcct
10	52,611,591	-	52,611,506	84	tgtccactag	GCT GAG GAA	CTG CAG CGG	gtgagagggc
11	52,610,660	-	52,610,529	132	ctttgttcag	GCC CGG CAG	GAG GAG AAG	gtgcgccccc
12	52,610,299	-	52,610,237	63	gtccccacag	AAC TCA CTG	CTG AAT AAG	gtgaggaccc
13	52,610,148	-	52,610,067	80	ctctccacag	GAG CAG CTC	TCC TAT TCC AG	gtgacagaag
14	52,609,033	-	52,608,889	145	gtgctcacag	G TCC CTT CCT	TCT TCC AAG	gtcagtagcc
15	52,607,645	-	52,607,457	188	tacaggacag	GAC TGG GAT	AAG GAA ATC AA	gtgagtccta
16	52,605,661	-	52,605,439	223	cctcttccag	G CTA ATT CAA	GAC AAG ACC	gtgagtactc
17	52,603,995	-	52,603,832	164	ctgtccccag	AAC CAT GTC	CCC CGG GGA AG	gtaggcagaa
18	52,603,739	-	52,603,612	128	gtgtctctag	T GAG AGC ACC	GTT TCT CTG G	gtgagtacta
19	52,603,190	-	52,603,096	94	ctgccaccag	CC GGG ACA CCC	AAC AAG AGG AA	gtgagtgtcc
20	52,602,875	-	52,602,794	82	tctctgctag	G CAC GAA CTT	TGG CTG GAG	gtattctgac
21	52,602,302	-	52,602,102	201	gtgacctcag	CTC TGG GTG	TCA CGC ACT	gtgagtgccc
22	52,602,173	-	52,599,111	63	cgcccttcag	CCC ACA GGA	ACA AAA CCC	gtgagtgcct
23*	52,598,949	-	52,598,923	27	aacgggtcag	GAG ACC AAG	TGG GAG CAG	gtaggggtgc
24	52,597,871	-	52,597,696	176	atggccccag	ATC CTG GCA	AGC TTC CAC AG	gtgggggctg
25	52,597,154	-	52,597,057	98	cactgctcag	G GTT AGT CTG	CAA ATC AGA G	gtgaggtccc
26	52,596,615	-	52,596,438	176	tcttctccag	AC GTG ATG GTG	AAT GCA CAA	gtgagctttg
27	52,596,338	-	52,596,208	69	tcttttccag	GCT CGG CAA	CTG GAT GAG	gtgggcgtgg
28	52,596,116	-	52,595,945	172	gtacatctag	GAC AGT GCC	CAG CCT GAA G TGC **TAG**	gtaagggact
29	52,595,630	-	52,595,559	72	ctctctccag	GC CAG ACT TCT	TGTGCACCTCCAG	gtgagtactc
*30	52,595,450	-	52,594,492	9	tcaatgaaag	TGACCTCAT	CACCAGTCC	tagcttttgt
		-						

Data are based on the analysis of human genome sequences in the NCBI, Ensembl and UCSC databases. Nucleotide numbers correspond to thoses of the assembled UCSC genome.
*Exons that are subject to alternative splicing.

Suppl. Table 7

Exon-intron structure of the human *Liprin-α4 (PPFIA4)* gene

Exon	Nucleotide no.			Size	Flanking sequences			
						ACACACTGCC...		
1	201,274,361	-	201,274,993		tttcccacag	**ATG** TGT GAG	CTC CCC CAG	gtaaggcccg
2	201,279,148	-	201,279,249	102	gggttttcag	GAA TTT GCC	AAC ACA CGG	gtaagtgggg
3	201,279,682	-	201,279,846	165	tccctgccag	CTG CTT CTG	GAT GAG AAG	gtgcccacct
4	201,280,130	-	201,280,204	75	cctcgagcag	GTG CGA GAG	CAC CAG CAG	gtaatctgcc
5	201,280,447	-	201,280,536	90	tgccctacag	GTA ATC TGC	CTG TGG AAG	gtaggtcatg
6	201,281,119	-	201,281,310	192	atccctggag	GAG GAT ACG	CTC CGG GAG	gtgcgtgagg
7	201,281,592	-	201,281,738	147	cttctcccag	GCT CTG GCC	CAC CGC CAG	gtacctcctc
8	201,281,999	-	201,282,137	139	acattgctag	TGT GAG GAG	CTC ACC AAG	gcaagtgggc
9	201,283,985	-	201,284,061	77	ctgcccctag	GCT GAA GAA	CTG GCA CGG	gtgagggcac
10	201,284,334	-	201,284,465	132	ggctgtgcag	GTG CGC CAG	GAG GAG AAG	gtgcccagag
11*	201,284,669	-	201,284,731	*63*	*tctccccccag*	*AAC ACG TTG*	*CAC CAC AAG*	gtacccggct
12	201,285,427	-	201,285,518	92	gctggcacag	GGC CGC CTG	GTC CAC TCC AG	gtactgcagc
13	201,287,519	-	201,287,628	109	accgctcaag	G TCG CAC ATG	TCT GCC AAG	gtgaggggt
14	201,289,504	-	201,289,712	209	ctttgctaag	GAC TGG GAG	GAG GAA ATC AG	gttagggcag
15	201,291,183	-	201,291,423	241	tcccttccag	G ATG ATT CAG	ATG ACC CTG	gtgagaggca
16	201,291,871	-	201,291,906	36	tcccttccag	CCC AGT GAC	AAG CTG CTG	gtgagaggca
17	201,292,125	-	201,292,259	134	gtctgttcag	TCG CCA GTG	GAA GGC AAG AG	gtaagtagag
18	201,292,235	-	201,292,725	193	caccctgtag	T GCC TTG GAG	CCT AAC GGA G	gtctgggcgg
19	201,294,929	-	201,295,022	94	ttccttgtag	TT CTG CTA ACA	CTA AAG AAG AA	gtaagagcca
20	201,295,521	-	201,295,602	82	ttcctataag	A CAC CAG CTG	TGG TTG GAG	gtaagcctga
21	201,295,968	-	201,296,168	201	gtgtctgcag	CTC TGG GTG	TCC AGG ACT	gtgagtggcc
22	201,296,721	-	201,296,783	63	ctgcctgcag	TCT TCT GGG	ACT AAA ACA	gtgagtctgg
23*	201,297,403	-	201,297,429	27	ttcctgctag	GAC AGT GAG	TGG GCT CAG	gtaagactcc
24	201,299,579	-	201,299,754	176	atttccctag	ACC CTG GCC	AGC TTC CAT CG	gtgagcgcgg
25	201,303,446	-	201,303,543	98	gtgcctgcag	A ACC AGT CTT	GAG ATC AAG G	gtaagctcgt
26	201,304,204	-	201,304,379	176	cacactccag	AT GTG TTA GTC	AAC ACC CAG	gtgggcagcc
27	201,307,443	-	201,307,511	68	tggactgcag	GCA CGC CAA	AAG CTG GAT GA	gtgagtacct
28	201,311,328	-	201,311,508	181	catggtgcag	G GGG ATG ACA	ATG CCT GAA G	gtgagtaaca
29*	201,311,719	-	201,311,827	109	cttctcccag	CT GGG ACG GCG	**TGA...** GTGGCTCGGG	gtaagtgggc
							GAC **TAG** CCA...	
30	201,312,092	-	201,314,487	2396	tctccctcag	CTC ACT CCC	AGACAATGTA	caaatggcct

Data are based on the analysis of human genome sequences in the NCBI, Ensembl and UCSC databases. Nucleotide numbers correspond to thoses of the assembled UCSC genome.
*Exons that are subject to alternative splicing.

Suppl. Table 8

Exon-intron structure of the mouse *Liprin-α4 (PPFIA4)* gene

Exon	Nucleotide no.			Size	Flanking sequences			
						ACCACATGTG...		
1	136,229,505	-	136,228,868	639	tctcccacag	ATC **ATG** TGT	CTT CCC CAG	gtaaggttcc
2	136,225,824	-	136,225,723	102	gggctttcag	GAA TTT GCC	AAC ACA AGG	gtaagtaagg
3	136,225,385	-	136,225,221	165	tctctcccag	CTG CTT CTG	GAT GAG AAG	gtacccacct
4	136,224,944	-	136,224,870	75	tcctgggcag	GTG CGA GAG	CAC CAG CAG	gtaagctgca
5	136,224,666	-	136,224,577	90	tgtcttacag	GTA TCT GCC	CTG TGG AAA	gtgggtaatg
6	136,224,026	-	136,223,835	192	gtccctggag	GAT GAC ACT	CTC CGA GAG	gtaggcgagg
7	136,223,539	-	136,223,393	147	ctccgcccag	GCT CTG GCT	CAC CGC CAG	gtaacgcggc
8	136,223,195	-	136,223,161	135	gtactgctag	TGT GAG GAG	CTC ACC AAG	gcaagtgggc
9	136,221,171	-	136,221,088	84	ctgcacctag	GCT GAG GAA	CTG GCA CGG	gtgagggcac
10	136,220,787	-	136,220,656	132	ggatgtgcag	GTG CGC CAG	GAG GAG AAG	gtgaggaagc
11	136,219,670	-	136,219,579	92	cctggcacag	G GCC GTC TGT	TCC ACT CCA G	gtactagagt
12	136,217,746	-	136,217,638	109	gtcactcaag	G TCA CAC GTG	TCT GCC AAG	gtaaggggtg
13	136,216,000	-	136,215792	209	ctttgctaag	GAC TGG GAG	GAG GAA ATC AG	gtggggtggg
14	136,214,625	-	136,214,385	241	ttctgagcag	G ATG ATC CAG	ATG ACC CTG	gtgagtctgg
15	136,214,050	-	136,214,015	36	tctctttcag	CCC AGC GAC	AAG CTG CTG	gtgagtgctt
16	136,2137,73	-	136,213,641	134	gtctgttcag	TCG CCA GTG	GAG GGC AAG AG	gtgagtgagc
17	136,213,355	-	136,213,192	164	catcctgtag	T GCC TTG GAG	CCT AAC GGA G	gtctctgcct
18	136,210,300	-	136,210,205	94	tcatttccag	TT CTG CTA ACA	CTA AAG AAG AA	gtaagagcct
19	136,209,745	-	136,209,664	82	ctcccccaag	A CAC CAG CTG	TGG CTG GAG	gtgagcctgg
20	136,209,313	-	136,209,114	201	atgtctgtag	CTC TGG GTG	TCC AGG ACT	gtgagtagcc
21	136,208,696	-	136,208,634	63	ctgcctgcag	TCT TCA GGG	ACC AAA ACA	gtgagtctgc
22	136,208,132	-	136,208,106	27	ctcctgctag	GAC AGT GAG	TGG GCC CAG	gtaagacccc
23	136,206,328	-	136,206,153	232	atgtccccag	ACC CTG GCC	AGT TTC CAT AG	gtgagccagg
24	136,200,961	-	136,200,864	98	gtgtctgcag	A ACC AGT CTT	GAG ATC AAG G	gtaaggttgc
25	136,200,357	-	136,200,182	176	tgtcctccag	AT GTG CTG GTC	AGC ACC CAG	gtagccctca
26	136,197,115	-	136,197,047	69	tgggtttcag	GCC CGC CAA	AAT TGG ATG AC	gtgagtacct
27	136,196,045	-	136,195,868	178	cttggtgcag	G GAG AAG AGA	ATG CCG GAA G	gtgagtgcca
							TGA CCCACCCCCC...	
28*	136,195,713	-	136,195,603	111	ctcctgccag	CC GGG ACG GCG	CCGGCTCGGG	gtaagtgggc
							GAC **TAG** CCCTTCC...	
29	136,195,405	-	136,193,360	2046	tctctcatag	CTC ACT CCC	AGACAATGTA	caaatggtgt

Data are based on the analysis of human genome sequences in the NCBI, Ensembl and UCSC databases. Nucleotide numbers correspond to thoses of the assembled UCSC genome.
*Exons that are subject to alternative splicing.

Suppl. Table 9

Human Liprin-α transcript variants produced by alternative splicing

Gene	Ensembl transcript ID	Tigr Gene Indices	GenBank entry number
Liprin-α1			
10	-	-	BX648037
Δ10	ENST00000253925, ENST00000389547	THC2610455, THC2466389[a]	DQ892401, NM_177423[a]
18	-	THC2655239, THC2652008[a]	BM724097, BG772359[a]
Δ18	ENST00000253925, ENST00000389547	DB074051, THC2664979[a]	DB256381, DB093696[a]
24+25	-	THC2652008,	BF115477, AW003540[a]
Δ24+25	ENST00000253925, ENST00000389547	THC2664979, THC2610455[a]	DA601551, BP288948[a]
30b	ENST00000389547	THC2661071	NM_177423, U22815[a]
31	-	THC2623316, THC2620206[a]	AK124621, AK123331[a]
Δ31	-	THC2789153	CB963045[a]
Liprin-α2			
6	ENST00000333447	THC2521513, DA097453a	XM_001088683, XM_001088353[a]
Δ 6	-	THC2512280	-
23	ENST00000333447	THC2478562, THC2533874a	NM_003625, AB210009[a]
Δ23		-	AB173244, XM_509243[a]
24	ENST00000333447	THC2478562, THC2533874a	NM_003625, AB210009[a]
Δ24		DA175569, THC2489420	BC104912, DA175569
23+24	ENST00000333447	THC2478562, THC2533874a	DA171009, NM_003625
Δ23+24		DA365677, THC2515077	DA365677, AK123372
Liprin-α3			
23	ENST00000334186	THC2464523	BC10152, BC101518[a]
Δ23	ENST00000334329	THC2610653	DB022704, BU931579[a]
Liprin-α4			
11	-	-	DC308173, EG328335
Δ11	ENST00000367238, ENST00000367240	-	-
23	ENST00000367238, ENST00000367240	NP1247464, THC2473050	BC132923, BC132925[a]
Δ23	ENST00000295706	THC2602563	AK023365, AF034801[a]
29	-	THC2760377, THC2602563	DA199274,AK170782
Δ29	ENST00000367238, ENST00000367240a	THC247305	BC132925, BC132923a

Data are based on the anaylsis of EST sequences in the UCSC, GenBank, ENSEMBL, and TIGR databases. **Δ** marks variants, in which the exon is absent. [a], databases contain additional EST sequences for this transcript variant.

Suppl. Tabel 10

Alternative splicing of mouse Liprin-α1-4

Gene	Ensembl transcript ID	Tigr Gene Indices	GenBank entry number
Liprin-α1			
10	-	-	-
Δ10	-	TC1612279, BG171917	XM_133979, XM_918243
18	-	-	DT917865, CF740050[a]
Δ18	-	TC1600458	-
24	-	-	-
Δ24	-	CB519424	-
25	-	-	-
Δ25	-	TC1707207	-
24+25	-	-	-
Δ24+25	-	CB519424	CX201127, CF733114[a]
31	-	TC1600458	CX239318, CN702858[a]
Δ31	ENSMUST00000093967	TC1707207	CF173556, AK146526
Liprin-α2			
6	ENSMUST00000029404	TC1583316	CV559156, CA328790[a]
Δ6	-	CV558903	CV558903
Liprin α3			
23	ENSMUST00000003961	TC1581164	AK147645, NM_029741[a]
Δ23	-	CB249091	-
Liprin-α4			
22			BY703827 (nur E22+23)
Δ22	ENSMUST00000027729	TC1601776	BG080124
28	-	-	AK170782
Δ28	ENSMUST00000027729	NP747047, TC1621807	AK003571, XM_988391[a]

Data are based on the anaylsis of EST sequences in the UCSC, GenBank, ENSEMBL, and TIGR databases. **Δ** marks variants, in which the exon is absent. [a], databases contain additional EST sequences for this transcript variant.

9 References

Ackley BD, Harrington RJ, Hudson ML, Williams L, Kenyon CJ, Chisholm AD, Jin Y (2005) The two isoforms of the Caenorhabditis elegans leukocyte-common antigen related receptor tyrosine phosphatase PTP-3 function independently in axon guidance and synapse formation. J Neurosci 25:7517-7528.

Andrews-Zwilling YS, Kawabe H, Reim K, Varoqueaux F, Brose N (2006) Binding to Rab3A-interacting molecule RIM regulates the presynaptic recruitment of Munc13-1 and ubMunc13-2. J Biol Chem 281:19720-19731.

Asperti C, Pettinato E, de Curtis I (2010) Liprin-alpha1 affects the distribution of low-affinity beta1 integrins and stabilizes their permanence at the cell surface. Exp Cell Res 316:915-926.

Asperti C, Astro V, Totaro A, Paris S, de Curtis I (2009) Liprin-alpha1 promotes cell spreading on the extracellular matrix by affecting the distribution of activated integrins. J Cell Sci 122:3225-3232.

Bard L, Boscher C, Lambert M, Mege RM, Choquet D, Thoumine O (2008) A molecular clutch between the actin flow and N-cadherin adhesions drives growth cone migration. J Neurosci 28:5879-5890.

Bloom FE, Aghajanian GK (1968) Fine structural and cytochemical analysis of the staining of synaptic junctions with phosphotungstic acid. J Ultrastruct Res 22:361-375.

Cahoy JD, Emery B, Kaushal A, Foo LC, Zamanian JL, Christopherson KS, Xing Y, Lubischer JL, Krieg PA, Krupenko SA, Thompson WJ, Barres BA (2008) A transcriptome database for astrocytes, neurons, and oligodendrocytes: a new resource for understanding brain development and function. J Neurosci 28:264-278.

Chao DL, Shen K (2008) Functional dissection of SYG-1 and SYG-2, cell adhesion molecules required for selective synaptogenesis in C. elegans. Mol Cell Neurosci 39:248-257.

Choe KM, Prakash S, Bright A, Clandinin TR (2006) Liprin-alpha is required for photoreceptor target selection in Drosophila. Proc Natl Acad Sci U S A 103:11601-11606.

Colon-Ramos DA, Margeta MA, Shen K (2007) Glia promote local synaptogenesis through UNC-6 (netrin) signaling in C. elegans. Science 318:103-106.

Coppola T, Magnin-Luthi S, Perret-Menoud V, Gattesco S, Schiavo G, Regazzi R (2001) Direct interaction of the Rab3 effector RIM with Ca2+ channels, SNAP-25, and synaptotagmin. J Biol Chem 276:32756-32762.

Dai Y, Taru H, Deken SL, Grill B, Ackley B, Nonet ML, Jin Y (2006) SYD-2 Liprin-alpha organizes presynaptic active zone formation through ELKS. Nat Neurosci 9:1479-1487.

Dick O, tom Dieck S, Altrock WD, Ammermuller J, Weiler R, Garner CC, Gundelfinger ED, Brandstatter JH (2003) The presynaptic active zone protein bassoon is essential for photoreceptor ribbon synapse formation in the retina. Neuron 37:775-786.

Dickinson BA, Jo J, Seok H, Son GH, Whitcomb DJ, Davies CH, Sheng M, Collingridge GL, Cho K (2009) A novel mechanism of hippocampal LTD involving muscarinic receptor-triggered interactions between AMPARs, GRIP and liprin-alpha. Mol Brain 2:18.

Dresbach T, Hempelmann A, Spilker C, tom Dieck S, Altrock WD, Zuschratter W, Garner CC, Gundelfinger ED (2003) Functional regions of the presynaptic cytomatrix protein bassoon: significance for synaptic targeting and cytomatrix anchoring. Mol Cell Neurosci 23:279-291.

Dunah AW, Hueske E, Wyszynski M, Hoogenraad CC, Jaworski J, Pak DT, Simonetta A, Liu G, Sheng M (2005) LAR receptor protein tyrosine phosphatases in the development and maintenance of excitatory synapses. Nat Neurosci 8:458-467.

Fernandez-Busnadiego R, Zuber B, Maurer UE, Cyrklaff M, Baumeister W, Lucic V (2010) Quantitative analysis of the native presynaptic cytomatrix by cryoelectron tomography. J Cell Biol 188:145-156.

Fouquet W, Owald D, Wichmann C, Mertel S, Depner H, Dyba M, Hallermann S, Kittel RJ, Eimer S, Sigrist SJ (2009) Maturation of active zone assembly by Drosophila Bruchpilot. J Cell Biol 186:129-145.

Gray EG (1963) Electron microscopy of presynaptic organelles of the spinal cord. J Anat 97:101-106.

Hallam SJ, Goncharov A, McEwen J, Baran R, Jin Y (2002) SYD-1, a presynaptic protein with PDZ, C2 and rhoGAP-like domains, specifies axon identity in C. elegans. Nat Neurosci 5:1137-1146.

Harlow ML, Ress D, Stoschek A, Marshall RM, McMahan UJ (2001) The architecture of active zone material at the frog's neuromuscular junction. Nature 409:479-484.

Hofmeyer K, Maurel-Zaffran C, Sink H, Treisman JE (2006) Liprin-alpha has LAR-independent functions in R7 photoreceptor axon targeting. Proc Natl Acad Sci U S A 103:11595-11600.

Hoogenraad CC, Milstein AD, Ethell IM, Henkemeyer M, Sheng M (2005) GRIP1 controls dendrite morphogenesis by regulating EphB receptor trafficking. Nat Neurosci 8:906-915.

Hoogenraad CC, Feliu-Mojer MI, Spangler SA, Milstein AD, Dunah AW, Hung AY, Sheng M (2007) Liprinalpha1 degradation by calcium/calmodulin-dependent protein kinase II regulates LAR receptor tyrosine phosphatase distribution and dendrite development. Dev Cell 12:587-602.

Isaac JT, Ashby M, McBain CJ (2007) The role of the GluR2 subunit in AMPA receptor function and synaptic plasticity. Neuron 54:859-871.

Kaeser PS, Kwon HB, Chiu CQ, Deng L, Castillo PE, Sudhof TC (2008) RIM1alpha and RIM1beta are synthesized from distinct promoters of the RIM1 gene to mediate differential but overlapping synaptic functions. J Neurosci 28:13435-13447.

Kaeser PS, Deng L, Chavez AE, Liu X, Castillo PE, Sudhof TC (2009) ELKS2alpha/CAST deletion selectively increases

neurotransmitter release at inhibitory synapses. Neuron 64:227-239.

Kalla S, Stern M, Basu J, Varoqueaux F, Reim K, Rosenmund C, Ziv NE, Brose N (2006) Molecular dynamics of a presynaptic active zone protein studied in Munc13-1-enhanced yellow fluorescent protein knock-in mutant mice. J Neurosci 26:13054-13066.

Katoh M (2003) Identification and characterization of human PPFIA4 gene in silico. Int J Mol Med 12:1009-1014.

Kaufmann N, DeProto J, Ranjan R, Wan H, Van Vactor D (2002) Drosophila liprin-alpha and the receptor phosphatase Dlar control synapse morphogenesis. Neuron 34:27-38.

Kiyonaka S, Wakamori M, Miki T, Uriu Y, Nonaka M, Bito H, Beedle AM, Mori E, Hara Y, De Waard M, Kanagawa M, Itakura M, Takahashi M, Campbell KP, Mori Y (2007) RIM1 confers sustained activity and neurotransmitter vesicle anchoring to presynaptic Ca2+ channels. Nat Neurosci 10:691-701.

Ko J, Na M, Kim S, Lee JR, Kim E (2003a) Interaction of the ERC family of RIM-binding proteins with the liprin-alpha family of multidomain proteins. J Biol Chem 278:42377-42385.

Ko J, Kim S, Valtschanoff JG, Shin H, Lee JR, Sheng M, Premont RT, Weinberg RJ, Kim E (2003b) Interaction between liprin-alpha and GIT1 is required for AMPA receptor targeting. J Neurosci 23:1667-1677.

Kohrmann M, Haubensak W, Hemraj I, Kaether C, Lessmann VJ, Kiebler MA (1999) Fast, convenient, and effective method to transiently transfect primary hippocampal neurons. J Neurosci Res 58:831-835.

Li Q, Lee JA, Black DL (2007) Neuronal regulation of alternative pre-mRNA splicing. Nat Rev Neurosci 8:819-831.

Mattauch S, Sachs M, Behrens J (2010) Liprin-alpha4 is a new hypoxia-inducible target gene required for maintenance of cell-cell contacts. Exp Cell Res.

Meinertzhagen IA (1996) Ultrastructure and quantification of synapses in the insect nervous system. J Neurosci Methods 69:59-73.

Mittelstaedt T, Schoch S (2007) Structure and evolution of RIM-BP genes: identification of a novel family member. Gene 403:70-79.

Mittelstaedt T, Alvarez-Baron E, Schoch S (2010) RIM proteins and their role in synapse function. Biol Chem 391:599-606.

Olsen O, Moore KA, Fukata M, Kazuta T, Trinidad JC, Kauer FW, Streuli M, Misawa H, Burlingame AL, Nicoll RA, Bredt DS (2005) Neurotransmitter release regulated by a MALS-liprin-alpha presynaptic complex. J Cell Biol 170:1127-1134.

Osten P, Khatri L, Perez JL, Kohr G, Giese G, Daly C, Schulz TW, Wensky A, Lee LM, Ziff EB (2000) Mutagenesis reveals a role for ABP/GRIP binding to GluR2 in synaptic surface accumulation of the AMPA receptor. Neuron 27:313-325.

Owald D, Sigrist SJ (2009) Assembling the presynaptic active zone. Curr Opin Neurobiol 19:311-318.

Patel MR, Shen K (2009) RSY-1 is a local inhibitor of presynaptic assembly in C. elegans. Science 323:1500-1503.

Patel MR, Lehrman EK, Poon VY, Crump JG, Zhen M, Bargmann CI, Shen K (2006) Hierarchical assembly of presynaptic components in defined C. elegans synapses. Nat Neurosci 9:1488-1498.

Pfenninger K, Sandri C, Akert K, Eugster CH (1969) Contribution to the problem of structural organization of the presynaptic area. Brain Res 12:10-18.

Prakash S, McLendon HM, Dubreuil CI, Ghose A, Hwa J, Dennehy KA, Tomalty KM, Clark KL, Van Vactor D, Clandinin TR (2009) Complex interactions amongst N-cadherin, DLAR, and Liprin-alpha regulate Drosophila photoreceptor axon targeting. Dev Biol 336:10-19.

Pulido R, Serra-Pages C, Tang M, Streuli M (1995) The LAR/PTP delta/PTP sigma subfamily of transmembrane

protein-tyrosine-phosphatases: multiple human LAR, PTP delta, and PTP sigma isoforms are expressed in a tissue-specific manner and associate with the LAR-interacting protein LIP.1. Proc Natl Acad Sci U S A 92:11686-11690.

Qiao F, Bowie JU (2005) The many faces of SAM. Sci STKE 2005:re7.

Samuels BA, Hsueh YP, Shu T, Liang H, Tseng HC, Hong CJ, Su SC, Volker J, Neve RL, Yue DT, Tsai LH (2007) Cdk5 Promotes Synaptogenesis by Regulating the Subcellular Distribution of the MAGUK Family Member CASK. Neuron 56:823-837.

Schoch S, Gundelfinger ED (2006) Molecular organization of the presynaptic active zone. Cell Tissue Res 326:379-391.

Schoch S, Castillo PE, Jo T, Mukherjee K, Geppert M, Wang Y, Schmitz F, Malenka RC, Sudhof TC (2002) RIM1alpha forms a protein scaffold for regulating neurotransmitter release at the active zone. Nature 415:321-326.

Serra-Pages C, Streuli M, Medley QG (2005) Liprin phosphorylation regulates binding to LAR: evidence for liprin autophosphorylation. Biochemistry 44:15715-15724.

Serra-Pages C, Medley QG, Tang M, Hart A, Streuli M (1998) Liprins, a family of LAR transmembrane protein-tyrosine phosphatase-interacting proteins. J Biol Chem 273:15611-15620.

Serra-Pages C, Kedersha NL, Fazikas L, Medley Q, Debant A, Streuli M (1995) The LAR transmembrane protein tyrosine phosphatase and a coiled-coil LAR-interacting protein co-localize at focal adhesions. EMBO J 14:2827-2838.

Shen JC, Unoki M, Ythier D, Duperray A, Varticovski L, Kumamoto K, Pedeux R, Harris CC (2007) Inhibitor of growth 4 suppresses cell spreading and cell migration by interacting with a novel binding partner, liprin alpha1. Cancer Res 67:2552-2558.

Shen K, Fetter RD, Bargmann CI (2004) Synaptic specificity is generated by the synaptic guidepost protein SYG-2 and its receptor, SYG-1. Cell 116:869-881.

Sheng M, Hoogenraad CC (2007) The postsynaptic architecture of excitatory synapses: a more quantitative view. Annu Rev Biochem 76:823-847.

Shin H, Wyszynski M, Huh KH, Valtschanoff JG, Lee JR, Ko J, Streuli M, Weinberg RJ, Sheng M, Kim E (2003) Association of the kinesin motor KIF1A with the multimodular protein liprin-alpha. J Biol Chem 278:11393-11401.

Siksou L, Rostaing P, Lechaire JP, Boudier T, Ohtsuka T, Fejtova A, Kao HT, Greengard P, Gundelfinger ED, Triller A, Marty S (2007) Three-dimensional architecture of presynaptic terminal cytomatrix. J Neurosci 27:6868-6877.

Smith SM, Renden R, von Gersdorff H (2008) Synaptic vesicle endocytosis: fast and slow modes of membrane retrieval. Trends Neurosci 31:559-568.

Spangler SA, Hoogenraad CC (2007) Liprin-alpha proteins: scaffold molecules for synapse maturation. Biochem Soc Trans 35:1278-1282.

Stryker E, Johnson KG (2007a) LAR, liprin {alpha} and the regulation of active zone morphogenesis. J Cell Sci 120:3723-3728.

Stryker E, Johnson KG (2007b) LAR, liprin alpha and the regulation of active zone morphogenesis. J Cell Sci 120:3723-3728.

Sudhof TC (2004) The synaptic vesicle cycle. Annu Rev Neurosci 27:509-547.

Tabuchi K, Sudhof TC (2002) Structure and evolution of neurexin genes: insight into the mechanism of alternative splicing. Genomics 79:849-859.

tom Dieck S, Altrock WD, Kessels MM, Qualmann B, Regus H, Brauner D, Fejtova A, Bracko O, Gundelfinger ED, Brandstatter JH (2005) Molecular dissection of the photoreceptor ribbon synapse: physical interaction of Bassoon and RIBEYE is essential for the assembly of the ribbon complex. J Cell Biol 168:825-836.

Tsuriel S, Fisher A, Wittenmayer N, Dresbach T, Garner CC, Ziv NE (2009) Exchange and redistribution dynamics of

the cytoskeleton of the active zone molecule bassoon. J Neurosci 29:351-358.

Tsuriel S, Geva R, Zamorano P, Dresbach T, Boeckers T, Gundelfinger ED, Garner CC, Ziv NE (2006) Local sharing as a predominant determinant of synaptic matrix molecular dynamics. PLoS Biol 4:e271.

van Roessel P, Elliott DA, Robinson IM, Prokop A, Brand AH (2004) Independent regulation of synaptic size and activity by the anaphase-promoting complex. Cell 119:707-718.

Varoqueaux F, Jamain S, Brose N (2004) Neuroligin 2 is exclusively localized to inhibitory synapses. Eur J Cell Biol 83:449-456.

Wagh DA, Rasse TM, Asan E, Hofbauer A, Schwenkert I, Durrbeck H, Buchner S, Dabauvalle MC, Schmidt M, Qin G, Wichmann C, Kittel R, Sigrist SJ, Buchner E (2006) Bruchpilot, a protein with homology to ELKS/CAST, is required for structural integrity and function of synaptic active zones in Drosophila. Neuron 49:833-844.

Wagner OI, Esposito A, Kohler B, Chen CW, Shen CP, Wu GH, Butkevich E, Mandalapu S, Wenzel D, Wouters FS, Klopfenstein DR (2009) Synaptic scaffolding protein SYD-2 clusters and activates kinesin-3 UNC-104 in C. elegans. Proc Natl Acad Sci U S A 106:19605-19610.

Wang X, Hu B, Zieba A, Neumann NG, Kasper-Sonnenberg M, Honsbein A, Hultqvist G, Conze T, Witt W, Limbach C, Geitmann M, Danielson H, Kolarow R, Niemann G, Lessmann V, Kilimann MW (2009) A protein interaction node at the neurotransmitter release site: domains of Aczonin/Piccolo, Bassoon, CAST, and rim converge on the N-terminal domain of Munc13-1. J Neurosci 29:12584-12596.

Wang Y, Sudhof TC (2003) Genomic definition of RIM proteins: evolutionary amplification of a family of synaptic regulatory proteins(small star, filled). Genomics 81:126-137.

Wittenmayer N, Korber C, Liu H, Kremer T, Varoqueaux F, Chapman ER, Brose N, Kuner T, Dresbach T (2009) Postsynaptic Neuroligin1 regulates presynaptic maturation. Proc Natl Acad Sci U S A 106:13564-13569.

Wyszynski M, Kim E, Dunah AW, Passafaro M, Valtschanoff JG, Serra-Pages C, Streuli M, Weinberg RJ, Sheng M (2002) Interaction between GRIP and liprin-alpha/SYD2 is required for AMPA receptor targeting. Neuron 34:39-52.

Zhai RG, Bellen HJ (2004) The architecture of the active zone in the presynaptic nerve terminal. Physiology (Bethesda) 19:262-270.

Zhen M, Jin Y (1999) The liprin protein SYD-2 regulates the differentiation of presynaptic termini in C. elegans. Nature 401:371-375.

Zito K, Scheuss V, Knott G, Hill T, Svoboda K (2009) Rapid functional maturation of nascent dendritic spines. Neuron 61:247-258.

Zurner M, Schoch S (2009) The mouse and human Liprin-alpha family of scaffolding proteins: genomic organization, expression profiling and regulation by alternative splicing. Genomics 93:243-253.